Genetically Engineered Small Extracellular Vesicles to Deliver Alpha-Synuclein siRNA Across the Blood-Brain-Barrier to Treat Parkinson's Disease

Carmen Daniela Sosa Miranda

Thesis submitted to the University of Ottawa
in partial fulfillment of the requirements
for the Master's of Science degree in
Cellular and Molecular Medicine

Department of Cellular and Molecular Medicine
Faculty of Medicine
University of Ottawa

ABSTRACT

Small extracellular vesicles (small EVs) are endogenous membrane-enclosed nanocarriers released from essentially all cells. They have been shown to carry proteins, lipids, nucleic acids to transmit biological signals throughout the body, including to the brain. Some evidence has suggested that small EVs can cross the blood-brain barrier (BBB), moving from the peripheral circulation to the central nervous system (CNS). The BBB is a dynamic barrier that regulates molecular trafficking between the peripheral circulation and the CNS. As a result, small EVs have attracted attention for their potential as a novel delivery platform for nucleic acid-based therapeutics across the BBB. Silencing RNAs (siRNAs) are a potent drug class but using "naked" siRNA is not feasible due to their short half-life, vulnerability to degradation and low penetration in cells. Despite the excitement for the development of small EV-based therapeutics, their clinical development is hampered by the lack of reliable methods for packing therapeutics into them. Reshke et al. has shown that cells can be genetically engineered to produce customizable small EVs packaged with siRNA against any protein by integrating the siRNA sequence into the pre-miR-451 structure. Mounting evidence has established that in a misfolded state, α-synuclein becomes insoluble and phosphorylated to form intracellular inclusions in neurons (known as Lewy bodies) which leads to Parkinson's disease (PD) pathogenesis. Given that increased α-synuclein expression causes familial and idiopathic PD, decreasing its synthesis by using siRNA is an attractive therapeutic strategy. Here, we genetically engineered cells to produce small EVs packaged with siRNA against α-synuclein integrated in the pre-miR451 backbone, tested their ability to cross an *in vitro* BBB, and deliver its cargo to silence endogenous α-synuclein in neuron-like cells. The therapeutic potential of α-synuclein siRNA delivery by these small EVs was demonstrated by the strong mRNA (60-70%) and protein knockdown (43%) of α-synuclein in

neuron-like cells. We also demonstrated that approximately at 4% and 2%, respectively of small EVs-derived from human brain endothelial cells (hCMEC/D3) and human embryonic kidney (HEK293T) were transported cross the *in vitro* BBB model. Interestingly, we observed that small EVs-derived from HEK293T deliver their cargo to induced brain endothelial cells (iBECs) (~74% α-synuclein mRNA reduction) but their rate of transport across BBB was lower and did not reduce α-synuclein mRNA expression in neuron-like cells, seeded on the far side of the BBB. Small EVs-derived from hCMEC/D3 reduced α-synuclein mRNA (40%) in neuron-like cells across the BBB model. This finding suggests that small EVs derived from different cell sources can undergo different intracellular trafficking routes, providing various opportunities to influence the efficiency of delivery and fate of intracellular cargo. Using small EVs-derived from hCMEC/D3, two different routes of administration, a single bolus intravenous (IV) or intra-carotid (ICD) injection, showed small EVs largely accumulated in the liver, spleen, small intestines and kidneys; and only a small amount of small EVs were detected in the brain. These results indicate that human brain endothelial cells may serve as a promising cell source for CNS treatments based on small EVs.

STATEMENT OF CONTRIBUTIONS

This MSc thesis entitled "Genetically Engineered Small Extracellular Vesicles to Deliver Alpha-Synuclein siRNA Across the Blood-Brain Barrier to Treat Parkinson's Disease" was written by me. Derrick Gibbings and Jagdeep K. Sandhu were responsible for the initial conceptualization and design of the project. I performed all experiments and was responsible for data collection, data analyses, and preparation of figures except for the ones listed below.

James Taylor (Derrick Gibbings lab) created and supplied me with HEK293T cells expressing GFP siRNA and hCMEC/D3 cells expressing GFP siRNA. As well, he performed all the lentiviral transduction experiments that were required during this project.

Kallol Dutta (Derrick Gibbings lab) performed the small EVs isolation by tangential flow filtration (TFF).

Claudie Charlebois (HHT NRC Team) performed the culturing and seeding of the induced brain endothelial cells (iBECs) in the polyethylene terephthalate (PET) membranes for the *in vitro* induced pluripotent stem cells (iPSC) BBB model experiments. Yonghong Guan (HHT NRC Team) carried out transendothelial electrical resistance (TEER) measurement for each transwell prior and 24 h after the experiment.

Mario Mercier (HHT NRC Team) prepared and injected CD1 mice for the *in vivo* biodistribution experiments as well as collected the tissues (brain, heart, lung, liver, kidney, spleen, and lymph nodes) for ex-vivo imaging with IVIS Lumina III. Dorothy Fatehi (HHT NRC Team) helped with the quantification of the fluorescent signals from each organ using the Living Image software.

Funding was provided by the National Program Office Ideation Programs-New Beginnings Fund NRC Research Proposal grant awarded to Jagdeep K. Sandhu and Derrick Gibbings.

The thesis presented here was read and edited by Derrick Gibbings and Jagdeep K. Sandhu prior to submission.

ACKNOWLEDGMENTS

I would firstly like to thank my supervisor, Dr. Derrick Gibbings, and co-supervisor, Dr. Jagdeep K. Sandhu, for opening the doors of research and giving me a chance to carry out this new project. Their unwavering support and enthusiasm encouraged me to be the best student I can be amidst the stresses of my graduate school and during COVID-19 pandemic. As well, for guiding me and helping me in every experiment throughout my project, but specifically for having the time and patience to teach me. I would also like to thank my thesis advisory committee Dr. Baptiste Lacoste and Dr. Maxime Rousseaux for providing me with helpful suggestions, feedback and guidance along this project.

Next, I am grateful to all current and past members in the Gibbing's lab that have made my experience a fulfilling and enjoyable one. I am grateful to past members (Maisa Alkailani, Kristofferson Tandoc, Jenna McCann) and current members (Ryan Reshke, James Taylor, Olanta Negeri, Alexandre Savard, Huishan Guo, Kaela O'Connor, Yunping Xue, Kallol Dutta, Charlotte Manser, Adnie Etienne), not only for their unconditional help with long and arduous experiments, but also for never saying no when I asked for help. Everyone in Gibbing's lab has helped me in some way or another during this project.

I am also grateful to all members in Sandhu's lab at the Human Health Therapeutics (HHT) Team, National Research Council Canada (NRC) for taking the time to show me key techniques, giving me suggestions for my project and always willing to help me. I am grateful to Umar Iqbal, Melissa Hewitt, Arsalan Haqqani, Dorothy Fatehi, Mario Mercier, Binbing Ling, Etienne Lessard, Anna Jezierski, Junzhuo Huang, Claudie Charlebois and Yonghong Guan. In particular, a big thank you to Melissa, who dropped everything she was doing to help me in many ways during my project.

I would like to give my utmost gratitude to my mom Rosy Miranda, and my dad César Sosa for all their sacrifice, love and motivation, my pillars of strength. You have both been supportive of me and my education from the beginning. Thank you for never letting me give up on the difficult things in life and helping me achieve my goals. My brothers César and Fabián for being my best friends and always believing in my potential. My accomplishments would not have been possible without you all by my side, so thank you.

Conor, thank you for your consistent motivation and support, and for being by my side since day one, throughout my undergraduate degree and now master's degree. You have been supportive throughout every aspect of my research and your willingness to listen means the world. You are a kind, honest, generous, hard-working, and just an amazing person; you will get far.

TABLE OF CONTENTS

ABSTRACT ... *ii*

STATEMENT OF CONTRIBUTIONS ... *iv*

ACKNOWLEDGMENTS ... *v*

LIST OF TABLES ... *viii*

LIST OF FIGURES ... *ix*

LIST OF ABBREVIATIONS ... *xi*

INTRODUCTION ... *1*

1.1 Blood-brain barrier ... 1
- 1.1.1 Overview: Structure, function, and regulation of the BBB ... **1**
- 1.1.2 Transport routes across the BBB ... **5**
- 1.1.3 Modeling the *in vitro* BBB of CNS disorders ... **10**
- 1.1.4 Overview of *in vitro* BBB models ... **11**
- 1.1.5 Application of BBB models in assessing CNS therapies ... **18**
- 1.1.6 Methods to delivery drugs to the CNS ... **19**

1.2 Extracellular vesicles ... 25
- 1.2.1 Extracellular vesicles biogenesis, general EV composition, and uptake ... **25**
- 1.2.2 Extracellular vesicle isolation and characterization ... **29**
- 1.2.3 Possible mechanisms for small EVs to cross the BBB ... **30**
- 1.2.4 Therapeutic applications for small EVs ... **32**

1.3 Silencing RNA ... 33
- 1.3.1 Small EV as a vehicle for delivery of nucleic acids ... **37**

1.4 Parkinson's disease ... 40
- 1.4.1 Parkinson's disease overview: pathology, risk factors, clinical and non-clinical features ... **40**
- 1.4.2 Genetics of Parkinson's disease ... **42**
- 1.4.3 Alpha-synuclein (α-synuclein) ... **44**

HYPOTHESIS AND OBJECTIVES ... *52*

METHODS ... *53*

1.5 Cell lines ... 53

1.6 Cell culture ... 53

1.7 Differentiation of human neuroblastoma SH-SY5Y cells ... 54

1.8 Transfection ... 54

1.8.1 Transfection of α-synuclein-targeting siRNA **54**

1.9 Generation of a stable cell line 57

1.10 Preparation of small EV depleted media 58

1.11 Small EV isolation 59

1.12 Nanoparticle tracking analysis 62

1.13 RNA extraction 62

1.14 cDNA synthesis and RT-qPCR 63

1.15 Measurement of copy number of siRNAs per small EV 64

1.16 Protein extraction and Western blotting 65

1.17 Endothelial cell differentiation of iPSCs 66

1.18 Preparation of transwell inserts and TEER measurements 67

1.19 Cell uptake assays.. 68

1.19.1 Treatment of differentiated SH-SY5Y cells with small EV containing α-synuclein siRNA **68**

1.19.2 *In vitro* human iPSC BBB model uptake **70**

1.20 Biodistribution of small EVs in mice 71

1.21 Statistical Analysis... 73

RESULTS 74

1.22 Integrating siRNA against α-synuclein into the pre-miR-451 backbone 74

1.23 Small EVs packaged with α-synuclein siRNA integrated in the pre-miR-451 backbone efficiently deliver siRNA to human neuron-like cells 79

1.24 Small EVs packaged with α-synuclein siRNA integrated in the pre-miR-451 backbone cross an *in vitro* human BBB model and reduce α-synuclein mRNA levels in neuron-like cells 87

1.25 *In vivo* biodistribution of small EVs in mice 97

DISCUSSION.. 104

CONCLUSION & FUTURE DIRECTION 119

REFERENCE 120

LIST OF TABLES

Table 1. Current *in vitro* BBB models. **17**
Table 2. Transfected silencing RNA (siRNA) sequences targeting human α-synuclein obtained from Alnylam Pharmaceuticals Patent. **55**
Table 3. Transfected Silencer® Select silencing RNA (siRNA) sequences obtained from ThermoFisher.. **55**
Table 4. α-synuclein silencing RNA sequences constructed using specific forward and reverse oligos for integration into modified pUC19 construct.. **58**
Table 5. Primer sets for RT-qPCR. **64**
Table 6. Antibodies used for Western Blot. **66**

LIST OF FIGURES

Figure 1. The structural diagram of the cellular components of the NVU and BBB junctions at the brain capillary **4**

Figure 2. The structural diagram of the different transport routes across the BBB. **9**

Figure 3. Biogenesis, general composition, and uptake of extracellular vesicle. **28**

Figure 4. Schematic of the silencing RNAs (siRNAs) transfection with Lipofectamine RNAiMAX method. **56**

Figure 5. Schematic of the two small EVs isolation methods: differential ultracentrifugation (UC), and tangential flow filtration (TFF). **61**

Figure 6. Schematic of the direct small EVs treatment of differentiated neuron-like cells. **69**

Figure 7. Methodology for *in vivo* biodistribution of CF770-labeled small EVs from Immortalized human brain microvascular endothelial cells after a single bolus administration (IV and ICD) in mice. **72**

Figure 8. Reprogramming the pre-miR-451 backbone with siRNAs. **76**

Figure 9. Characterization of small EVs. **77**

Figure 10. α-synuclein Knockdown measured by RT-qPCR and Western Blot in HEK293T cells. **78**

Figure 11. Reprogramming the pre-miR-451 hairpin structure with α-synuclein siRNA. **83**

Figure 12. Small EVs packaged with α-synuclein siRNA integrated in the pre-miR-451 backbone efficiently deliver siRNA to human neuron-like cell line. **85**

Figure 13. Packing efficiency of small EVs α-synuclein siRNA reprogrammed into pre-miR-451 hairpin structure. **86**

Figure 14. α-synuclein knockdown efficiency and uptake in the *in vitro* human BBB model using α-synuclein siRNA packaged small EVs. **95**

Figure 15. Small EVs packaged with α-synuclein siRNA integrated in the pre-miR-451 backbone efficiently deliver siRNA to neuron-like cells in the *in vitro* human iPSC BBB model. **96**

Figure 16. Biodistribution of CFF70-labeled small EVs from human immortalized cerebral endothelial after a single bolus IV injection in CD-1 mice. **102**

Figure 17. Biodistribution of CFF70-labeled small EVs from human immortalized cerebral endothelial after a single bolus ICD injection in CD-1 mice. **104**
Figure 18. Proposed transport mechanism of hCMEC/D3-derived small EVs across the *in vitro* iPSCs BBB Transwell model. **116**

LIST OF ABBREVIATIONS

AAV9: Adeno-associated virus serotype 9
AD: Alzheimer's disease
AF-iPSC(s): Amniotic fluid-derived induced pluripotent stem cell(s)
Ago: Argonaute
AJ(s): Adhesion junction(s)
AMT: Adsorptive-mediated transcytosis
ApoBDs: Apoptotic bodies
ASO(s): Antisense oligonucleotide(s)
Aβ1-40: Amyloid β1–40 peptide
BBB-on-a-chip: Microfluidic organ-on-a-chip blood-brain barrier model
BBB: Blood-brain barrier
BEC(s): Brain endothelial cell(s)
bp: Base Pair
CBF: Cerebral blood flow
cc-siRNAs: Cholesterol-conjugated small interfering RNAs
CCP: Clathrin-coated pits
CNS: Central nervous system
C_q: Quantitation cycles
CSF: Cerebrospinal fluid
CX: Connexin
DA: Dopaminergic
DIV-BBB: Dynamic *in vitro* BBB model
DPC: Dynamic polyconjugates
EGF: Epidermal growth factor
EV(s): Extracellular vesicle(s)
FABP: Fatty acid binding proteins
FUS: Focused ultrasound
GalNAc: N-acetylgalactosamine
GBA: Glucocerebrosidase
GFP: Green fluorescent protein
GLUT-1: Glucose transporter 1
GWAS: Genome-wide association study
hCMEC/D3: Human immortalized cerebral microvascular endothelial cell transduced with the catalytic subunit of human telomerase (hTERT) and SV40 large T antigen
HEK293T: Human embryonic kidney cells transformed with SV40 large T antigen
HNE: 4-hydroxynonenal
iAstro: Induced astrocyte cells
iBEC: Induced brain endothelial cells
ICV: Intracerebroventricular
ILVs: Intraluminal vesicles
iNeu: Induced neuronal cells
iPSC: Induced pluripotent stem cells
IR: Insulin receptors
ISEV: International Society for Extracellular Vesicles

IV: Intravenous
JAM: Junctional adhesion molecules
L-dopa: Levodopa
Lamp2b: Lysosomal associated membrane protein 2b
LAT: Large neutral amino-acid transporters
LB(s): Lewy bodies
LDLR: Low density lipoprotein receptor
LEPR: Leptin receptor
LN(s): Lewy neurites
LNP(s): Lipid nanoparticle(s)
LPS: Lipopolysaccharide
LRRK2: Leucine-rich repeat kinase 2
miRNA(s): MicroRNA(s)
MISEV: Minimal Information for Studies of Extracellular Vesicles
mL: Milliliter
MRI: Magnetic resonance imagining
mRNA(s): Messenger RNA(s)
MVB(s): Multivesicular bodie(s)
MV(s): Microvesicle(s)
NAC: Non-amyloid component
ncRNA(s): Non-coding RNA(s)
NP(s): Nanoparticle(s)
NRC: National Research Council Canada
nt(s): Nucleotide(s)
NTA: Nanoparticle tracking analysis
NVU: Neurovascular unit
PBS: Phosphate-Buffered Saline
PC(s): Pericyte(s)
PD: Parkinson’s disease
PDMS: Polydimethylsiloxane
PFF(s): Preformed fibril(s)
PLGA: Poly (lactic-co-glycolic acid)
pre-miRNA(s): miRNA precursor(s)
PTM(s): Post-transcriptional modification(s)
qPCR: Quantitative polymerase chain reaction
RBD: Sleep behavior disorder
REM: Rapid eye movement
RISC: RNA-induced silencing complex
RMT: Receptor-mediated transcytosis
RNA: Ribonucleic acid
RT: Reverse transcription or room temperature
RVG: Rabies virus glycoprotein
S129: Serine 129
SEM: Scanning electron microscopy
sEV(s): Small extracellular vesicle(s)
siRNA(s): Silencing or short interfering RNA(s)

SNARE: Sensitive factor attachment protein receptor
SNpc: Substantia nigra pars compacta
TEER: Transendothelial electrical resistance
TFF: Tangential flow filtration
TfR: Transferrin receptor
TJ(s): Tight junction(s)
TSG101: Tumour susceptibility gene 101
TTR: Transthyretin
UC: Ultracentrifugation
VAMP2: Vesicle-associated membrane protein 2
WGA: Wheatgerm agglutinin
WT: Wild-type
α-synuclein: Alpha-synuclein
μBBB: Microfluid 3D Blood-brain barrier
μg: Microgram
μL: Microliter

INTRODUCTION

1.1 Blood-brain barrier

1.1.1 Overview: Structure, function, and regulation of the BBB

The central nervous system (CNS) is primarily composed of the brain and spinal cord. It controls most activities and functions across the entire body[1]. Due to its "central" role in organizing life, most of the life-devitalizing disorders are due to dysfunctions in the CNS[2]. There are several types of CNS disorders which include infections (e.g., encephalitis, meningitis), vascular (e.g., stroke), structural (e.g., traumatic brain injury), functional (e.g., epilepsy), inflammatory (e.g., multiple sclerosis), genetic (e.g., Huntington disease) and neurodegenerative [e.g., Parkinson's disease (PD)][3]. To date, drug delivery to the CNS remains among the major challenges in the field with the main obstacle being the inability of drugs to effectively cross the restrictive vascular structure of the brain, the blood-brain barrier (BBB), in order to reach the CNS[4,5].

The BBB was named early in the twentieth century for its ability to prevent the leakage of substances from the blood into the brain. The most known experimental evidence is from Ehrlich and Goldman. They demonstrated during histological tissue staining experiments that many dyes did not stain the CNS after their peripheral injection suggesting a separation between the CNS and the peripheral circulation[6–8]. Throughout the years, the BBB has emerged as a complex, dynamic, and adaptable barrier that regulates the exchange of molecules (ions, amino acids, or/and cells) and prevents unwanted substances/pathogens in the blood from entering the brain. The basic building blocks of this vascular barrier are the brain endothelial cells (BECs) which form a tightly-sealed monolayer lining the walls of the brain capillaries[9,10]. These BECs are connected by highly electrical resistive tight junctions (TJs, e.g., adhesion molecules, claudins, and occludins), adhesion junctions (AJs, e.g., cadherin-5, vascular endothelial cadherin) and gap junctions (e.g., connexins and pannexins)[11] (

Figure *1*). Interestingly, changes in the expression and distribution of claudin proteins in TJs lead to the formation of discontinuous TJs, which indicate a disconnection between BECs, resulting in BBB breakdown[12]. The dysfunction of the Wnt/β-catenin pathway, which promotes the formation of TJs during BEC development, has also been implicated in discontinuous TJs and BBB breakdown[13]. Moreover, the BECs in the BBB express specific BBB transporters in order to regulate the entry and exit of molecules across the cells, however they lack fenestrations (pores in peripheral endothelial cells that allow quick exchange of molecules between blood and tissues)[4,14]. Due to these TJs, AJs, gap junctions and BECs transporters, the BBB has a very low permeability compared to the peripheral blood vessels. Only molecules with molecular weight less than 500 Da can passively diffuse across the BBB under normal conditions[15,16].

BECs are not the only cells that make up the structure and function of the BBB. There are different cell types including mural cells (pericytes, and smooth muscle cells), glia (astrocytes, microglia, and oligodendrocyte), and neurons which all contribute to the regulation of BBB permeability and overall CNS function. More specifically, BECs maintain close interaction with surrounding cells, specifically with pericytes and astrocytes. The brain capillary pericytes (PCs) are contractile mural cells that are embedded around the BECs in a BEC:PC ratio between 1:1 and 1:3[17,18]. They help maintain BBB integrity, modulate transport signaling factors at the capillary level and, by modulating capillary diameter (with concentrated contraction-stimulated intracellular calcium ion), they can regulate the capillary blood flow[17]. Additionally, these PCs have specific transporters that can modulate the movement of substances between the circulating blood and the brain parenchyma (refers to the functional tissue in the brain)[18,19]. For example, PCs and endothelial cells can have direct contact between one another, which is formed by N-cadherin and the gap junction connexin CX43 hemichannels, allowing for intercellular communication[20–22]. Studies have shown that a reduction in PC coverage can cause a loss of TJs between the BECs, resulting in increased BBB permeability[18,23]. The other primary component of the BBB are astrocytes, which are a star-shaped glial cell in the CNS[24,25]. The unique feature of these cells is their end-feet that wrap around the BECs and basal lamina, linking up the BECs with the other CNS cells, microglia, and neurons[26]. This interaction of astrocyte end-feet with BECs is indispensable in maintaining BBB properties and regulating blood flow in response to neuronal activity[27]. Specifically, astrocytes express important gap junction proteins such as CX30 and CX43[27]. It has been reported that astrocyte-specific CX43 knockout or CX43/CX30 double knockout results in loss of astrocyte end-feet which ultimately leads to a BBB leakage, and leukocyte infiltration[28,29].

The intercellular interactions between the BECs and the other CNS cells are collectively referred to as the neurovascular unit (NVU), a recent concept in the neuroscience field. The NVU plays an important role in the maintenance of a highly selective BBB and in responses to the demands of neuronal stimuli by regulating the cerebral blood flow (CBF)[30]. The cellular components of the NVU is combination of the CNS cells mentioned above (neurons, glia, mural cells, and BECs), basement membrane, and extracellular matrix components[31,32]. These components of the NVU share a tight and complex interaction with each other and due to these interactions, they have been classified as a single functional unit (**Figure *1***). Taken together, the BBB acts as a protective monolayer that shields the brain from non-desirable molecules, and is maintained and regulated by the dynamic, close proximity and highly interactive communication among the cellular components of the NVU at the capillary level.

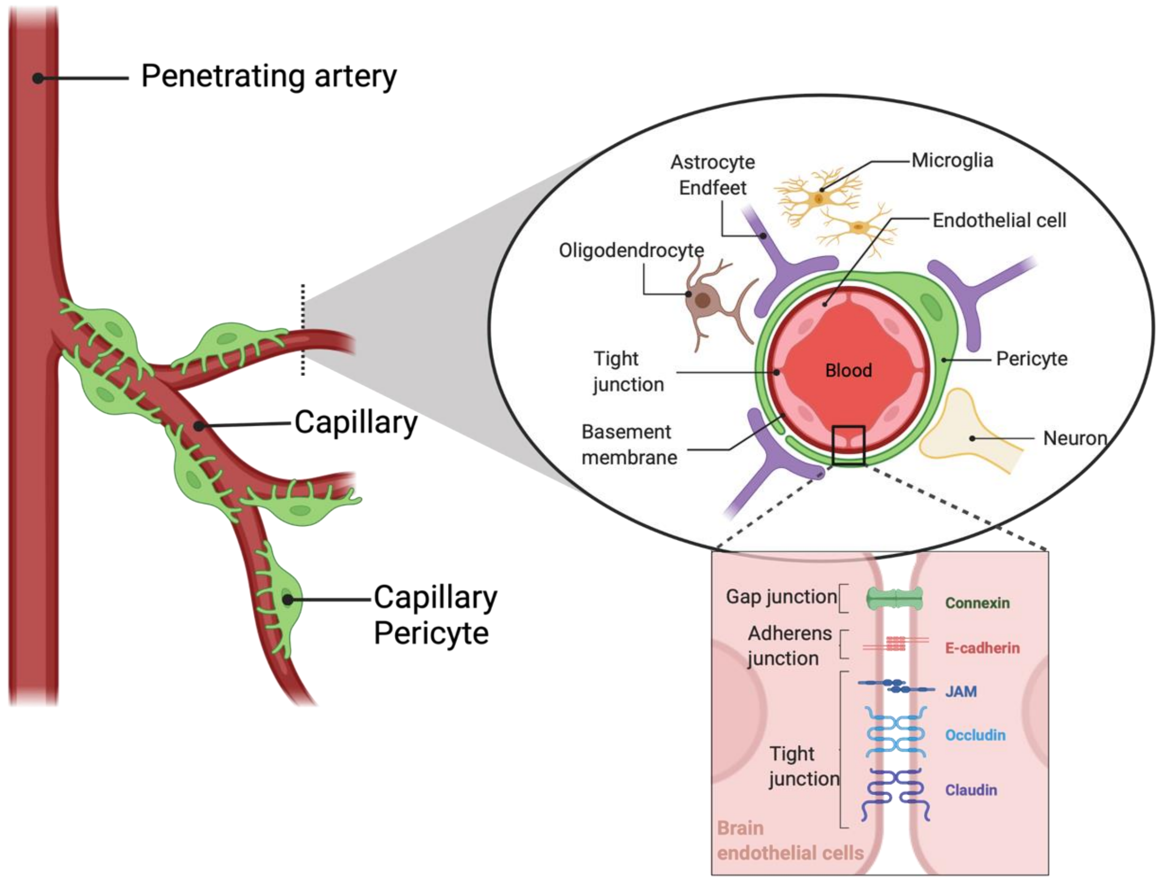

Figure 1. The structural diagram of the cellular components of the NVU and BBB junctions at the brain capillary. At the capillary level, the NVU is composed of mural cells (including endothelial cells, pericytes), glial cells (astrocytes, microglia, and oligodendrocyte), and neurons. The BBB is formed by endothelial cells at the level of the cerebral capillary. These endothelial cells interact with astrocytic end-feet, neurons and pericytes to form a functional BBB. Adjacent endothelial cells are connected by tight junctions, adherens junctions, and gap junctions. The tight junction is mainly composed of claudin, occludin, and junctional adhesion molecules (JAM), the adherens junction is composed of vascular endothelial cadherin, while the gap junction is composed of connexin. BBB, blood-brain barrier. NVU, neurovascular unit. Illustration created using BioRender.

1.1.2 Transport routes across the BBB

As mentioned above, the BBB is a selective membrane that only allows specific molecules to transport across the BECs. The existence of transport systems in capillary BECs reinforce the BBB properties by tightly regulating what enter and exit the brain[15,16]. In general, the transport routes across the BBB can be separated into several mechanisms which are: diffusion transport in the form of paracellular and transcellular transcytosis, carrier-mediated transcytosis, receptor-mediated transcytosis (RMT) and adsorptive-mediated transcytosis (AMT)[1,33]. The different mechanisms of transport across the BBB are illustrated in **Figure 2**.

Firstly, some small molecules can passively cross the BBB through the paracellular (between adjacent BECs) or transcellular (through the cell cytoplasm) diffusion routes[34]. Paracellular diffusion is accomplished by the regulation of TJ permeability in BECs. The driving force for this non-specific transport route is the negative concentration gradient from blood to brain. Therefore, water and some small hydrophilic molecules with molecular weight lower than 500 Da are able to passively diffuse through TJs and cross the BBB. In contrast, transcellular diffusion is accomplished by the distinctive distribution of membrane transporters on both side of the BECs. Only selectively small molecules with desirable lipid solubility and non-ionized compounds can transport to/from the BBB using this route[25]. Similar to paracellular diffusion, the driving force is simply the negative concentration gradient, and this is also a non-specific route. Using this transport, the lipophilic molecules are able to transcellularly diffuse by penetrating the BECs to cross the BBB[35].

Secondly, the BECs have unique expression of influx and efflux transporters on both luminal (blood side) and abluminal (brain side) sides. They allow selective uptake of nutrients, such as glucose, amino acids, and ions from the blood, and restrict the accumulation of xenobiotics and neurotoxic substances in the brain. Therefore, many nutrients that are important for CNS function enter the brain through carrier-mediated transport, which conveys the nutrients from one side of the membrane to the opposite side along the concentration gradient[36]. For example, large neutral amino-acid transporters (LAT) carry amino acids and nucleosides, while glucose molecules use the glucose transporter (GLUT-1)[37,38]. GLUT-1 is a member of the family of sodium-independent glucose transporters and the BECs express it in large densities since glucose is evidently important in maintaining CNS functions.

Transcytosis is a phenomenon that occurs in many different cell types from intestinal cells to endothelial cells in multicellular organisms[39]. At its simplest, it is the transport of a molecule's cargo from one side of a cell to the other within a membrane-bounded transporter(s)[40]. Therefore, it selectively moves its cargo between two different environments while still maintaining the distinct environments of both[40]. There are steps along this transcytosis route which include endocytosis, intracellular vesicular trafficking, and exocytosis to the other side of the cell[39]. The first step, endocytosis, could involve either adsorptive-mediated transcytosis (AMT, charge dependent) or receptor-mediated transcytosis (RMT). Firstly, positively charged molecules (e.g., polymers, cationic lipids, albumin, and nanoparticles) could interact with negatively charged molecules present in the cell membrane of BECs and promote their internalization by absorptive endocytosis[42]. In the luminal surface of the capillary BECs, the specific proteoglycans (e.g., syndecan-1 and glypican) are expressed which trigger the accumulation of negative charges on this luminal membrane side[33]. Therefore, studies have shown that cationic proteins (e.g., histone, wheat germ agglutinin, HIV virus)[41–43] can cross the BBB using these negative charge accumulations through the AMT route. The AMT has a lower affinity compared to RMT; however, it has higher capacity and does not require interaction between receptors and ligands[42]. Therefore, the RMT route is dependent on the interaction between ligand and receptor, thus it has the potential for higher selectively compared to AMT.

The most well-known receptors expressed in the BECs include the transferrin receptor (TfR), the low-density lipoprotein (LDL) receptor related proteins (LRP), and the insulin receptor (IR) which are known to selectively bind and internalize their ligands through RMT[44,45]. Clathrin-mediated transcytosis is a well-known route of RMT and is mediated by around 20 different receptors in the BECs[46,47]. Clathrin is a protein which plays an important role in the formation of coated vesicles that transport molecules to the cytoplasm of a cell[48,49]. Briefly, this process involves[50]: (i) the binding of the natural or targeting ligand to the specific receptor on the luminal surface of BECs; (ii) the endocytosis of the ligand-receptor complexes which are placed in the clathrin-coated pits (CCP) composed of the assembly of clathrin and the adaptor protein AP2; (iii) after CCP-budding and CCP detachment from the plasma membrane, the vesicle leaves behind its clathrin coat and fuses with early sorting endosome; (iv) these are routed across cells (transcellular/transvascular) through complex endosomal sorting pathways (e.g., Rab GTPase); (v) cargo is released by either fusing back to the abluminal surface of the BEC (recycling) or by sorting into multivesicular bodies (MVBs); (vi) in the MVBs, some internalized cargoes are either directly carried intact to the abluminal side of the capillary BECs and released to the abluminal side and/or are directed to the endo-lysosomal pathways which leads to their degradation in lysosomes. These complex endosomal sorting pathways may be dependent on the specific receptor/ligand cargo[50]. Caveolae-mediated transcytosis is another well-known route and is a clathrin-independent transcytosis pathway[51]. Caveolae are 70-100 nm diameter bulb-shaped plasma membrane invaginations and are formed by specific lipid binding proteins (e.g., caveolins, cavins, EHD2). These caveolae vesicles are involved in the formation of ligand-receptor complexes, for example these vesicles promote the advanced glycation end-products (RAGE)-mediated Aβ influx into the brain[52]. After the caveolae have formed the ligand-receptor complexes, it undergoes clathrin-mediated transcytosis, endocytosis, endosomal sorting pathways into the MVBs, and the release of the cargo on the abluminal side of the BEC or degradation by lysosomes.

In short, there are different transport routes to cross the BBB which tightly regulate the passage of molecules into the CNS and impact the way CNS drugs can efficiently deliver to the brain. It is important to note that all these transporters that enhance the transport of nutrients and small molecules to the BBB are potential candidates for increasing drug delivery to the CNS. Some of these transporters will be discussed in a later section.

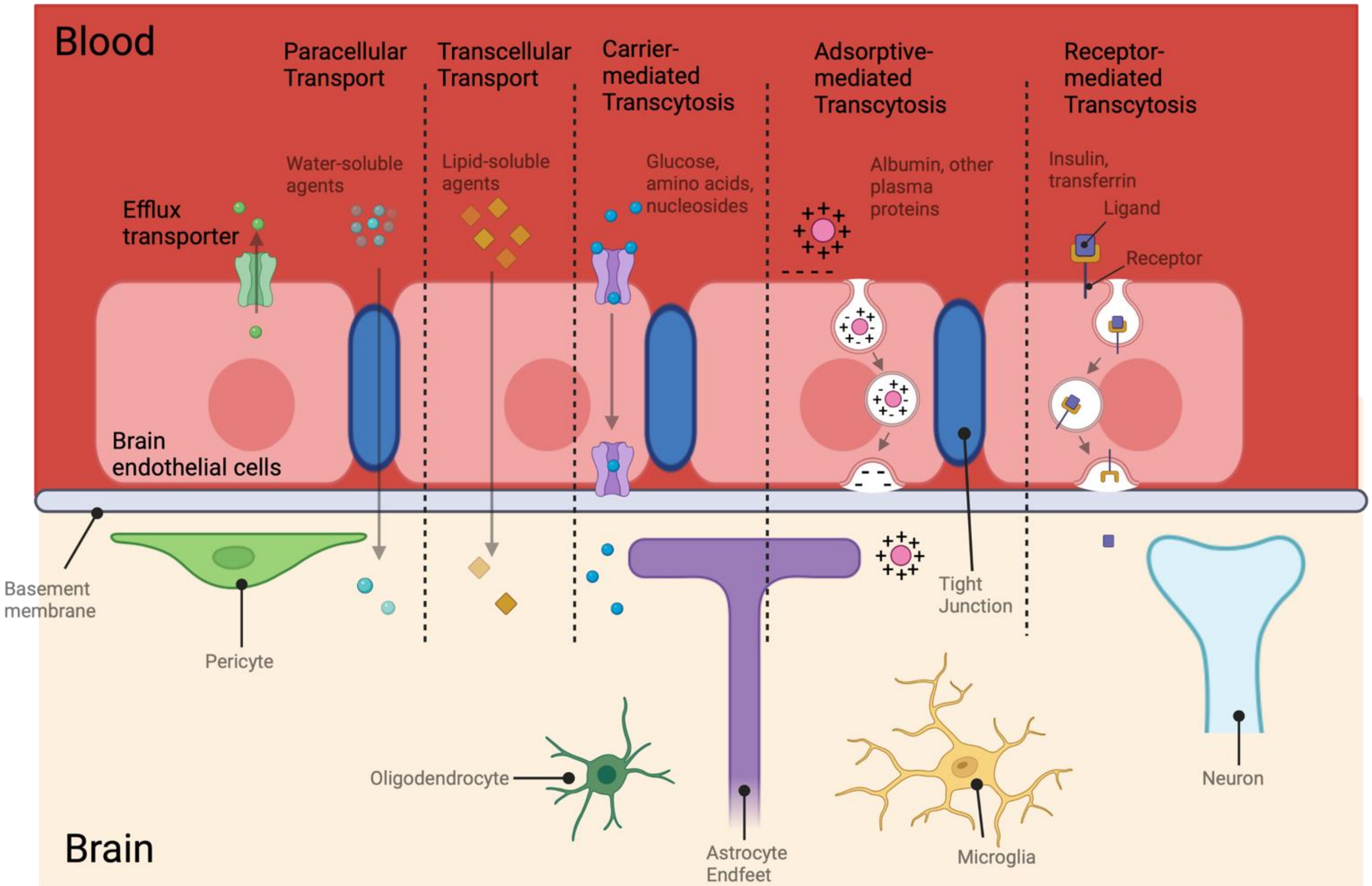

Figure 2. The structural diagram of the different transport routes across the BBB. Molecules can cross the BBB using a variety of transport mechanisms. Hydrophilic-soluble molecules of a low molecular weight (lower than 500 Da) can pass between BEC using paracellular transport. Lipophilic-soluble molecules of a low molecular weight can (lower than 500 Da) diffuse passively through BECs using transcellular transport. Some compounds including glucose and amino acids use transporters to cross the BBB using carrier-mediated transcytosis. Other compounds rely on adsorptive-mediated transcytosis (AMT) or receptor-mediated transcytosis (RMT). BECs, brain endothelial cells. Adapted from[1], Multidisciplinary Digital Publishing Institute. 2021. Illustration created using BioRender.

1.1.3 Modeling the *in vitro* BBB of CNS disorders

The complex physiology of the human brain, the difficulty to reach sufficient drug concentrations within a specific region, and the inadequate animal models of human CNS pathology are the key limitations of CNS drug development. *In vitro* BBB models have been developed to aid the pre-clinical evaluation and selection of potential BBB-penetrating drugs[53]. It is important to note that these *in vitro* models do not entirely reproduce the *in vivo* conditions due to the complex and highly interactive nature between the BBB components of the NVU, meaning there is no perfect *in vitro* BBB model[54]. Therefore, it is key to carefully select the *in vitro* BBB model in line with the requirements of the particular study. There are different types of *in vitro* BBB models that have been established and they are commonly classified into the static 2D and dynamic 3D BBB models. The advantages and disadvantages for each current model are shown in **Table 1**.

Even though *in vivo* animal models can recapitulate the physiological events of the complex human BBB, there are some key differences between the mouse BBB and the human BBB. Studies have shown differences related to the abundance and function of key BBB transporters[55–57]. For example, a recent study performed RNA sequencing on brain microvessels from human and mouse tissue in order to identify mouse-human species differences in gene expression that have relevance to the BBB regulation and drug delivery[58]. They identified genes with species-specific expression in the mouse or human brain vascular transcriptomes including 142 mouse-enriched genes (Vtn, Slco1c1, Slc6a20a, Atp13a5, Slc22a8), and 211 human-enriched genes (SLCO2A1, GIMAP7, and A2M)[58]. Therefore, it is important to understand differences in BBB gene expression between humans and mice for CNS drug development. In addition, Roux et al. have reported the BBB permeabilities of 8 clinical positron emission tomography radioligands with known pharmacokinetic parameters in human brain *in vivo* compared with an *in vitro* iPSC-based human BBB model[59]. They showed a good correlation between *in vitro* and *in vivo* drug brain permeability. As well, they demonstrated interspecies differences in the prediction of drug BBB permeability between rodent BBB model and the iPSC human BBB model[59]. This highlights that human *in vitro* BBB models are more accurate at predicting drug delivery to the *in vivo* CNS than mouse models. Another approach to overcome this limitation has been the development of humanized mouse models in order to express human genes in mice[60]. However, the consequences of expressing human genes may be impacted by complex species-specific gene and protein interactions. Ultimately, the expression of these human genes can potentially limit the full function of newly expressed proteins. Therefore, the approach to overcome all of these limitations has been to develop adequate human *in vitro* BBB models.

1.1.4 Overview of *in vitro* BBB models

These models differ significantly in their composition, but nearly all incorporate three main key components: (i) barrier cells grown on a semipermeable membrane dividing two compartments; the abluminal and luminal sides, (ii) extracellular matrix deposited on a semipermeable surface modeling the basement membrane, (iii) brain microenvironment which can be introduced on the abluminal side of the model system to induce specific BBB phenotypes in BECs. Some models also introduce shear stress forces though liquid mixing or laminar flow[61]. An important measurement of BBB tightness for BBB models is the transendothelial electrical resistance (TEER). It measures the electrical resistance of the tight junctions between BEC monolayers and serves as a reliable method to validate the integrity and permeability of the BBB[62]. The TEER values measured *in vivo* (rats) have been showed to be as high as 5900 Ω cm^2 which is larger than what is achieved by the majority of the currently available *in vitro* BBB models[63]. In order to replicate *in vivo* TEER values in BBB models, BECs have been cocultured with other NVU cells[54], exposed to physiological shear stress[64,65] or treated with various chemicals[66].

In addition, one of the key components in building any *in vitro* BBB model is the type of cells that are used. Most *in vitro* human BBB models have been derived either from primary biopsied brain tissue[67] or immortalized cell lines[68]. Primary cells purified from brain tissue in culture have some benefits including established BBB physical properties (TEER around 150–400 Ω cm^2), which partially demonstrate BEC phenotypes among other BBB functions (i.e., expression of efflux and influx transporters)[54,69,70]. Nevertheless, *in vitro* models using primary cells have limitations including scalability, a rapid loss of BEC phenotype identity (de-differentiation), poor availability of human brain tissues, ethical issues, time-consuming purification with limited yield, and a considerable risk of contamination with other cell types[62,63]. While immortalized BECs are able to overcome scalability and the constant phenotype during culturing issues, they lack sufficient barrier properties, such as discontinuous TJs[32,62]. The most used immortalized BECs cell lines are TY08, HMEC-1 and hCMEC/D3 which have variations in phenotypes and morphology[54]. Despite all of that, these cell lines are often still used for high throughput screening of BBB models due to their high proliferation rate and constant BBB phenotypes[61].

To overcome these weaknesses, *in vitro* BBB models have been developed from human adult stem cells, human endothelial progenitor cells[71], human hematopoietic stem/progenitor cells[72], human embryonic stem cells, and induced pluripotent stem cells (iPSCs)[62,73,74]. Specifically, iPSCs can be reprogrammed from adult somatic cells (i.e., fibroblasts or T-cells) to produce stable, scalable, and self-renewable cells that possess the potential to differentiate into any cell of the body. For example, Lippmann et al. have developed a coculture BBB model with iPSC-derived endothelial cells and neuronal progenitor cells in combination with chemical treatment in order to increase BBB formation[66]. In this model, they demonstrated that retinoic acid (RA) treatment can increase the TEER values up to 4000 Ω cm^2 and maintain it higher than 2000 Ω cm^2 for 4 days. Therefore, these iPSC BBB models acquire many BBB properties including high TEER values, the expression of specific BEC transporters, and efficient transcytosis[63].

1.1.4.1 2D models: BEC monolayers and BBB *in vitro* transwell coculture system

There are two commonly known static BBB models: BEC monolayers and co-culture transwell systems. Currently, BEC monolayers are widely used and are the simplest BBB *in vitro* model. These models are assembled in a transwell system, where BECs are seeded on the upper chamber membrane (luminal side) whereas the bottom chamber (abluminal side) usually does not have any cell type. The microporous membrane (0.2-0.4 μm) in these wells permits the traffic of small molecules however it stops the migration of cells between both sides[75]. In order to further mimic the anatomic *in vivo* BBB structure, BECs are cocultured with other NVU cells. The coculture 2D BBB models include the BECs coculture with any one of the following: astrocytes, pericytes, neurons, or microglia while some models include three cells (e.g., BEC-astrocyte-pericyte) in the transwell system. Additionally, these coculture models are based on the ability of BEC to interact with other cells of the NVU to increase the expression of transporters, TJs in BECs and to further induce BBB properties and phenotypes[54].

Although these models lack the microenvironment and cell-cell communications and other important physiological factors including shear stress forces, it is still useful for drug transcytosis studies, paracrine signaling, and modelling diseased human BBB. For example, Vatine et al. have generated iPSCs from patients with Monocarboxylate transporter 8 (MCT8) mutations, a specific membrane transporter of thyroid hormone (TH) broadly expressed in the CNS[76]. Since BBB controls TH entry into the brain, iPSC-derived BECs were used to model the disease MCT8-

deficient human BBB. They have demonstrated that TH transport across the BBB is dependent on MCT8, likely driving the decreased concentration of TH transporter observed in MCT8-deficient brains[76]. Therefore, this study provides the first iPSC-based disease models of the human BBB, showing a critical BBB mechanistic insight and a new tool for future CNS drug development. In addition, Mantle et al. have assessed the permeability of four FDA-approved drugs (donepezil, memantine, rivastigmine, and galantamine) across a human iPSC-derived BBB model[77]. Since the mechanism of action for these four drugs requires brain permeability, they were all expected to be CNS-permeable; however, *in vivo* data are not publicly available for all these four Alzheimer's diseases (AD) drugs. Specifically, they found memantine permeability measured *in vitro* (43.0×10^{6} cm/s) is very close to the value of 55×10^{6} cm/s measured *in vivo* in humans[78]. This supports the use of *in vitro* BBB models as screening tools for drug development. These are clear examples in how *in vitro* BBB models can be utilized for proof-of-concept drug testing and clinically relevant models of diseased human BBB.

Many 2D models have been used, however the National Research Council Canada (NRC) has developed a reproducible human BBB model that contains all the principal components of the *in vivo* BBB[62]. This model consists of one type of cell produced from proprietary amniotic fluid-derived induced pluripotent stem cells (AF-iPSCs): brain endothelial cells (iBECs). This human BBB model exhibits the critical components of the BBB, including high barrier integrity measured by TEER and polarized expression of efflux transporters[62]. They showed an average of TEER values of 500 Ω cm^2 (ranging between 300-800 Ω cm^2) without the addition of any chemical treatment or coculture with other NVU cells. As well, this high baseline TEER values translate into a low sucrose permeability (2.8×10^{-5} cm/min) similar to that observed in other human iPSC-derived BBB models (3.4×10^{-5} cm/min)[74] and much lower than that observed in hCMEC/D3

(1.65×10^{-3} cm/min)[68]. Importantly, like the *in vivo* BBB, it has a functional RMT pathway that transports natural ligands across the BBB through iBECs. At the NRC, this model is routinely deployed for evaluating the BBB-crossing of biological drugs (mainly antibody therapeutics) by many small- and medium-sized enterprises. The iBEC are used to assemble an *in vitro* BBB model in a transwell system, where iBECs are seeded on the upper chamber (luminal side) and neurons or astrocytes on the bottom chamber (abluminal side) of the transwell[62]. In this master's project, this *in vitro* iPSC human BBB model will be utilized, and its implications will be further discussed.

1.1.4.2 3D models: dynamic *in vitro* model, microfluid model, and BBB on-a-chip

During physiological conditions in the brain, steady blood flow generates shear stress resulting in the regulation of the BBB microenvironment, transport, differentiation of BECs, TJ protein expression, and further maintenance of the barrier function[64]. For example, it has been shown that the shear stress generated by blood flow increases ZO-1 expression in BEC cells, ultimately reducing BBB permeability[79]. Therefore, dynamic 3D models have been developed incorporating shear stress by using artificial microvessels. The dynamic 3D platforms that have been modified to increase the resemblance of the BBB microenvironment are broadly categorized into three groups: dynamic *in vitro* BBB model (DIV-BBB), microfluidic BBB, and BBB on-a-chip. Firstly, the DIV-BBB model incorporates the shear stress and various NVU cells using a microporous hollow fiber. In this model, BECs and specific NVU cell (i.e., astrocytes and/or pericytes) are cultured on the inner (luminal) and outer (abluminal) sides of the artificial capillaries (microporous fibronectin-coated surface of hollow fiber made up polypropylene), respectively[64,32]. The shear stress force is produced by pushing the culture media into the system using a speed pump (5–23 dyne/cm^2) mimicking physical fluidic flow in capillaries and maintaining a physiological microenvironment by using a gas-permeable tubing system to interchange O_2 and CO_2[80,81].

Microfluid 3D BBB (μBBB) models have been produced to overcome the limitations of the BBB-DIV platform, which generally are comprised of microporous membrane segments (mainly polydimethylsiloxane (PDMS)-based systems) creating a sandwich-like structure on the chip[82,83]. There are two perpendicular crossing channels (~200 μm tall): (i) the luminal side (2 mm) seeded with BEC and (ii) an abluminal side (5 mm) which is filled with hydrogel and seeded with NVU cells. In order to induce the shear stress and exchange of O_2 and CO_2, the aforementioned speed pumps and gas-permeable tubing system are used. This μBBB model is further improved by utilizing a flow chamber with built-in oxidative-sensitive Ag/AgCl electrodes for TEER measurement[84]. Even though these models have several advantages, there are still limitations such as not being able to directly observe the BEC phenotypes (since they are inside the fiber), the high cost and time-consumption (9-12 days) to achieve a stable TEER value, and the inability to produce large scalable drug transport experiments[82,83].

More recently, a system was developed called bioengineered microfluidic organ-on-a-chip based models (BBB-on-a-chip). These systems typically use crossing, parallel, or X-shaped channels seeding BECs into hydrogels or two PDMS layers that contain electrodes for TEER measurements being separated by a thick polycarbonate membrane (10 μm) with 0.4 μm pores[85,86]. These cell culture channels are transparent layers allowing for clear visualization under microscopy and provide areas for built-in electrodes in order to facilitate TEER measurement. One advantage of using BBB on-a-chip devices is the ability to incorporate fluid flow inducing shear stress with studies showing a PDMS-based system with shear rates up to 12 dyne/cm^2. Subsequently, they can achieve gas exchange through pumping and gas-permeable tubing systems.

Importantly, these models have illustrated the incorporation of patient-derived iPSCs which increase the recapitulation of the complex architecture and physiological microenvironment of the human BBB[87,88]. It has been observed that iBECs do not enlarge or align with the direction of fluid flow in response to shear stress, which is a phenotype unique to *in vivo* BECs of the brain. In addition, these iBECs do not change their morphology but they do respond at the transcriptional level to shear stress. Based on the studies of new iPSC-based BBB-chip technologies, they may be able to provide a better understanding of the human BBB compared to common 2D or 3D cell-based models, due to human-like physiology, and can further be used for drug transcytosis studies, multicellular network studies, and other BBB dysfunction features.

Table 1. Current *in vitro* BBB models. The advantages and disadvantages of the prevalent 2D and 3D BBB models.

BBB models		**Advantages**	**Disadvantages**
2D models (static system)	BEC monolayers	Simplistic model to study drug transport studies or endothelial-based pathology studies, highly scalable, high-throughput screening assays, cellular and molecular assays in BECs	Low TEER (~ 150 Ω cm^2), high paracellular permeability, BECs difficulty adhering to the side of culture dishes, lack of cell-cell interaction in coculture, limited in BEC phenotypes, lack of flow and shear stress induction
	Transwell coculture system	BEC-NVU cell interaction, improved physical property of barrier (higher TEER, lower permeability & better transporter expression), and improved BEC phenotypes due to close coculture cell interaction	Lack of flow and shear stress induction, inability to address all aspects of NVU simultaneously, physical barrier properties limited by different BEC-NVU cells interaction
3D models (dynamic system)	DIV-BBB	Good topographic distribution of cellular BBB components resembling *in vivo* conditions, flow and shear stress induction, improved BBB barrier properties	Thick basal membrane, difficulty assessing cell-cell interaction, limitation in drug transport studies or leukocytes

		and physical phenotypes (high TEER, cell polarization and transporter expression), viable up to several months	transmigration due to artificial microvessel pore sizes
	Microfluid Chips (μBBB)	Replication of *in vivo* flow chamber and shear stress, cell-cell contacts, mimics microvasculature with microfluidic channels, improved physical barriers properties, possibility to build-in multicellular interactions	Limitation in scalability and for cell-cell interaction, expensive and requires specialized manufacture, rigid extracellular matrix
	BBB on-a-chip	Better replication of *in vivo* fluid flow and possibility for built-in multicellular interactions, established from human iPSCs, mimics microchannel size to microvascular structures, more realistic microcirculation environment, real-time monitoring of barrier properties	Exclusion of shear stress in some models, low throughput, difficulty in measuring TEER values and drug transport, rigid extracellular matrix, limitation in reproducing capillary dimensions and recapitulate *in vivo* cell phenotype, expensive media requirements for iPSCs

1.1.5 Application of BBB models in assessing CNS therapies

How are these models beneficial and applicable in assessing CNS therapeutics? All of these models have limitations in replicating the complex BBB, however they are extremely beneficial for the initial stages of novel drug development. At the early pre-clinical stages, a huge number of compounds need to be screened and optimized. As such, the aforementioned *in vitro* BBB models allow individuals to do so. Importantly, selecting a proper *in vitro* model not only allows for accurate data interpretation but also increases the chances for the drug to progress through the clinical phases faster. As well, these models can be used to evaluate/predict safety and to decrease brain neurotoxicity, immune responses, and brain edema[60]. Therefore, preclinical evaluation of

CNS therapies requires reliable, scalable, and reproducible human BBB models that can recapitulate physiological cellular and molecular features of the BBB.

1.1.6 Methods to delivery drugs to the CNS

The BBB is the main "gatekeeper" and guardian barrier of the CNS. Currently, the biggest challenge is to pass through the BBB and efficiently deliver therapeutic to the brain. Therefore, several strategies have been developed to enhance the delivery of therapeutics to the CNS by breaching the BBB using a variety of techniques. These approaches can be segregated into two groups: invasive, and non-invasive.

1.1.6.1 Invasive approaches

Invasive approaches are physical methods which deliver a drug to the brain using mechanical techniques to breach the BBB. These methods are commonly used in the most severe cases and emergency circumstances, where the drug needs to be directly and locally administered in order to reach a specific brain region[3]. These approaches include intra-cerebral administration (directly into brain vasculature), intraventricular or intrathecal administration [direct delivery in the cerebrospinal fluid (CSF)][89]. With this approach, the administration site needs to be very precise in order to observe an effect, since the distribution of the drug into other brain regions is not effective by simple diffusion[90]. For example, it has been reported that direct injection to the cerebral ventricle of adeno-associated virus serotype 9 (AAV9) encoding a human intracellular cholesterol transporter 1 gene (NCP1) shows an improvement in lifespan, locomotor function and disease pathology in a mouse model of NPC[91]. Other examples of this approach are Spinraza[92] and Zolgensma[93], both drugs are used to treat spinal muscular atrophy (SMA). Spinraza is a survival motor neuron-2 (SMN2)-directed anti-sense oligonucleotide (ASO) which is administered intrathecally in pediatric and adult patients[92]. While Zolgensma is an AAV9 vector-based therapy containing a SMN1 transgene and is administered during a long intravenous infusion in infants younger than 2 years old[93]. Clinical trials are ongoing for the use of Zolgensma in adults, however its administration will be an invasive approach using intrathecal injection.

Another invasive approach is placing intracerebroventricular (ICV) devices, which are implanted osmotic pumps (e.g. Ommaya reservoir)[94] or intravenous (IV) catheters, into the brain parenchyma and/or cerebral ventricle. This method of administration occurs over several days or weeks by simple diffusion and therefore the administered drugs have a slow coefficient depending on lipophilicity, molecular weight, polarity, affinity, and the region of administration[3]. It has been reported that ICV infusion of dopamine or dopamine agonists using an implanted catheter in the cerebral ventricle of a rat Parkinson's disease (PD) model was able to increase dopamine levels in the rat CNS[95]. However, this ICV infusion was complicated due to pump intolerance and the constant disconnection of the pump from the catheter, making it difficult to use this method within a clinical setting[95]. Lastly, the BBB permeability can be physically disturbed by disrupting the connections between BECs and TJs resulting in leakage between cells. This can be obtained by hyperosmotic shock (osmotic disruption in BECs causing BECs to shrink)[95] or magnetic resonance imaging (MRI)-guided focused ultrasound[96]. Even though the BBB disruption opens the door for drugs to enter the CNS, it also increases the potential for neurotoxic agents to accumulate and the release of important CNS nutrients. All these methods require an aggressive and physical technique to be performed in order to deliver the CNS therapeutics into a specific brain region.

1.1.6.2 Non-invasive approaches

While the approaches described above have shown effective delivery of drugs directly into the CNS, they are quite aggressive in their approach and are not routinely used. It is also important to take into consideration that most patients with neurodegenerative disorders are elderly and performing these aggressive methods can be more detrimental than helpful. Therefore, treatments against neurodegenerative disorders should optimally be systematically delivered via oral and/or IV routes of administration. In order to increase the drug intake and accumulation in the brain, one approach involves the chemical modification of drugs at their molecular level. The chemical modification approach is performed by either attaching a lipophilic moiety into the drugs, which increases their lipophilicity, or using prodrugs (e.g., ganciclovir)[85] which are able to breach the BBB and must be transformed to an active state for efficiency[97,98]. Even though these molecular changes can increase the capacity of a drug to cross the BBB, some drugs do not tolerate chemical modifications and also these modifications might alter their biological function which ultimately reduces their effectiveness[99] or make them ineffective.

Therefore, an alternative approach is to use molecular Trojan Horses[100]. Molecular Trojan horses are genetically engineered proteins (ligands or antibodies) against endogenous BBB receptors and can be fused to target drugs to trigger their transport into the CNS[100]. As mentioned previously, the initial internalization and potential transport across the BECs could occur via paracellular and transcellular diffusion (non-specific), carrier-mediated transport, adsorptive-mediated transcytosis (AMT) or receptor-mediated transcytosis (RMT)[40]. Since the RMT transport process takes place via a specific receptor, it has the potential for higher selectivity compared to AMT. Therefore, the most studied receptors undergoing RMT are transferrin receptor (TfR)[101,102], lipid transporters [low-density lipoprotein receptor-related proteins 1 and 2 (LRP-1 and -2, low density lipoprotein receptor (LDLR))][103], leptin receptor (LEPR)[104], and insulin receptor (IR)[105]. The NRC has isolated and developed proprietary BBB-transmigrating single-domain antibodies (VHHs or nanobodies), FC5[106] and insulin-like growth factor 1 receptor, for the delivery of therapeutic payloads across the BBB[53]. All of these receptors have been studied as molecular carriers to deliver therapeutic cargoes across the BBB.

TfR is the transporter studied the most and has been reported to be responsible for transporting iron into the brain by binding to the iron-carrying transferrin protein[102,107]. TfR is highly expressed on BECs[108] compared to peripheral endothelial cells[109,110] and has been shown to be internalized by BECs *in vivo* via clathrin-coated vesicles[111]. Drugs can be engineered to target TfR receptors through conjugation to TfR proteins or antibodies (Ab) specific to the TfR receptor of any species. Several studies have utilized this approach in delivering drugs to the brain, including vasoactive intestinal peptide (VIP)[112], epidermal growth factor (EGF)[113], amyloid β1–40 peptide (Aβ1-40)[114], and β-galactosidase[115]. Specifically, there are two recent studies from JCR Pharmaceuticals[116] and Denali Therapeutics[117] that describe a novel platform capable of trafficking protein therapeutics to the brain through binding to TfR. In Denali Therapeutics study, Kariolis et al. showed the development of a novel BBB transport vehicle that exploits receptor-mediated transcytosis (RMT) by TfR[117]. The authors fused the TfR-binding Fc fragment to β-secretase 1 (BACE1) to produce an antibody transport vehicle carrying anti-BACE1 target. They showed in cynomolgus monkeys that this antibody transport vehicle carrying anti-BACE1 treatment reduces Aβ-40 levels in the cerebrospinal fluid and in various brain regions[117]. This study suggests that this TfR antibody transport vehicle can successfully cross the BBB in this species and can produce therapeutic effects. The BBB selectivity for the TfR has been of special interest since its expression is limited to the endothelial cells of the brain as opposed to peripheral endothelial cells[109,110]. However, it has also been reported the presence of high blood levels of TfR which increases targeting competition with the endogenous ligand[118]. Therefore, there are still challenges associated with using anti-TfR antibodies to deliver drugs to the brain via RMT including specificity to the brain tissue, potential lysosomal degradation[119], and low drug transport into the brain parenchyma[118].

Similarly, studies have shown that using a peptide derived from the rabies virus glycoprotein (RVG) can also facilitate systemic delivery of therapeutics to the brain in a non-invasive manner[120,121]. RVG is a cell penetrating peptide that can pass through cell membranes and facilitate the cellular entry of proteins, macromolecules and drugs[122,123]. Therefore, RVG peptide has been shown to be available to cross the BBB and enter NVU cells, possibly through binding its RVG peptide to the nicotinic acetylcholine receptor without compromising the BBB[124]. Kumar et al. have shown that systematic treatment with RVG bound to an antiviral siRNA provided robust protection against fatal viral encephalitis in mice[122]. However, this delivery system could be improved since they reported that RVG bound siRNA was only partly protected against degradation by serum proteins[124]. Thus, RVG peptide delivery system has limitations including potential lysosomal degradation within BECs, short half-life, and difficulty to reach significant drug concentrations within a specific brain region[125]. For instance, the usage of chemically stabilized siRNA (e.g., GalNAc, will be further discussed in **section 1.3**) or encapsulation of siRNA within nanoparticle can greatly enhance the serum half-life and bioavailability.

Lastly, another approach is to encapsulate drugs in nanosized delivery systems in order to protect and increase their distribution in the brain parenchyma. In recent years, the application of nanotechnology in terms of medicine, nanomedicine, is experiencing rapid growth and consists of natural or synthetic polymers. Nanoparticles (NPs) have been developed to overcome the limitations of free therapeutics and navigate specific types of biological barriers (e.g., BBB) including systemic, cellular, intracellular, and microenvironmental. They can be classified according to the nature of the nanomaterial from which they are prepared[3]. Some of the most common NPs include polymeric-based (e.g., poly (lactic-co-glycolic acid) [PLGA]), lipid-based (e.g., lipid micelles, liposomes, lipid nanocapsules), and biological-based [e.g., extracellular vesicles (EV)]. Therefore, it has been reported that, depending on the nanomaterial of the NPs, passive transport is allowed across the BBB and, subsequently, targeted administration to specific tissues or cells controlling drug delivery. For example, polymeric PLGA is one of the most studied organic nanomaterials and is composed of polymerized glycolic acid and lactic acid monomers[126]. They are biocompatible, biodegradable, and easy to prepare. However, the disadvantages of polymeric NPs involve aggregation, poor drug packing, and potential toxicity associated with the degradation processes and their remaining materials[127,128]. In contrast, liposomes are synthetic lipid-based and consist of a thin file hydration with aqueous solution core surrounded by one or more amphiphilic lipid bilayers[129]. Consequently, they can encapsulate both hydrophilic drugs in the aqueous solution core and hydrophobic therapeutics in their phospholipid bilayers[129,130]. Recent studies have reported their potential to deliver drugs to the brain, across the BBB, by either passive or active transport[131]. Their limitations consist of low stability, short half-life, rapid clearance and sterilization difficulties after isolation[132,133].

Recently LNPs have shown successful commercialization with ONPATTRO for siRNA delivery targeting transthyretin (treatment of hereditary amyloidosis)[134] and BioNTech/Pfizer and Moderna mRNA vaccines against COVID-19[135]. Even though these strategies are being used to encapsulate drugs in nanocarriers like liposomes or polymeric NPs to improve stability, most of these carriers have difficulties in crossing the BBB to reach the CNS and due to their synthetic nature might also be immunogenic[127,128]. EVs are small vesicles (nanometers in size) comprised of an aqueous core surrounded by a lipid bilayer and are natures' own endogenous communication vectors that mediate intercellular transfer of cellular contents to adjacent cells or distant organs[136].

EVs, compared to polymeric and lipid-based NPs, have many additional advantages as drug nano-vehicles since they have lower toxicity and immunogenicity and can naturally cross biological barriers (e.g., BBB)[137]. A recent study has demonstrated that despite having lower packing efficiency of miR-219A-5p (microRNA) compared to PLGA and liposomes, EVs were better at crossing the *in vitro* BBB model[138]. Overall, NLs can be used as nanocarriers to better stabilize and protect drugs during their transport to the CNS and as it will be discussed, EVs have shown greater potential as vehicles, but also as a therapeutic tool, for CNS diseases due to their natural intrinsic properties. The next section will discuss evidence supporting the use of EVs in nanomedicine.

1.2 Extracellular vesicles

1.2.1 Extracellular vesicles biogenesis, general EV composition, and uptake

Extracellular vesicles (EVs) are highly conserved and lipid-bound nanoscale vesicles which are actively secreted by all types of cells into the extracellular space. They can be found in body fluids including plasma, urine, semen, saliva, CSF, amniotic fluid, breast milk, and many other[139]. There are three main subtypes of EVs: apoptotic bodies (ApoBDs), microvesicles (MVs), and small extracellular vesicles (small EVs) (**Figure 3**). Specifically, EVs are differentiated according to their biogenesis, size, internal content, pathways of release from cells, and specific function. ApoBDs or "little sealed sacs" are 500 nm - 2 μm in size and are released by dying cells containing information and substances from these dying cells. MVs bud directly from the plasma membrane and vary in size between 100 - 1,000 nm in diameter. They are distinguishable by their biogenesis, which occurs via the direct outward budding of the plasma membrane.

Small EVs have recently emerged as a novel lipid nanocarrier for the delivery of small molecule drugs, proteins[121] and gene-based biotherapeutics[140].These small EVs are smaller in size, varying between 40-160 nm in diameter (~100 nm on average)[141,142]. They are formed through a process involving double invagination, first of the plasma membrane to form endosomes, and then the invagination of the endosomal membrane to form MVB containing intraluminal vesicles (ILVs) - future small EVs[143]. The first invagination of the plasma membrane leads to the formation of an early sorting endosome or directly merges with a pre-formed early sorting endosome. Second inward invagination in late sorting endosome occurs in the endosomal limiting membranes and this process generates MVB containing ILVs (future small EVs). Lastly, MVB can either fuse with autophagosomes or lysosomes leading to its content degradation. Alternatively, they can fuse with the plasma membrane, through the help of MVB-docking proteins, to release its ILV cargo which are now called small EVs. Small EVs biogenesis is illustrated in **Figure 3**. Heterogeneous populations of small EVs, likely formed by distinct mechanisms, have been identified in recent studies including exomeres[144], migrasomes[145], and Arc-containing EVs[146,147]. This heterogeneity is defined based on their size, cargo, functional properties on recipient cells, and cellular origin. Interestingly, cells may release several of these small EV types simultaneously, generating a complex heterogeneous population of vesicles that could regulate different biological functions.

Small EVs are natures' own endogenous communication vectors that mediate intercellular transfer of cellular contents to adjacent cells or distant organs[148]. This was demonstrated in studies where the transfer of endogenous mRNA and miRNA from donor cells to target cells in a biologically active form resulted in a change of cellular function[149,150].Therefore, small EVs can interact or enter the acceptor cells by different uptake pathways. These distinct entry pathways of intact small EVs may involve receptor-mediated endocytosis[151], clathrin-coated pits[152], lipid raft-mediated uptake[153], phagocytosis[154], caveolae[155], and micropinocytosis[155]. As well, small EV can directly bind and trigger cellular receptors, inducing intracellular signaling, or directly fuse with the plasma membrane to transmit their cargo into the cytoplasm. The cellular journey of internalized small EVs and/or their cargo alone is yet to be fully discovered. Upon its entry into the cell through one of the endocytic pathways, internalized small EVs can fuse with early sorting endosome and get stored in the MVB. Then, their fate inside their recipient cells can be: (i) degradation by lysosomes; (ii) fusing with the MVB membrane to release small EV contents into the cytoplasm, and ultimately making a cellular impact; and/or (iii) trafficking small EVs from the MVB back to the plasma membrane in a recycling mechanism, leading to its release into the extracellular space. The "turnover rate" for the internalization/uptake of small EVs could vary depending on the nature of their cargo, their surface receptors, the recipient cell's panel of available receptors, state of activation, and metabolic status that could all modulate uptake of small EVs.

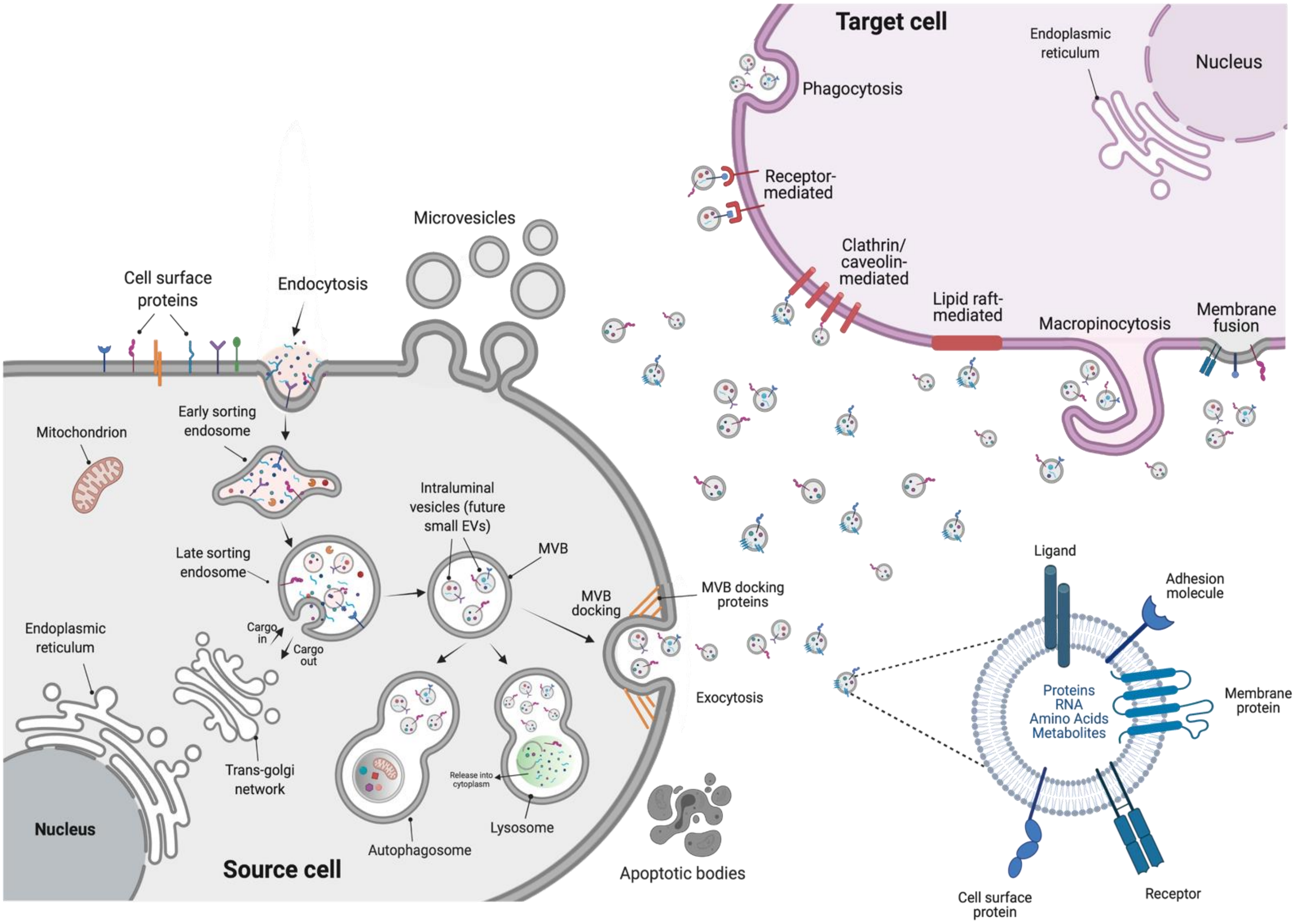

Figure 3. Biogenesis, general composition, and uptake of extracellular vesicle. Small EVs are formed via the endocytic pathway through investigation of the endosomal membrane, forming MVBs that can fuse with the plasma membrane to release small EVs into the extracellular space. MVs are formed from the outward budding and fission of the plasma membrane. ApoBDs are formed from dying cells containing information and substances from these dying cells. Small EVs are generated by almost all cells, and they carry nucleic acids (mRNA, siRNA), proteins, lipids, and metabolites. They are regulators of neighboring and long-distance intercellular communication which impacts function. The specific cargo of small EVs is mostly dependent on their biogenesis, cell source and culture conditions. Different endocytic pathways have been suggested for small EVs: receptor-mediated endocytosis[151], clathrin-coated pits[152], lipid raft-mediated[153], phagocytosis[154], caveolae, and micropinocytosis[155]. Small EVs, small extracellular vesicles. MVBs, multivesicular bodies. MVs, microvesicles. ApoBDs, apoptotic bodies. Illustration created using BioRender.

1.2.2 Extracellular vesicle isolation and characterization

Current isolation methods are not capable of fully separating the various populations of small EVs. Moreover, one major limitation is the lack of standard methods for isolating small EVs with good yield, reproducibility, and population purity. In 2018, the International Society for Extracellular Vesicles (ISEV) proposed comprehensive Minimal Information for Studies of Extracellular Vesicles (MISEV) guidelines which focuses on the terminology, isolation, and characterization of EVs[156]. They urged the scientific community to define EVs by their physical characteristics and isolation methods rather than a presumed pathway of biogenesis. Therefore, in this project we will follow physical characteristics to define EVs as suggested in MISEV 2018 guidelines. Throughout this project, particles < 200 nm detected after differential ultracentrifugation (UC) or Tangential flow filtration (TFF) will be termed “small EVs”.

Until recently, differential ultracentrifugation-based (UC) methods remained the gold standard for isolating small EVs. In UC, small EVs are isolated based on sedimentation using high centrifugal forces in order to remove cell debris or larger microvesicles (low speed spins), followed by high-speed spins in order to pellet small EVs. This technique is limited by a time-consuming protocol, non-scalability, low small EV recovery (low yield), small EV aggregation, possible contaminants which co-isolate (e.g., non-vesicular macromolecule, and aggregated proteins), and disruption of small EV integrity due to high shear forces[157,158]. Other methods have been developed to overcome some challenges associated with UC. Therefore, alternative isolation techniques are based on size, mass, immunoaffinity capture, and small EV precipitation. Tangential flow filtration (TFF) is an ultrafiltration technique that uses membrane filtration and fluid flow for efficient isolation of small EVs with high yield from large volumes. TFF separates small particles according to their molecular size. It is important to note that even these current methods are not able to produce a pure small EV population[159]. The population is a mixture of isolated small EVs and other components of the extracellular space which are co-isolated because of an overlap in their properties (i.e., similar size), which can vary between protocols. This is due to the complexity of the extracellular milieu and biological fluids from which small EVs are enriched.

Many methods have been developed to assess the size, concentration, integrity, and purity of small EVs. The most common techniques include nanoparticle tracking analysis (NTA), western blotting, scanning electron microscopy (SEM), among others. Considering that small EVs originate from a variety of different cell types, they share common structural and functional characteristics, such as tetraspanins (CD9, CD63, CD81), TSG101, and Alix which all can be detected using western blotting. The NTA method allows real-time visualization and analysis resulting in the measurement of concentration and size distribution of isolated EVs[156]. It is also important to note that according to the ISEV, there are no markers that can distinguish different population of EVs from each other because EVs are heterogeneous.

1.2.3 Possible mechanisms for small EVs to cross the BBB

As mentioned above, small EVs have gained relevance due to their prominent function in intercellular communication and their ability to transmit functional changes between neighboring cells and distant ones. Indeed, evidence suggests that small EVs can cross the BBB. Morad et al. showed that intact breast cancer-derived small EVs were able to cross the BBB in two different *in vitro* BBB, 2D (cell monolayer system) and 3D (microfluidic organ-on-a-chip system) models[160]. Even though there is a lack of *in vivo* evidence demonstrating small EVs crossing the BBB by transcytosis, some *in vitro* studies suggest otherwise.

Kusuma et al. have reported that small EVs can penetrate human umbilical vein endothelial cells (HUVEC) in a time and concentration dependent manner since small EVs incubated at 4°C had lower uptake by HUVECs[161]. These findings suggest that small EVs are internalized by endocytosis in an energy dependent manner. Interestingly, when small EVs were treated with protease K and trypsin, their internalization by HUVECs were decreased, indicating that the interaction between surface molecules on small EVs and adaptor molecules on the surface of HUVECs could contribute to the small EVs transport to the cytoplasm of the endothelial cells. In 2016, Chen et al. demonstrated that, under normal conditions, small EVs were internalized by BECs *in vitro* 2D BBB model by either the clathrin or caveolin dependent pathway and then trafficked in BECs via endocytic mechanisms[162]. Using the same model, they also showed that under inflamed conditions (TNF-α activated) mimicking stroke-like pathology, the small EVs cross the BBB by a transcellular route. Interestingly, in the absence of TNF-α, small EVs were not found in the abluminal side of the model, indicating the effects of CNS diseases in the route or efficiency of small EV transport through the BBB. A recent study examined the ability of 10 small EV populations derived from mouse, human, cancerous, and non-cancerous cell lines to cross the *in vivo* BBB in mice[163]. They showed that all small EVs crossed the BBB, but rates varied by up to 10-fold. Also, wheatgerm agglutinin (WGA) regulated the transport of five small EV populations, indicating transport by AMT. Lipopolysaccharide (LPS), an activator of the innate immune system, also increased uptake independent of BBB disruption for six small EV populations. They concluded that the uptake rate response, linear vs. non-linear, to either LPS or WGA are not predicted by the source of origin or the small EVs derived from cancerous/ noncancerous cell line. This data indicated that small EVs were transported across the BBB nearly universally, however the mechanisms of uptake are diverse suggesting that the different properties of small EVs could influence their brain uptake.

Even though, to date, evidence has suggested that small EVs can cross the BBB, the mechanism that small EV utilize to cross the BBB has yet to be fully elucidated. There are limited number of studies exploring these transport mechanisms and further studies need to be performed to answer basic questions. These questions include: What is the BBB/small EVs interaction(s)? What is the percentage and number of intact small EVs that actually cross the BBB? How many small EVs are degraded by lysosomes in BECs? Can intact small EVs cross the BBB and result in a functional change within NVU cells? In this project, we aim to answer some of these questions by using engineered human embryonic kidney (HEK293T), human immortalized cerebral microvascular endothelial (hCMEC/D3) derived small EVs and testing their transcytosis potential in the *in vitro* iPSC BBB as a model system.

1.2.4 Therapeutic applications for small EVs

As discussed, small EVs have been shown to cross the BBB and have many advantages as vehicles for delivery of biotherapeutics. One advantage is that small EVs are resistant to degradation in blood circulation due to their hydrophilic shell containing anti-phagocytosis CD47 protein which evades phagocytosis by macrophages and monocytes[164,165]. As well, their lipid bilayer protects cargo from degradation. Therefore, small EVs can be packaged with therapeutic cargo including RNA, small molecules, or proteins by either exogenous or endogenous packing methods.

In exogenous packing, small EVs are packed with therapeutics post-isolation using sonication, extrusion, freeze-thaw cycles, electroporation, membrane permeabilization with saponin, or co-incubation[166–168]. In endogenous packing, the packing occurs in the parent cells, before the isolation of small EVs, by transfection or engineering parental cell to express a particular therapeutic of interest[169,170]. For example, small EVs have been used as delivery vehicles for anticancer drugs to the brain[171]. It has been reported that brain endothelial cell lines (bEnd.3 cells) derived from small EVs were packed with doxorubicin by simple coincubation and injected into the cardiac vein of zebrafish embryos containing U87MG tumor cells[171]. These treated embryos showed reduction in tumor cell growth compared to embryos treated with the drug alone or buffer control. Additionally, the surface proteins of small EVs can be modified to increase their biodistribution in the CNS or to target specific cells. This approach was demonstrated in delivering small interfering RNA (siRNAs) against BACE1 to the mouse brain by IV injection of targeted small EVs[120]. BBB targeting was achieved by engineering dendritic cells to express lysosomal associated membrane protein 2b (Lamp2b) fused with RVG, harvesting small EVs, and packing siRNA by electroporation. They showed that systemically injected RVG-siRNA small EVs efficiently crossed the BBB and silenced the mRNA (60%) and protein (62%) levels of BACE1 in neuronal cells, resulting in reduced brain amyloid levels in transgenic mice. This suggests that RVG can improve siRNA delivery to the CNS, but the impact of siRNAs encapsulated in small EVs was not assessed and further studies have shown this impact, which will be discussed in the next section.

1.3 Silencing RNA

Before discussing small EVs as vehicles for delivery of nucleic acids, we will discuss different strategies for the systemic delivery of therapeutic nucleic acids targeting the CNS. Therefore, gene therapy has emerged as a potent therapeutic strategy for the treatment of CNS diseases. One main strategy that can be used is the silencing of the disease-causing gene by RNA interference (RNAi)[172]. Antisense oligonucleotides (ASOs) and siRNA are smaller nucleic acids and are the two most studied strategies for silencing gene expression.

ASOs and siRNA share the fundamental principles of binding-to and degrading complementary mRNA to modulate gene expression[173,174]. siRNAs are double-stranded and mimic endogenous miRNA. miRNA transcripts (pri-miRNA) are cleaved by Drosha to release a hairpin (pre-miRNA) which is exported out of the nucleus. Once in the cytoplasm, most pre-miRNAs are processed by Dicer to form a miRNA duplex of ~21 nucleotide double stranded (ds) RNA, with 3' overhangs and 5' monophosphates[175], which are then loaded into the Argonaute (Ago2) complex. Ago2 plays an important role in the RNA silencing processes, as an essential component of the RNA-induced silencing complex (RISC)[176,177]. Short double-stranded miRNA complexes or therapeutic siRNAs are directly loaded into Ago2 and one of the strands of the RNA derivatives is selectively removed (passenger strand). This mature miRNA or siRNA (guide strand) guides the Ago2 complex to a complementary mRNA sequence, which promotes the binding and cleavage of the mRNA at a specific site inducing its rapid degradation and interfering with the translation of this target protein. In contrast to siRNA which acts in the cytoplasm, miRNA requires transport into the nucleus, an additional barrier to RNAi delivery. Moreover, ASOs are single-stranded oligonucleotides and must be chemically modified to be active inside cells[178]. Compared to siRNA, ASOs require a higher dose due to their lower binding efficiency to RISC[179]. Therefore, siRNA is more suitable for drug efficiency since it does not require genome integration and can be easily synthesized[180].

A big challenge faced by RNAi therapeutics after systemic administration is the circulatory system. Naked RNAi is not feasible due to its short half-life, vulnerability to degradation by serum nucleases[181], low penetration into target cells, rapid renal clearance[178], and proneness to stimulate a host immune response[182,183]. As well, studies have reported that around 300 siRNA copies per cell are necessary to silence an mRNA targeting sequence by 50%[184,185] and around 2,000 siRNA copies per cell in order to achieve 80%[184,186] reduction. Therefore, there are approaches to improve the systemic delivery of RNAi therapeutics: (i) chemical modifications of the ASOs/siRNA structure itself, preserving its molecular nature and functional activity; (ii) encapsulation of ASOs/siRNA into a nanocarrier system.

Firstly, the alterations in the chemical structure are focused on either the backbone (e.g., replacement of non-bridging oxygen with boron, nitrogen or methyl), the sugar group (e.g., 2′-O-methyl (2′-OMe), 2′-fluoro (2′-F), 2′-O-methoxyethyl (2′- MOE) groups), or the nucleobases[187]. To date, chemical modifications predominate ASOs while conjugation and nanocarrier systems have been studied more in-depth for siRNA. This is due to siRNA and ASOs differing in their composition, specifically their strand characteristics. Modifications in siRNA can lead to impaired binding into the RISC complex, ultimately decreasing siRNA function efficacy[188]. Therefore, the preferred candidates, whether approved or in clinical trials, to treat brain diseases are ASOs. There are two United States Food and Drug Administration (FDA)-approved ASOs: (i) Nusinersen (also known as Spinraza) to treat spinal muscular atrophy (SMA) using two chemical modifications in the backbone (phosphorothioate) and sugar units (2′-MOE) of the ASOs targeting Survival of Motor Neuron 2 (SMN2)[92]; (ii) Eteplirsen (also known as Exondys 51) is an ASO with phosphoroimidate morpholino modification at the backbone against Duchenne Muscular Dystrophy[189]. However, Spinraza is still administrated directly to the CSF around the spinal cord by intrathecal injection, an invasive approach, while Exondys 51 is administered via IV infusion.

In terms of siRNA, they can be encapsulated into nanocarriers or conjugated to certain ligands in order to effectively avoid renal clearance and, most importantly, to increase their delivery to desired organs or cells. Therefore, LNP nanocarriers, dynamic polyconjugates (DPC™), and GalNAc (N-acetylgalactosamine)[190,191] siRNA conjugates have shown efficient siRNA delivery to the liver, specifically the hepatocytes. Furthermore, Alnylam Pharmaceuticals have developed Onpattro (Patisiran) which is the first FDA approved therapy based on siRNA using a LNP drug delivery system[134]. In Onpattro, the LNPs are packaged with siRNA harboring two chemical modifications (2'-OMe and 2'F) targeting transthyretin (TTR) mRNA for the treatment of polyneuropathies induced by hereditary transthyretin amyloids. This drug, approved in 2018, acts to inhibit the synthesis of the TTR protein by > 80% in the liver using systemic delivery. The success of Onpattro could rely on the fact that LNPs and siRNA naturally accumulate in the liver, where the target mRNA (TTR) is mostly synthesized.

Despite Patisiran (a lipid-based siRNA therapy) achieving clinical application, Alnylam continue to develop more siRNA therapeutics since the GalNAc-siRNA conjugation delivery strategy seems to be superior in comparison to lipid-based nanocarrier in terms of both potency and safety for liver-targeted delivery. Moreover, the newly FDA-approved GIVLAARI™ (Givosiran) from Alnylam for the treatment of adults with acute hepatic porphyria (AHP) is the second siRNA (targeting aminolevulinic acid synthase 1, ALAS1) therapeutic, but first worldwide GalNAc-based siRNA conjugation design[192,193]. GalNAc is a ligand of the asialoglycoprotein receptor (ASGPR) which is an endocytic receptor that is highly and specifically expressed in hepatocyte membranes (~500,000 copies/cell) in the liver[194]. ASGPR- and clathrin-mediated endocytosis can efficiently transport galactose-derived ligands, present in GalNAc, from the cell surface to the cytoplasm within 15 minutes. It allows for subcutaneous injection once every month dosing at significantly lower dosages, compared to Patisiran (80 minute IV infusion once every 3 weeks). Therefore, many GalNAc-conjugated siRNA therapeutics with sophisticated chemical modifications are undergoing clinical studies by different researchers groups including Arrowhead (targeting alpha-1 antitrypsin deficiency), Dicerna (targeting lactate dehydrogenase A), and

Arbutus Biopharma (targeting Hepatitis B)[195]. Most of these studies are for hepatic delivery of siRNA, thus limitation of LNPs and GalNAc-siRNA as therapeutics in treating CNS diseases is that their key protein is not synthesized in the liver. Studies have shown that LNP delivery vehicles are able to transfer approximately 0.05% to 1% of their contained siRNA to the cytoplasm of cells[184,186,196]. For all these reasons, high siRNA doses and effective delivery vehicles are required to achieve therapeutic doses that will properly silence a gene. This high siRNA dose can lead to toxicity and stimulate an immune response, which is the major reason why multiple clinical trials of silencing RNAs have been halted[197,198].

Therefore, a major challenge in this field is the development of a safe and efficient vehicle to deliver siRNA therapy to other organs, in particular to brain. As elucidated above, small EVs seem to be able to achieve delivery of RNA to organs other than the liver[33,120,121] and are able to deliver 10 times more efficiently than commercially available lipid nanoparticles[199]. Hence, small EVs can be safer and more efficient nanocarriers of siRNAs if siRNAs can be packaged inside them.

1.3.1 Small EV as a vehicle for delivery of nucleic acids

Small EVs can also be utilized to deliver therapeutic nucleic acids to the CNS. Despite the tremendous amount of excitement for the development of small EV-based therapeutics, their clinical development is hampered by the lack of reliable methods for packing therapeutics within them. Current methods involve packing small EVs with therapeutics after their isolation from parental cells. The most common packing strategies include (i) passive incubation with isolated small EVs or (ii) active packing with transfection and electroporation. As discussed earlier, Alvarez-Erviti et al. were the first ones who encapsulated siRNA into small EVs to treat CNS disorders[120]. They packed BACE1 siRNA by electroporation in RVG-small EVs isolated from dendritic cells and their results supported the ability of small EVs to cross the BBB and deliver cargo to neurons in mice. Copper et al. also used electroporation to encapsulate α-synuclein siRNA into small EVs isolated from murine dendritic cells and showed that α-synuclein siRNA-EVs were able to decrease α-synuclein mRNA expression in the brains of transgenic mice[121]. α-Synuclein aggregates are found in Lewy bodies (LBs), which is a characteristic of PD, and their implications will be discussed in **section 1.4.3**. While these studies suggested that small EVs could be packed with siRNA by electroporation and injected intravenously to silence key genes in the brain[200], subsequent research reported that <0.1% of siRNA was actually associated with small EVs and siRNAs were not being inside small EVs, but attached to the small EVs surface, resulting in the observed effects likely being due to extremely high doses of free siRNA[121]. Similarly, cholesterol-conjugated small interfering RNAs (cc-siRNAs) can attach siRNA to the outside surface of the small EVs and, as a result, suffer from poor delivery[201]. Although there exists preclinical proof-of-concept for siRNA-mediated silencing of CNS genes, many hurdles remain in the translation of these strategies to the clinic.

Sequentially, small EVs are produced as heterogeneous populations and are packaged with a highly selective range of RNA cargoes from their cell of origin[202]. It has been challenging to fully characterize these RNA cargoes due to their complexity, low concentration within small EVs, small size, and the overall heterogeneity of small EVs. There have been studies reporting different types of RNAs within small EVs including mRNAs, mature miRNA, and many non-coding RNAs (ncRNAs)[203–205]. Additionally, miRNA precursors (pre-miRNAs) and siRNA have been identified in small EVs[150,206]. Interestingly, miRNAs are infrequently present ranging from 1 copy of specific miRNA per 1 million (10^6) small EVs to one copy per small EV[207]. This is concerning since 300-2,000 copies of siRNA are needed per cell in order to silence a target mRNA. Many miRNAs including precursors miR-16, miR451, and miR-134 have been reported to be present at very low numbers in small EVs (1 copy per 10,000 small EVs to 1 copy per 10)[207,208]. Although, miR451 has shown a low copy number in small EVs, they are 500-10,000 fold enriched in small EVs compared to its levels in cells of many types[199]. Precursor miR-451 (pre-miR-451) is the only known miRNA whose biogenesis bypasses the Dicer protein[209]. This is due to its unique stem loop that is too short (42 nt long) to be bound and cleaved by the Dicer protein, hence follows a unique Dicer-independent pathway (**Figure *8*A**). Instead of binding to Dicer, pre-miR-451 binds directly to Ago2 which cleaves one strand of the hairpin after which exonucleases remove the tail of the pre-miRNA to form the mature miR-451.

A recent study from the Gibbings' lab has shown that cells can be genetically engineered to produce customizable small EVs packaged with siRNA against any protein by integrating the siRNA sequence into the pre-miR-451 structure[210,211]. Reshke et al., have demonstrated that any siRNA sequence inserted in this RNA backbone would usually be enriched 100 - 1000-fold in small EVs compared to its expression from another pre-miRNA backbone[199]. As well, they have shown that reprogramming the pre-miR-451 hairpin structure with siRNA enriches them 1000-fold in small EVs. These small EVs can silence their target mRNAs in primary mouse motor neurons *in vitro* and in neurons *in vivo* after direct IV injection into the brain. As a result, this project will be utilizing this cell's endogenous RNA sorting machinery (pre-miR-451 backbone) to pack siRNA against a specific target into small EVs and test their ability to cross the BBB using the iPSC-derived *in vitro* BBB model discussed previously. The specific target of siRNA will be discussed in the next section.

1.4 Parkinson's disease

As mentioned above, this project will be using small EVs containing specific siRNA integrated in the pre-miR-451 backbone to selectively induce the downregulation of a target gene expression using the iPSCs *in vitro* BBB model. Here the specific siRNA will be against α-synuclein, and its dysfunction/aggregation has been strongly implicated in the pathogenesis of Parkinson's disease (PD).

1.4.1 Parkinson's disease overview: pathology, risk factors, clinical and non-clinical features

PD, with its evolving layers of complexity, is caused by the progressive death of dopaminergic (DA) neurons in the *Substantia Nigra pars compacta* (SNpc), ultimately leading to motor and non-motor symptoms[212]. Additionally, its neuropathological hallmark is the accumulation of α-synuclein (alpha-synuclein) protein that results in the formation of cytoplasmic inclusions, known as LB and Lewy neurites (LN)[213]. LBs are round and dense cytoplasmic depositions of amyloid-like aggregates where the major component is the accumulation of misfolded α-synuclein, a protein predominantly expressed in the brain[214]. While LBs are primarily composed of this protein they also contain other proteins such as ubiquitin, tau, parkin, lipid content, heat shock proteins, cytoskeletal proteins (i.e., neurofilaments, tubulin), proteasomal, lysosomal components, among others[215]. A hundred years has passed since Trétiakoff first described neuropathological changes within the SNpc of PD patients[215]. He reported a substantial loss of the darkly pigmented areas in the SNpc resulting from the cell death of SNpc neurons, which contain the neuromelanin pigment, as well as the presence of cytoplasmic inclusion LBs and LNs[216,217]. Microscopically, the pathological hallmark of PD is the presence of both the loss of dark pigmentation within the SNpc and the presence of abnormal cytoplasmic deposits or LBs within DA neuronal cell bodies.

Moreover, PD is the second most common age-related disease after Alzheimer's disease (AD), with prevalence and incidence exponentially increasing with age[218]. The median age of onset is 60 years and in fact, aging is considered the single most important risk factor for PD[219,220]. Even though PD impacts both sexes, the frequency is higher in men (around 1.4 times) than women[2,214,221]. Most patients with PD are classified as idiopathic cases (e.g., arising spontaneously); thereby the etiology of this multifactorial disease remains mostly unknown[214]. Subsequently, the relevant causes and modifying risk factors of PD are a complicated interplay of both environmental/lifestyle and genetics. Approximately 90% of PD cases are classified as idiopathic, while only 10% are associated with genetics. A complete assessment of all the potential causative factors that are present in an individual's environment is not possible since an individual's environment is in constant flux. Nonetheless, several environmental factors increase PD risk including pesticide and heavy metal exposure, rural area living, agricultural occupation, traumatic head injury, consumption of dairy products, type 2 diabetes mellitus, a potential history of COVID-19[222–224] (at the present there is only unempirical evidence supporting this notion), and many others[219,220]. Interestingly, there are findings that patients who have undergone vagotomy[225] or appendectomy[226] have a lower risk of developing PD. Ultimately, the risk of developing PD is distinctly multifactorial, and a further understanding of PD's various risk factors and their interplay can uncover new pathogenic mechanisms, identify biomarkers, improve early diagnostics, and individualize treatment.

Beyond the motor symptoms, PD patients develop several non-motor symptoms that can precede the motor symptoms by several years. Importantly, in early stages of the disease, many cases report a major disturbance of non-motor symptoms in comparison to motor ones. Some of these non-motor symptoms includes hyposmia, rapid eye movement (REM) in sleep behavior disorder (RBD), olfactory dysfunction[227], fatigue, depression and constipation[228–230]. However, the diagnosis of PD currently relies on the presence of motor symptoms and the earliest stages can be difficult to recognize due to a long delay (an average of 10 years) between the earliest symptoms and development of clear motor symptoms. The most common motor symptoms which lead to a PD diagnosis include bradykinesia, muscular rigidity, rest tremor, postural, and gait impairment, often appearing as the disease progresses[231,232]. Other non-motor symptoms that appear in mild or late PD stages include cognitive decline and autonomic impairment. Current drugs can only manage PD motor symptoms by increasing dopamine levels or stimulating dopamine receptors, however dopaminergic neuron cell death still continues. Levodopa (L-dopa) is the prime example of a dopamine replacement therapy and remains the "gold standard" treatment for PD[233]. It provides only temporary relief and does not impact non-motor symptoms. Additionally, its chronic use is associated with severe side effects or patients becoming unresponsive[233]. Therefore, the development of new disease-modifying treatments that can slow and ultimately halt disease progression is one of the greatest unmet medical needs for PD.

1.4.2 Genetics of Parkinson's disease

Even though PD is generally an idiopathic disease, ~20% PD cases are genetic. It is important to note that the risk factors of PD in an individual are an interplay between environmental and polygenic factors (one phenotype influenced by more than one gene)[234]. Therefore, the genetic contribution to PD was limited to a 1997 study which first identified familial segregation of the A53T point mutation in the SNCA gene on chromosome 4q21-23 (which encodes the protein α-synuclein identified the following year) with an early-onset autosomal dominant PD phenotype[235]. SNCA was the first gene to be associated with inherited PD and subsequently α-synuclein was identified as a major component of LBs and LNs[213]. Furthermore, duplications or triplications in SNCA gene has also been shown to contribute to some autosomal dominant early-onset and idiopathic PD cases, indicating that over-expression of wild type α-synuclein is sufficient to cause PD pathogenesis[236–238].

Since then, with the advancement of genetic techniques and genome-wide studies (including GWAS), there have been many other causative genes that have been linked to the disease. To date, there are over 20 loci that have been identified as genetic risk factors for PD[239–241], yet with a certain degree of heterogeneity regarding phenotypes (PD only or PD plus other disorders), age-at-onset (early or adult onset), and inheritance association (autosomal dominant or recessive). Yet, mutations which cause PD, despite being rare in frequency, have been unequivocally established and account for the majority of autosomal dominant (e.g., SNCA, LRRK2, VPS35) or autosomal recessive cases of inherited PD (e.g., PRKN, PINK2, DJ-1, ATP12A2, FBXO7)[242]. Additionally, several point mutations in the SNCA gene (A30P, E46K, H50Q, G51D, A53T or A53E) or gene multiplications of the wild type allele has now been reported[237,243–246]. While a greater understanding of genes causing PD has been achieved, our understanding of the mechanism of progressive DA cell loss in the SNpc still remains unclear. Therefore, SNCA is unique since it is the only gene which can cause PD and has a clear link to the Lewy Body pathogenesis of PD.

1.4.3 Alpha-synuclein (α-synuclein)

1.4.3.1 Location and structure of α-synuclein protein

Although SNCA point or multiplication mutations that cause familial PD are rare, the common variations in the SNCA gene have shown the strongest association with susceptibility to PD across populations worldwide as well as at the GWAS level[247]. Therefore, the contributions of SNCA gene have been extensively investigated in PD pathogenesis. Aggregated α-synuclein is the dominant pathology in disorders known as synucleinopathies[248]. α-synuclein is a small 14-kDa protein consisting of 140 amino acids, encoded by the SNCA gene on human chromosome 4. It is abundantly expressed in many brain regions, especially in the neocortex, hippocampus, SNpc, thalamus, and cerebellum, as well as being present at high levels in red blood cells (RBCs) and in small amounts in other tissues including heart and muscle[249,250]. The significance of this different localization has not been fully elucidated.

Human α-synuclein consists of three distinct functional domains: (i) The N-terminal region forms an amphipathic α-helix structure which interacts with lipid membranes. Due to this N-terminal region containing one of the two conserved sequence characteristic for fatty acid binding proteins (FABP)[251], it can also regulate the association of α-synuclein with mitochondrial membranes[252,253]. It has been shown through *in vitro* studies which indicate that the α-helical conformation interacts with lipid membranes, small unilamellar vesicles, and micelles through its repeat motifs due to their negatively charged head groups[254,255]. (ii) The central region, known as the non-amyloid component (NAC), contains highly hydrophobic motifs. It has been reported that several small deletions in this region or even one deletion of few amino acids (A76 and V77) can dramatically impair the ability of α-synuclein to polymerize into its mature form[256]. Moreover, this α-synuclein domain has been hypothesized to be responsible for conformational changes from random coil to β-sheet structure[257,258], which leads to an increased propensity to form cylindrical β-sheets[259], amyloid-β-like fibrils, and protofibrils[260]. Several studies have highlighted that these α-synuclein oligomers and fibrils might be the responsible entities for α-synuclein pathology[261,262], leading to LB formation[263] (more details in next **section 1.4.3.3**). As well, it has been shown that this region of the protein contains a chaperone-binding site which promotes target protein binding as a result of its β-sheet formation[264]. There is evidence that α-synuclein promotes the regulation of sensitive factor attachment protein receptor (SNARE) structure during their assembly/disassembly process through direct interaction of this α-synuclein chaperone-binding site with the SNARE proteins[265]. Thus, the α-synuclein defect can cause neurological problems since its deficiency decreases SNARE complex assembly[265]. (iii) The C-terminal domain contains many negatively charged amino acids and is a target for various post-transcriptional modifications (PTMs), including phosphorylation at Serine 129 (S129). Many studies have shown that the accumulation of phosphorylated α-synuclein at the S129 site in the brain of PD patients (and in animal models) is associated with an increased propensity of both the aggregation of α-synuclein and the development of LBs[266]. Notably, α-synuclein is only phosphorylated in small amounts (around 4%) in healthy brains while abundant accumulation of phosphorylated S129 α-synuclein (around 90%) has been observed in brains with Lewy pathology[267,268]. Phosphorylation of S129 in α-synuclein regulates its binding with lipid membranes and increases its interaction with metal ions, leading to protein aggregation[269,270].

As a result of these domains, the native α-synuclein is an intrinsically disordered protein which means that it lacks a well-defined structure, and its physiological conformation is still controversial. Thus, it has been reported that the physiological conformation of α-synuclein is in a dynamic balance between "natively unfolded" monomeric and oligomeric states[271,272]. Bartels et al. found endogenous α-synuclein isolated from various cell types had several conformational states, mainly as a folded tetrameric α-helical oligomer in all cells[273,274]. They also reported that *in vitro* α-synuclein tetramers are resistant to fibrillization and aggregation while recombinantly expressed monomers are more prone to aggregation into amyloid-like fibrils. Later studies confirmed that native α-synuclein purified from mouse brain formed stable tetramers, however native α-synuclein also formed largely unstructured monomers, which were prone to aggregation, suggesting that native brain α-synuclein in cytoplasm is also monomeric[271]. All of this suggests that α-synuclein can be present as an α-helix structure, in association with phospholipids, or an unfolded conformation in the cytoplasm of the cell. These different conformations depend on the surrounding environment and their binding partners (lipid membranes and/or vesicles). This further suggests that α-synuclein plays specific roles in various cellular locations, depending on its dynamic structure, which leads, in part, to what makes understanding its function difficult.

1.4.3.2 Potential function of α-synuclein

The physiological functions of α-synuclein and its mechanisms of action in normal cells and in PD are still yet to be fully explored. Several immunohistochemical studies have detected high concentration of α-synuclein at the presynaptic terminals within neurons of mammals[275–277] and colocalizing with presynaptic proteins including synapsin 1, synapsin III, and synaptophysin[278]. As mentioned before, the biochemical structure of α-synuclein predicts a function as a molecular chaperone which can be capable of binding to other intracellular proteins[279]. Burre et al. reported that triple-knockout mice lacking (α,β,γ)-synucleins developed age-dependent neurological impairments, decreased SNARE-complex assembly, and premature neuronal death[265]. As well, they demonstrated that α-synuclein acts as a molecular chaperone to support the assembly and disassembly of SNARE-complex by directly binding to a specific SNARE protein, known as synaptobrevin-2/vesicle-associated membrane protein 2 (VAMP2)[265]. It has been also indicated that, *in vitro*, large oligomers of α-synuclein (which are its pathological form, more details below in **section 1.4.3.3**) bind to an N-terminal domain in synaptobrevin-2 protein which inhibits the SNARE assembly, resulting in neurodegeneration[280]. Later studies showed that under normal conditions, α-synuclein can regulate the fusion and clustering of synaptic vesicles[281–283]. Overexpression of α-synuclein in mouse striatum triggers the redistribution of the SNARE proteins (SNAP-25, syntaxin-1 and synpatobrevin-2) leading to impairment in proper vesicle trafficking and recycling[284]. Therefore, according to this evidence, α-synuclein has been implicated in synaptic activity through regulation of vesicle docking, fusion, and neurotransmitter release. As a result, dysfunction of α-synuclein (either by knockout or overexpression conditions) increases the predisposing factor for synaptic dysfunction, and the development of neuropathology in PD and related neurodegenerative disorders.

In addition to these functions, some recent studies have shown that α-synuclein plays other roles including: regulation of blood glucose levels, reduction of apoptosis by suppression of protein kinase C activity in DA neurons[285], regulation of calmodulin activity, prevention of unsaturated fatty acid oxidation by acting as an antioxidant[286], and the inhibition of phospholipase D2[287]. These functions could potentially indicate a more important role for α-synuclein beside its synaptic activity; however, its mode of action still remains controversial (e.g., phospholipase D inhibition, dopamine and serotonin transporters)[287] and more studies need to be performed to fully understand its function.

1.4.3.3 Contribution of α-synuclein in Parkinson's disease pathogenesis

Due to its contribution to PD pathogenesis, α-synuclein has been studied in a variety of PD patients and a variety of animal models including mice, Drosophila, and *Caenorhabditis elegans*. Studies have reported that elevated levels of α-synuclein oligomers were presented in the brains of patients with PD compared to healthy subjects (no PD cases)[288,289]. Other studies, using transgenic mice or flies that over-expressed wild type or point mutation (A30T or A53T) in α-synuclein, have shown movement deficiency and neuronal cytoplasmic inclusions[278,290–292]. Aggregated α-synuclein were present in DA neurons in over-expressed wild type or point mutation (A30T or A53T) in human α-synuclein transgenic nematodes *Caenorhabditis elegans* model[293]. As well, over-expression of wild type human α-synuclein causes energy and metabolism abnormalities (body mass loss, lower food consumption, lower plasmatic levels of insulin and leptin) in Thy1-α-synuclein transgenic mice compared to control ones[294]. These studies illustrate a portion of the evidence supporting the underlying notion that α-synuclein plays a central role in PD pathogenesis.

As mentioned before, α-synuclein has been isolated in several conformational states, however during its pathological misfolding states, monomeric α-synuclein has been shown to acquire a β-sheet-rich amyloid-like structure and self-assembles into metastable oligomers before forming fibril-like structures that are found within LBs[295,296]. This aggregation and accumulation process is not well understood but it leads to the formation of a wide variety of α-synuclein amyloid-like fibrils which are characterized by a cross-β organization[261,262]. Even though the process is still to be fully eluded, the susceptibility of α-synuclein to form fibrils and inclusions can be correlated with several factors. These include point mutations (A53T, E46K and A30P)[297], gene duplication and triplication of the SNCA gene which are sufficient to elevate protein expression[298], unknown environmental factors[299], oxidative stress[300], PTMs[301], and high concentration of metal[302].

1.4.3.4 Evidence for the spreading and seeding capabilities of α-synuclein

Moreover, α-synuclein aggregates have been found in different brain regions of postmortem PD brains depending on the disease stage, indicating a spread through the CNS in a "prion-like" manner propagating from cell-to-cell[303,304]. The exogenous treatment of preformed α-synuclein fibrils (PFFs) to cultured cells recapitulated the self-assembly process of endogenous α-synuclein into amyloid-like fibrils[305]. Similarly, injection of synthetic α-synuclein fibrils into the striatum of transgenic mice can lead to the formation of aggregated α-synuclein, the development of LB pathology, nigrostriatal degeneration, and most importantly, cell-to-cell transmission[306]. This is the first *in vivo* evidence that synthetic α-synuclein PFFs alone was shown to promote the formation and propagation of α-synuclein *in vivo* neuropathology[306]. Recent studies have also injected PFFs into wild type mice and non-human primates which showed similar results by inducing progressive α-synuclein aggregation[307,308]. Peelaerts et al. injected structurally well-defined human α-synuclein strains (such as oligomers, ribbons, and fibrils) into mice brain ultimately observing that distinct α-synuclein strains had different seeding capacities, which result in strain-specific pathology and phenotypes[309]. Other studies using engrafted tissue have also shown direct host-to-graft transmission of α-synuclein *in vivo*[310,311]. This was specifically shown by transplanting mouse DA neurons into the striatum of mice over-expressing human α-synuclein, the transmission of α-synuclein between the host and grafted neurons was demonstrated 6 months after transplantation[310]. Taken together, these studies among others suggest that, when exogenously α-synuclein fibrils were added into cells or an animal model, they were taken up by cells and act as "seeds" to promote the aggregation of endogenous α-synuclein.

The mechanisms in which aggregated α-synuclein propagates cell-to-cell is still not well defined, however there is growing evidence that α-synuclein could be transferred by EVs[281]. Zhang et al. has reported that 4-hydroxynonenal (HNE), a lipid peroxidation product, increases aggregation of endogenous α-synuclein in primary neurons and promotes the secretion of EVs containing oligomeric α-synuclein[281]. This leads to EVs being released from HNE-treated neurons in order to be internalized by neurons and, by harboring their pathogenic α-synuclein in the cytoplasm, results in neuronal degeneration. As well, they performed focal injection of EVs containing α-synuclein into striatum of wild type mice which resulted in the spread of synuclein pathology to connected brain regions. This data suggests an event for late-onset PD where HNE promotes intracellular accumulation and, in turn, the release of EVs containing aggregated α-synuclein species[265]. It is important to note that the potential α-synuclein propagation is still controversial in the field due to the currently gathered data being acquired in experimental animals (primarily rodents) and not humans. Another point of difference is the different rates of α-synuclein progression between PD and prions. PD is not rapidly progressive like prions and, in the contrary neurodegenerative disorders, are generally a slow progressive disorders[312]. Hence, reducing α-synuclein aggregation remains an extremely attractive target for PD therapeutic development due to its ability to aggregate, accumulate, propagate cell-to-cell, seeding propensity in order to increase neuronal toxicity, the presence of LBs, and, ultimately, PD pathogenesis.

1.4.3.5 Therapeutic silencing of alpha-synuclein in PD

There are no disease-modifying therapies targeting the reduction of α-synuclein levels. This reduction of total protein levels can be achieved through different approaches including decreasing its mRNA expression, inhibiting its protein accumulation, interfering with its prion-like spread (by inhibiting neighboring uptake), and increasing its intracellular clearance mechanisms. For example, Alnylam Pharmaceuticals showed encouraging results, which for the first time, demonstrated the suppression of α-synuclein mRNA by 40 - 50% using siRNA against α-synuclein in the SNpc of non-human primates[313]. Indeed, this study, and others, reported that α-synuclein mRNA levels can be reduced in order to improve PD pathology and motor symptoms[314,315]. However, α-synuclein siRNA was continuously infused into the SNpc of squirrel monkeys using stereotactic surgery over a one-month period (invasive delivery) and levels of α-synuclein returned to normal 3 weeks post-infusion. Therefore, questions arise such as "Is it safe to decrease α-synuclein expression?" or "Is it effective to decrease α-synuclein levels?" Caution needs to be used when manipulating the overall α-synuclein expression due to its functional implications in synaptic transmission, its role in maintaining neuronal activity, and its other physiological roles that have not yet been characterized. Thus, a therapy aiming to decrease α-synyclein expression could have a significant impact in endogenous α-synuclein levels. Recent reports have shown that α-synuclein reduction of > 90% in rat and non-human primate SNpc is implicated in nigrostriatal system degeneration[316,317]. As well, it was mentioned previously that α-synuclein knockout mice also lead to the SNARE assembly dysfunction which impacts the overall neuronal survival[284]. Before this approach is considered a viable option for PD patients, it is crucial to determine the appropriate degree of α-synuclein reduction which is safe while still allowing α-synuclein aggregation and pathology to be slowed. The degree to which α-synuclein is reduced is a balancing act between functional levels and pathogenic α-synuclein expression reduction.

HYPOTHESIS AND OBJECTIVES

In this project, we will be manipulating the cell's endogenous RNA sorting machinery (pre-miR-451 backbone) to pack siRNA against α-synuclein into small extracellular vesicles, test their ability to cross the BBB and inhibit α-synuclein in neurons using the iPSC *in vitro* BBB model. Therefore, our objectives are (i) to integrate siRNA against human α-synuclein into the pre-miR-451 backbone, (ii) test delivery efficiency of small EVs packaged with α-synuclein siRNA integrated in the pre-miR-451 backbone in culture, (iii) to assess their ability to cross the *in vitro* human BBB model/test the efficiency of α-synuclein knockdown in neuronal cells, and (iv) to evaluate the biodistribution of small EVs, derived from brain endothelial cells, following systemic delivery in mice.

METHODS

1.5 Cell lines

(1) HEK 293T WT (ATCC)

(2) SH-SY5Y WT (generous gift from the Human Health Therapeutics Team (HHT), National Research Council Canada (NRC), Ottawa, ON, K1A 0R6, Canada)

(3) hCMEC/D3 WT (generous gift from the Human Health Therapeutics (HHT) Team, National Research Council Canada (NRC), Ottawa, ON, K1A 0R6, Canada)[318]

1.6 Cell culture

Human embryonic kidney HEK 293T cells and human neuroblastoma SH-SY5Y cells were cultured in DMEM (Wisent Bioproducts, 081-150) supplemented with 10% heat-inactivated FBS (Wisent Bioproducts, 081-150) and 1% penicillin-streptomycin (Wisent Bioproducts, 450-201-EL). Immortalized human brain microvascular endothelial hCMEC/D3 cells were maintained in EBM-2 basal medium (Lonza, CC-3156) supplemented with 1:1 of each growth-factors (Hydrocortisone 100 μL, hFGF-B 1 mL, VEGF, R3-IGF-1 250 μL, ascorbic Acid 250 μL, hEGF 250 μL, GA-1000 250 μL, and heparin 250 μL) of the EGM-2 SingleQuot Kit (Lonza, CC-4176) and 2% FBS. The culture dishes were coated for 1 h at 37ºC with 0.1 mg/ml rat tail collagen type I (VWR, CACB354236), diluted in 20 mM acetic acid. All cell lines were maintained at 37°C with 5% CO_2 in humidified incubators. Confluent cells were detached with Trypsin/EDTA (0.25%/EDTA 2.21 mM in HBSS) (Wisent Bioproducts, 325-043-EL), neutralized with at least equal volume of culture medium, and centrifuged at 500 xg for 5 minutes (only for hCMEC/D3). The hCMEC/D3 cell pellet was then re-suspended in fresh media for plating or freezing medium for storage. The concentration of cell suspensions was determined using a hemocytometer (Sigma, Z359629 or Thermo Fisher Scientific, 0267110).

1.7 Differentiation of human neuroblastoma SH-SY5Y cells

Human SH-SY5Y neuroblastoma cells were plated in a 24-well plate at a density of 5×10^4 cells per well (~50% confluence) in complete media: DMEM (Wisent Bioproducts, 081-150) supplemented with heat inactivated 10% FBS (Wisent Bioproducts, 081-150) and 1% penicillin-streptomycin (Wisent Bioproducts, 450-201-EL). After 24 h of cell plating, differentiation was induced by lowering the FBS in culture media to 1% without antibiotics and adding 10 µM all trans-retinoic acid (RA) (Sigma-Aldrich Cat.no. R2625) at day 1, 4, 7 and 10. This treatment was replaced every 3 days to replenish RA in culture media. Depending on cell density or level of differentiation required, cells were used on day 8 or day 11.

1.8 Transfection

1.8.1 Transfection of α-synuclein-targeting siRNA

HEK 293T cells were seeded at 5×10^4 cells per well in a 12-well plate. They were grown to 60-80% confluence and transfected with Lipofectamine RNAiMAX (Thermo Fisher Scientific, 13778150) and Opti-MEM (Thermo Fisher Scientific, 31985-070) at a final concentration of 10 µM of α-synuclein siRNA in 1 mL of antibiotic-free DMEM supplemented with 1% heat inactivated FBS. HEK 293T transfected with scrambled siRNA served as control. The manufacturers' recommended protocol for transfection of a well of a 6-well plate was followed (**Figure *4***). Then, 24 h post-transfection culture media was removed, and cells were washed with 1x PBS and were collected by adding 1 mL Trizol Reagent for RNA isolation for RT-qPCR. Alternatively, 48 h post-transfection cells were lysed for protein isolation. For total protein collection, cells were washed twice in cold 1x PBS, scraped, and incubated with lysis buffer [50 mM Tris-HCl (pH 7.4), 75 mM NaCl, 0.5 mM EDTA, 0.5% Triton-X, 1X protease inhibitor cocktail (Sigma Aldrich)] at -80ºC for 10 minutes. Lysates were centrifuged for 5000 xg for 10 minutes and supernatants were stored at -20ºC until further use for Western blotting.

Table 2. Transfected silencing RNA (siRNA) sequences targeting human α-synuclein obtained from Alnylam Pharmaceuticals Patent. (US patent US007595306B2)

siRNAs Names	**Sequence** (5'→ 3')
Sequence #1 (sq1)	5'-CAGUGGCUGAGAAGACCAAdTdT-3'
Sequence #2 (sq2)	5'-UCCUGACAAUGAGGCUUAUdTdT-3'
Sequence #3 (sq3)	5'-CUACGAACCUGAAGCCUAAdTdT-3'

Table 3. Transfected Silencer® Select silencing RNA (siRNA) sequences obtained from ThermoFisher.

siRNA Names	**siRNA ID#**	**Sequence** (5'→ 3')
Sequence #4 (sq4)	S13204	5'-CCAUCUCACUUUAAUAAUAtt-3'
Sequence #5 (sq5)	S13206	5'-AGAGGGUGUUCUCUAUGUAtt-3'

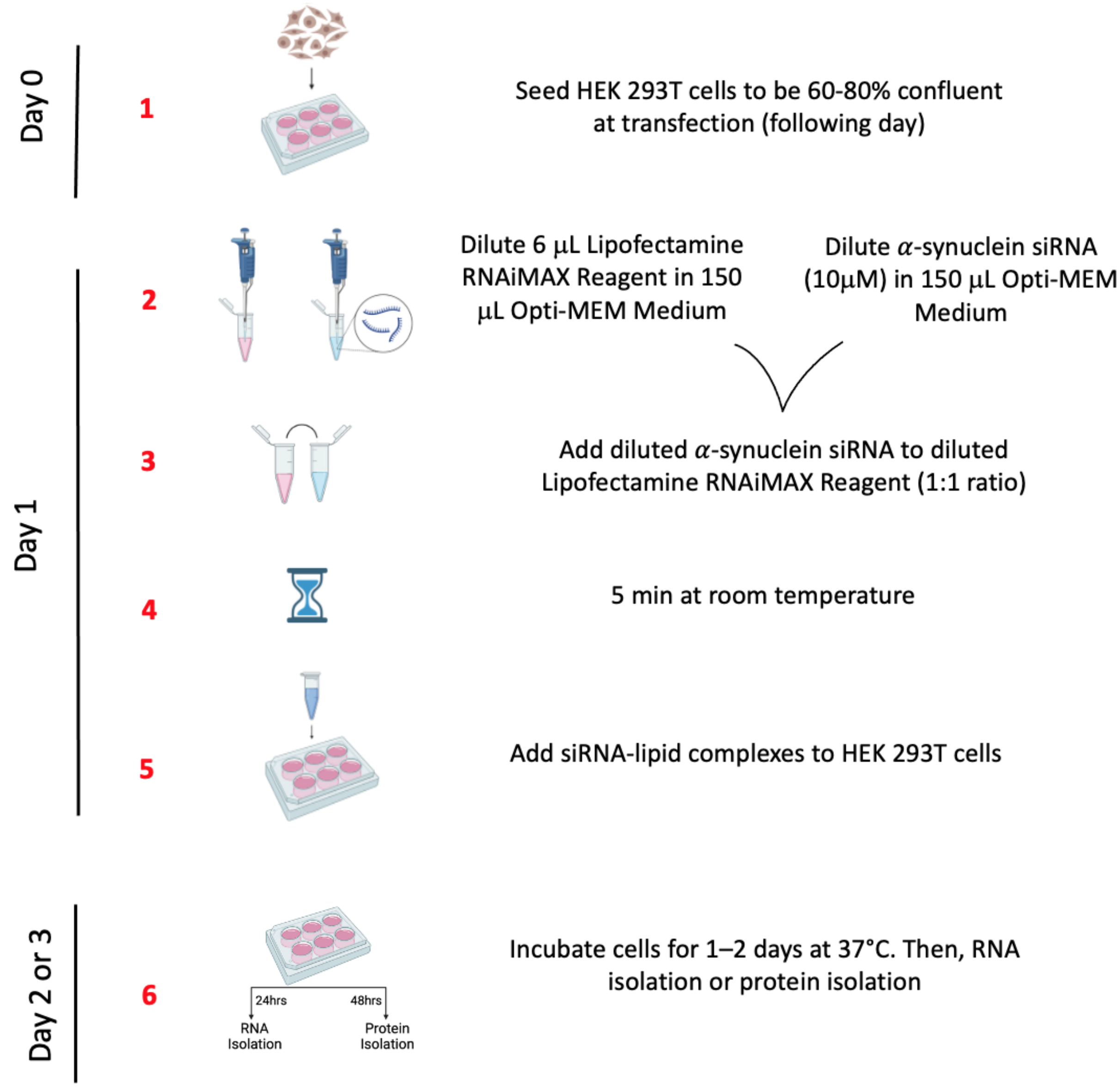

Figure 4. Schematic of the silencing RNAs (siRNAs) transfection with Lipofectamine RNAiMAX method. (Illustration created using BioRender).

1.9 Generation of a stable cell line

Published siRNA sequences to target α-synuclein were adapted and reprogramed into the pre-miR-451 hairpin for packaging into small EVs (US patent 0186591) (**Table 2 and Table 3**). Where published siRNA sequences contained less complementary sequence than the length of the 22 nt mature miR-451, bases complementary to the target were added at the 3' end of the antisense strand. The mature antisense strands were designed as shown in **Table *4***. The specific oligonucleotide sequences were cloned into the modified pUC19 (Puromycin) construct encoding the 5' and 3' regions of pre-miR-451 backbone with BbsI sites flanking an EcoRV site in the middle. These were cloned between the BamHI and NheI sites of pCU19 as a BglII- NheI fragment. These α-synuclein siRNA sequences integrated in pUC19 constructs were verified by forward DNA sequencing at the OHRI StemCore DNA Sequencing Facility. Then, these constructs encoding reprogrammed pre-miR-451 in pUC19 were cloned into a vector allowing production of lentiviral particles. The DNA fragments of each construct were amplified by PCR using Herculase II DNA polymerase (Agilent, catalogue no. 600677) as recommended by the manufacturer and combined into a single vector by Gibson assembly (NEB, catalogue no. E2611S). The resulting vector enabled transduction of cells in cell culture to produce stable cell lines expressing puromycin resistance and the reprogrammed miR-451 construct from a CAG-enhanced CMV promoter. Lentiviral particles produced from transfected HEK293T cells were concentrated by ultracentrifugation and added to HEK 293T cells using standard culture methods. After 3 days, cells were split into media containing puromycin (final concentration 2 μM) to select for transduced cells. Transduction was confirmed by observing the Turbo-GFP fluorescent signals using a ZOE Fluorescent Cell Imager.

Table 4. α-synuclein silencing RNA sequences constructed using specific forward and reverse oligos for integration into modified pUC19 construct.

siRNA	Antisense strand sequence	Forward oligos	Reverse oligos
Sequence #1 (sq1)	UUGGUCUUCUCAGCCACUGUUG	aaggTTGGTCTTCTCAGCCACTGTTGAGTGGCTGAGAAGACCAT	aagaATGGTCTTCTCAGCCACTCAACAGTGGCTGAGAAGACCAA
Sequence #2 (sq2)	AUAAGCCUCAUUGUCAGGAUCC	aaggATAAGCCTCATTGTCAGGATCCCCTGACAATGAGGCTTAA	aagaTTAAGCCTCATTGTCAGGGGATCCTGACAATGAGGCTTAT
Sequence #3 (sq3)	UUAGGCUUCAGGUUCGUAGUCU	aaggTTAGGCTTCAGGTTCGTAGTCTTACGAACCTGAAGCCTAT	aagaATAGGCTTCAGGTTCGTAAGACTACGAACCTGAAGCCTAA
Sequence #4 (sq4)	UAUUAUUAAAGUGAGAUGGGAU	aaggTATTATTAAAGTGAGATGGGATCATCTCACTTTAATAATT	aagaAATTATTAAAGTGAGATGATCCCATCTCACTTTAATAATA
Sequence #5 (sq5)	UACAUAGAGAACACCCUCUUUU	aaggTACATAGAGAACACCCTCTTTTGAGGGTGTTCTCTATGTT	aagaAACATAGAGAACACCCTCAAAAGAGGGTGTTCTCTATGTA

1.10 Preparation of small EV depleted media

Media depleted of small EVs was prepared by adding all the necessary nutrients, 10% heat inactivated FBS (Wisent Bioproducts, 081-150) and 1% penicillin-streptomycin (Wisent Bioproducts, 450-201-EL) to DMEM. Then, approximately 250 mL of complete media were aliquoted into 50 mL tubes and centrifuged at 5000 xg for 30 minutes at 4°C. The supernatant was transferred into ultracentrifuge tubes and centrifuged for 2 h at 100,000 xg at 4°C. Lastly, the supernatant of each ultracentrifuge tube was filtered with a sterile bottle-top vacuum-connected 0.22 µm filter. The small EVs-depleted media was ready to be used and was stored at 4°C.

1.11 Small EV isolation

Cells were grown to 70-80% confluence in DMEM (Wisent Bioproducts, 081-150) supplemented with 10% heat inactivated FBS (Wisent Bioproducts, 081-150) and 1% penicillin-streptomycin (Wisent Bioproducts, 450-201-EL) at 37 °C in a humidified atmosphere of 5% CO_2. DMEM culture media was removed, washed with 1x phosphate buffered saline (PBS) to remove contaminating small EVs originating from the FBS in the culture media; then replaced with small EV-depleted media. Small EVs-depleted media was left on cells overnight (16-24 h is ideal since small EVs release begins to plateau after ~24 h) and was collected the next day. Small EVs were enriched using two methods: differential ultracentrifugation or tangential flow filtration. These two processes can be seen in **Figure 5**.

For differential ultracentrifugation, the first centrifugation steps are at 300 xg for 10 minutes at 4^{o}C to remove contaminating live cells. Then the supernatant was transferred to a new 50 mL tube and centrifuged at 2,000 xg for 10 minutes at 4^{o}C to remove large contaminating dead cells or debris. The supernatant was again transferred into new ultracentrifugation tubes and centrifuged at 10,000 xg (SW-32Ti rotor, Beckman-Coulter Life Sciences) at 4^{o}C for 30 minutes to remove the aggregates of biopolymers, bulky apoptotic bodies, and other structures with their buoyant density higher than the small EVs[319,320]. A final high spin at 28,500 rpm (100,000 xg) (SW-32 Ti Swinging-Bucket rotors, Beckman-Coulter Life Sciences) at 4^{o}C in thick wall polycarbonate ultracentrifuge tubes (Beckman-Coulter Life Sciences, no. 355631) for 2 h to precipitate the small EVs. The pellet of small EVs was vigorously resuspended in 1 mL 1x PBS and re-centrifuged for a wash at 49,000 rpm (100,000 xg) (TLA-100.3 Fixed-Angle Rotor, Beckman-Coulter Life Sciences) at 4^{o}C in new 1.5 mL polypropylene tubes (Beckman-Coulter Life Sciences, no. 357448) for 30 minutes. Ultimately, the re-pelleted small EVs were resuspended in 100 μL 1xPBS and analyzed using Nanoparticle Tracking Analysis (NTA) on a ZetaView PMX-110. NTA is commonly used to determine both the size and relative concentration of microvesicles, which includes small EVs, in the supernatants of small EVs depleted media and/or body fluids after isolation. As described, treatment of the small EVs ensued prior to RNA isolation with 500 μL Trizol reagent (Thermo Fisher Scientific, no. 15596018). It is important to note that numerous protocols for EV isolation differ not only in the number of steps but also in the conditions of differential centrifugation spins. As mentioned above, low speed centrifugation (<10,000 xg) is usually used to remove particles with a higher buoyant density such as cells, cell debris, apoptotic bodies, and proteins aggregates, while high centrifugal forces (100,000 xg) are used for small EVs sedimentation[158,321,322].

For TFF, the first two low speed centrifugations were performed. Media containing small EVs was centrifuged at 300 xg for 10 minutes and then supernatants were subsequently spun at 2000 xg for 10minutes, all spins at 4°C. Supernatants were then passed through a 0.22 μm filter (ThermoFisher no. 168-0045) and then the sample was concentrated using the KR2i TFF system (Spectrum Labs) with a 75 cm^2 modified polyethersulfone hollow fibre column with 500 kDa cut-off (Spectrum, D02-E500- 10-S) at a crossflow rate of 140 ml $minutes^{-1}$ and transmembrane pressure around 2.5-4.0 psi to achieve a shear rate of 2,000 s^{-1} [159,199,323]. Ultimately, the concentrated media underwent 10x buffer exchange in 1x PBS, and then ultrafiltration TFF was combined with ultracentrifugation in order to further separate small EVs and to pellet them, 100,000 xg for 30 minutes. All small EVs were then re-suspended in 1 mL 1x PBS and was ready for quantification using NTA on a ZetaView PMX-110.

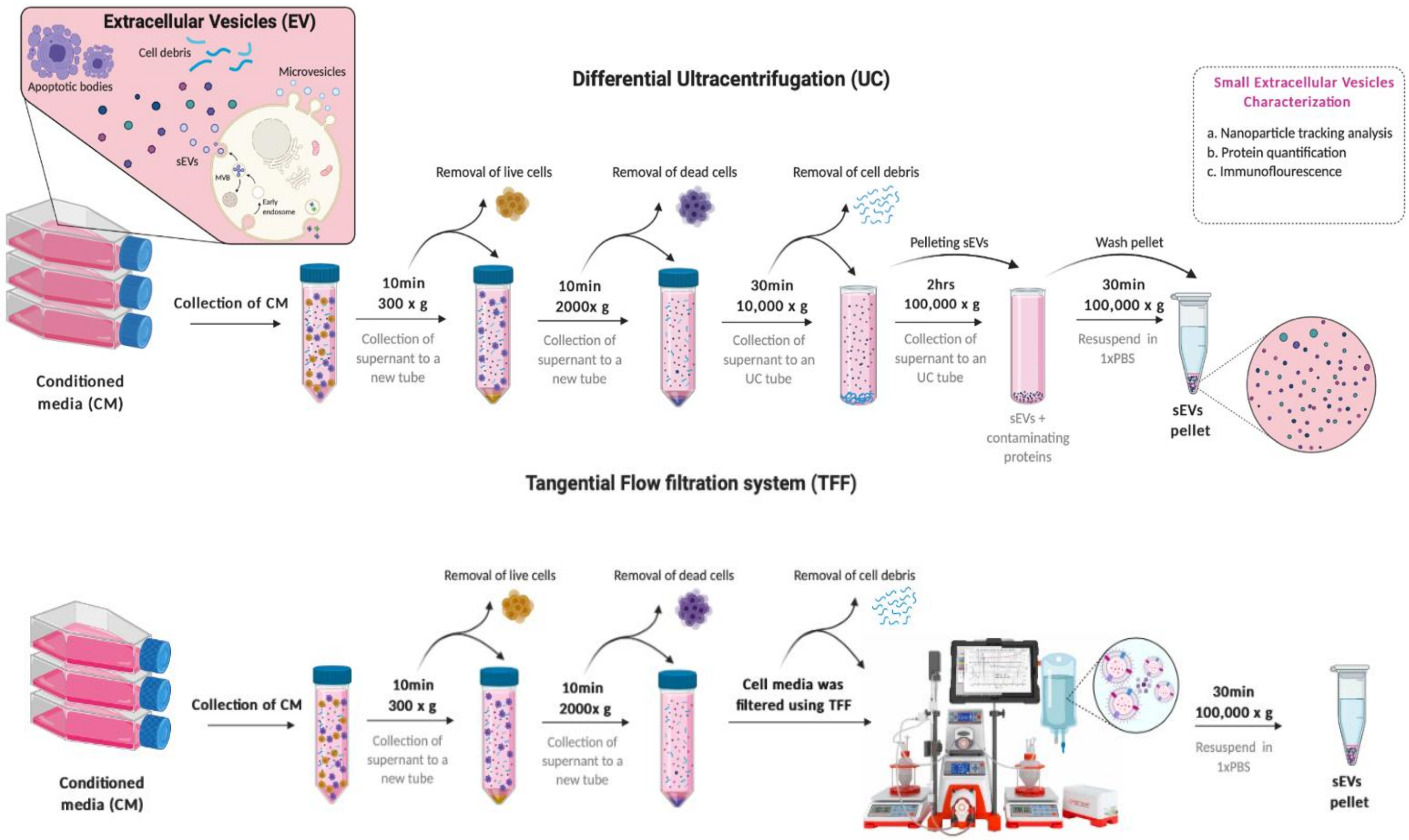

Figure 5. Schematic of the two small EVs isolation methods: differential ultracentrifugation (UC), and tangential flow filtration (TFF). (Illustration created using BioRender).

1.12 Nanoparticle tracking analysis

Small EVs were analyzed and quantified using a Nanoparticle Tracking Analysis (NTA) on a ZetaView PMX-110 (ParticleMetrix). The ZetaView NTA was calibrated for every experiment using 102 nm polystyrene beads (Microtrac, 900383). Isolated small EVs were diluted in 1x PBS ($1x10^4$ - $1x10^6$ in a total volume 1 mL) to be in the instrument's range for accurate measurement. Approximately 800-900 µL of each sample was injected into the machine. When the cell quality, particle drift and concentration reached an acceptable level according to the built-in particle-drift sensor, video acquisition was measured with the following settings: Sensitivity 85, Shutter Speed 40, Frame Rate (fps) 30, Resolution Highest, Camera Gain 770, Positions Measured 11, Minimum Brightness 15, Minimum Size (pixels) 10, Maximum Size (pixels) 500. The resulting quantification included particle size distribution, median particle size, and the particle concentration (after accounting for the dilution factor). The Gibbings lab has validated the linear range of the NTA instrument using serial dilutions of 110 nm polystyrene beads of known concentration (5.0×10^{12} particles per ml) (Microtrac, 400168). **Figure *9*** shows analyzed data from the Nanoparticle Tracking Analysis (NTA).

1.13 RNA extraction

A standard Trizol extraction protocol was performed following the manufacturer's instructions (Thermo Fisher Scientific). Total RNA was extracted from cells, using 1 mL of TRIzol Reagent (Invitrogen no. 15596026) followed by 0.2 mL of chloroform (Thermo Fisher Scientific, BP1145-1) at a ratio of 5:1 (Trizol:chloroform). After vigorous mixing, the sample was incubated at room temperature (15 minutes), then centrifuged at 12,000 xg for 15 minutes at 4°C. The aqueous phase was precipitated by adding 10 µg of GlycoBlue glycogen (Thermo-Fisher

Scientific, R0551 or AM9515) and isopropanol (0.5 mL per mL of Trizol reagent) for 10 minutes at room temperature. The RNA was pelleted at 12,000 xg for 15 minutes at 4°C. The resulting pellet was washed with 75% nuclease-free ethanol (1 mL per mL of Trizol reagent) and centrifuged at 12,000 xg for 15 minutes at 4°C. The dry RNA pellet was then resuspended in 20 μL of nuclease-free water and incubated at 55°C for 5 minutes using the thermomixer. Quantification and analysis were completed with Nanodrop 2000 spectrophotometer (Thermo Fisher Scientific, ND-2000). The final RNA solution was stored at -80°C.

1.14 cDNA synthesis and RT-qPCR

cDNA was synthesized with 500 ng of RNA using M-MuLV Reverse Transcriptase enzyme (NEB, no. M0253S) supplemented with 100 μM Oligo(dT)18 primer and dNTP mix (Thermo Fisher Scientific) following the manufacturer's protocol. cDNA was diluted 1:16 in nuclease-free water and immediately used in quantitative PCR (qPCR). Each qPCR reaction was carried out using 2x GoTaq ® qPCR master mix (Promega) with primer sets indicated on **Table 5**. Primer sets for qPCR were designed using the NCBI Primer-BLAST tool. Amplification efficiency of primer sets for each gene of interest was evaluated through standard curve analysis using pooled RNA samples from the cell type of interest. The thermocycler conditions for all primer sets was as follows: 95°C for 2 minutes, (95°C for 15 seconds, 60°C for 1 minutes) x 42 cycles, followed by a melt curve to assess product dissociation. To calculate fold-change in mRNA levels the ΔΔCt method was used. For differentiated SH-SY5Y knockdown experiments, mRNA levels were normalized to housekeeping genes hGAPDH and hβ-actin (ΔCt values). Test conditions were normalized to control conditions for each biological replicate (ΔΔCt), and biological replicates were averaged. Fold change in each condition was expressed relative to control (1.0). NRT (no reverse transcriptase) and NTC (no template control) reactions were also performed with each primer set as controls in order to assess primer-dimer formation and background genomic DNA amplification for each qPCR experiment.

Table 5. Primer sets for RT-qPCR. The primer sets were designed using the NCBI Primer-BLAST tool based on the following criteria: (i) product length must be between 120 to 180 bp, (ii) primers should be between 18-23 nt long and have melting temperatures of 58-60°C, (iii) primers must have minimal unintended targets and span exon-exon junctions to avoid amplification of genomic DNA.

Primer Set Name	**Forward oligos**	**Reverse oligos**
h-SNCA	CTTGCCTTCAAGCCTTCTGC	TCCTTGGTTTTGGAGCCTACAT
h-GAPDH	AGGTCATCCCTGAGCTGAACG	GCCTGCTTCACCACCTTCTTG
h-β-actin	GGCATGGGTCAGAAGGATT	GGGGTGTTGAAGGTCTCAAA

1.15 Measurement of copy number of siRNAs per small EV

Trizol LS (ThermoFisher, no. 10296028) was used to isolate RNA from known numbers of small EVs (quantified by nanoparticle tracking analysis on a ZetaView PMX-110) and RNA was extracted as described above. RNA was quantified with Nanodrop 2000 spectrophotometer (Thermo Fisher Scientific, ND-2000) and 500 ng were added to a reverse transcription reaction using miScript II microRNA reverse transcription kit using the HiSpec buffer option (Qiagen, catalogue no. 218161). RT–qPCR was performed according to the manufacturer’s instructions using the miScript SYBR Green PCR kit (catalogue no. 218075, Qiagen) on a Bio-Rad CFX-384 instrument using 10 µl reaction volumes. The primer sequence for siRNA targeting α-synuclein was as follows: TTAGGCTTCAGGTTCGTAGTCT. qPCR was performed on small EV samples, simultaneously with qPCR reactions using purified products of known concentration as templates with dilution series ($1x10^{-2}$ to $1x10^{-9}$) to generate a standard curve. The standard curve Ct values were used to calculate the number of RNA molecules in sample Ct values. As the number of small

EVs in the original sample was known, this allowed calculation of the number of molecules of specific siRNAs per small EV.

1.16 Protein extraction and Western blotting

Cells were washed with 1x PBS and lysed from cell pellets in ice-cold cell lysis buffer [0.1 M Tris (pH 7.4), 5 M NaCl, 0.5 M EDTA, 1% Triton-X 100] containing protease inhibitor cocktail. Cell lysates were incubated at -80°C for 30 minutes and centrifuged at 1000 rpm for 5 minutes at 4°C. Protein concentration in cell lysates was determined by Bradford Protein Assay following the manufacturer's protocol (Biorad) or Micro BCA^{TM} protein assay kit (Thermo Fisher, no. 23235) for small EVs. Samples were prepared for electrophoresis by combining appropriate volumes of each sample to give 25 µg of total protein with Laemmli loading buffer [50 mM Tris (pH 6.8), 2% SDS, 10% glycerol, 5% β-mercaptoethanol, 0.1 M DTT] and distilled water to equal a total volume of 20 µL. Proteins were denatured by boiling at 99°C for 5 minutes and separated by 10% polyacrylamide gel electrophoresis (SDS-PAGE) at 100 V for 1.5 h. Proteins were transferred to polyvinylidene fluoride (PVDF) membranes (Millipore) at 100 V for 70 minutes, an ice box was placed inside the machine. For α-synuclein protein detection, the membrane was microwaved for 1 minute in 0.4% paraformaldehyde (PFA) diluted in 1x PBS. After the microwave, the membrane was rinsed with 1x TBST [10 mM Tris-HCl (pH 8), 150 mM NaCl, 0.05% Tween 20]. Then, membranes were blocked in 5% milk in 1% TBST for 1 h at room temperature and probed with primary antibody overnight at 4°C followed by three washes in TBST for 10 minutes each. Membranes were then incubated with HRP-labelled secondary antibody diluted in 5% milk in 1% TBST at room temperature for 1 h and washed again 3 times for 10 minutes washes in 1% TBST. All antibodies used are listed in **Table 6**. Proteins were visualized using Luminata Crescendo Western HRP chemiluminescent substrate (Millipore) on an Image Quant LAS4010 Biomolecular

Imager (GE Healthcare). Rainbow markers (Amersham) were used to determine the protein sizes. Quantitative analyses on band intensity levels were performed using ImageJ. Mean band intensity was normalized to each sample's β-actin levels.

Table 6. Antibodies used for Western Blot.

Antigen [Clone]	Source	Dilution
α-synuclein [MJFR1]	Abcam (Epitomics) Rabbit monoclonal #ab138501	1:2000
β-actin [AC-15]	Millipore Sigma Mouse monoclonal #A5441	1:7500
CD9 [EPR2949]	Abcam Rabbit monoclonal #ab92726	1:1000
Flotillin-2 (C42A3)	New England Biolabs (NEB) Rabbit monoclonal #3436S	1:1000
Alix [3A9]	New England Biolabs (NEB) Mouse monoclonal #2171S	1:1000
Calnexin [C5C9]	New England Biolabs (NEB) Rabbit monoclonal #2679S	1:2000
CD63 [NVG-2]	BioLegend Mouse monoclonal #143904	1:5000
TSG101 [4A10]	GeneTex Mouse monoclonal #GTX70255	1:5000

1.17 Endothelial cell differentiation of iPSCs

The protocol published by Ribecco-Lutkiewicz et al from the NRC-HHT was adapted for the differentiation of endothelial cells from human iPSCs[62]. In short, once the iPSCs reached 60-

70% confluency the media was switched from mTeSR1 to low osmolality KOEB media composed of KnockOut DMEM/F12 medium (~ 276 mOsm/kg, Gibco) supplemented with 20% KnockOut serum replace-ment, 1x Glutamax, 1x non-essential amino acids and 55 μM β-mercaptoethanol (all from Life Technologies) for 5-7 days. The media was switched to endothelial differentiation media (EM) composed of human serum free endothelial media (Life Technologies) supplemented with 1% platelet-poor plasma derived serum (PDS, Alfa-Aesar) and 20 ng/ml bFGF for 9-10 days, once the cells formed a uniform monolayer of endothelial-like cells (cobblestone-like morphology). After 9-10 days in EM, the cells were dissociated with Accutase (Stem Cell Technologies) at 37 °C for 10-15 min. Through a 40 μm sieve and after dissociation, the cells were filtered to eliminate residual basement membrane, endothelial cell clusters and re-suspended in EM containing 10 μM ROCK Inhibitor. Then, iBECs were plated onto 0.5% gelatin coated Transwell inserts as described in the next **section 1.18**. The characterization of iBEC was performed at the end of the differentiation process (~21 days from iPSCs) following culturing onto gelatin coated inserts.

1.18 Preparation of transwell inserts and TEER measurements

Transwell inserts were prepared according to the published protocol by Ribecco-Lutkiewicz et al. at the NRC-HHT[62]. Briefly, transwell inserts (1 μm pore size, BD-Falcon, no. 353103) with polyethylene terephthalate (PET) membranes were coated with 0.5% gelatin and incubated overnight at 37 °C in 5% CO_2. Then, the gelatin was removed and 5×10^5 iBECs (at day 10) were seeded in each transwell insert in 1 mL complete endothelial medium (EM) without FBS (Life Technologies), supplemented with 1% platelet-poor plasma derived serum (Alfa-Aesar), 20 ng/ml bFGF (Life Technologies) and 10 μM Y27362 (ROCK Inhibitor) overnight at 37 °C in 5% CO_2. The following day, complete EM medium (without ROCK Inhibitor) was exchanged with fresh media for each transwell insert. To ensure BBB integrity, transendothelial electrical resistance (TEER) was measured for each transwell insert prior to experiments using a CellZscope apparatus (Nanoanalytics). The standard settings used were: 1 cm diameter electrodes and frequency range (1 Hz-100 kHz), points per decade and logarithmic spacing. TEER values for the empty inserts were subtracted from the TEER values for the inserts with cells to obtain final TEER values (represented as Ωcm^2).

1.19 Cell uptake assays

1.19.1 Treatment of differentiated SH-SY5Y cells with small EV containing α-synuclein siRNA

Small EVs derived from the following stable cell lines were isolated by TFF: wild-type, GFP siRNA and α-synuclein siRNA HEK293T cells; and wild-type, GFP siRNA and α-synuclein siRNA immortalized brain endothelial cells (hCMEC/D3). After isolation, the concentration of small EVs was quantified using Nanoparticle Tracking Analysis (NTA) on a ZetaView PMX-110. Then, 50,000 small EVs were incubated per one differentiated SH-SY5Y cell in a 24 well plate. The differentiated SH-SY5Y cells were treated prior to small EVs with all trans-retinoic acid (RA) (Sigma-Aldrich no. R2625) at 10 μM for 7 or 10 days depending on the initial cell density. After 72 h of incubation, the cells were treated with either Trizol reagent or cell lysis buffer for RNA and protein isolation, respectively. A diagram of this assay can be seen below (**Figure *6***).

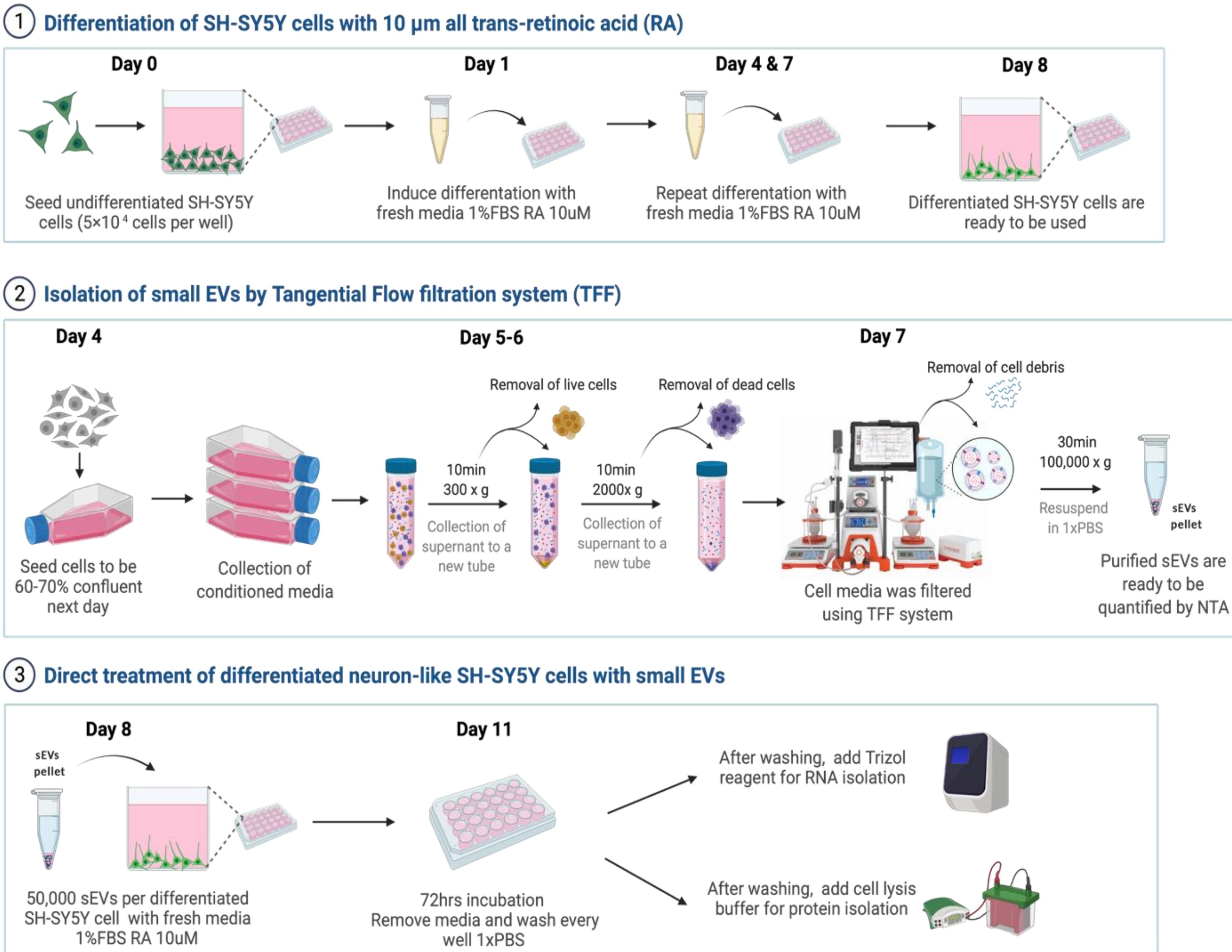

Figure 6. Schematic of the direct small EVs treatment of differentiated neuron-like cells. (Illustration created using BioRender).

1.19.2 *In vitro* human iPSC BBB model uptake

Small EVs derived from the following stable cell lines were isolated by TFF: wild-type, GFP siRNA and α-synuclein siRNA HEK293T cells; and wild-type, GFP siRNA and α-synuclein siRNA immortalized brain endothelial cells (hCMEC/D3). After isolation, the small EVs were labeled with 2 μM CellTracker™ Red CMTPX Dye (ThermoFisher, no. C34552) by incubating for 2 h at 37°C. Then, the last spin of ultracentrifugation was performed 100,000 xg at 4°C for 30 minutes (49,000 rpm with the TLA 100.3 rotor) to remove free dye and pellet was resuspended in 1 mL 1x PBS. The concentration of labeled small EVs was quantified using Nanoparticle Tracking Analysis (NTA) on a ZetaView PMX-110. Then, 50,000 labeled small EVs per one differentiated SH-SY5Y cell [seeded in the lower chamber (abluminal side)] were placed on the upper chamber (luminal side) of the 24-well transwell inserts containing a confluent monolayer of iBECs, shown in **Figure 14A**. The inserts were incubated at 37°C and 100 µl of the media was carefully removed from the upper and lower chamber of each insert at 1 h, 2.5 h, 4.5 h and 24 h. Following each collection, 100 µl pre-warmed media was added back to the upper and lower chamber for each insert and the plates were returned to the incubator. The sample collection was also carried out in 3 inserts without labeled small EVs at the same time points as negative controls. After the last collection, the inserts were placed in a new 24-well plate with fresh media at the lower chamber and returned to the incubator for 72 h. At the end of the experiment, iBECs were treated with 500 µl Trizol reagent for RNA isolation. In addition, the plate containing the differentiated SH-SY5Y cells at the lower of the chamber was returned to incubator for 72 h, cells were treated with 1 mL Trizol reagent for RNA isolation. The fluorescent values were measured by a Clariostar microplate reader using ex/em 577/602 nm spectra. Small EV uptake was calculated by using a standard curve of labeled small EVs from the same batch and plotting the lower chamber fluorescent values in the linear regression equation, taking into consideration the amount of total small EVs used and the 100 µl media removed at each point time.

1.20 Biodistribution of small EVs in mice

Small EVs derived from wild-type immortalized brain endothelial cells (hCMEC/D3) were isolated using the Tangential Flow Filtration (TFF) system as described in later section. After isolation, small EVs were labeled by mixing 0.2 M carbonate buffer pH 9.4 (Thermofisher, 28382), CF770-NHS Ester (Succinimidyl Ester) (Biotium Inc, no. 92150) and small EVs derived from hCMEC/D3 for 2 h at room temperature with slow mixing. Then, the sample was subjected to 2 rounds of washes using Zeba™ Spin Desalting Columns (40K MWCO, 2 mL, Thermofisher, no. 87769) by centrifuging the columns at 1000 ×g for 2 minutes to remove free dye. Then, the columns were placed into a new collection tube and sample was added slowly to the center and centrifuged 1000 ×g for 2 minutes to collect the purified sample. CF770-labeled small EVs were injected either by intravenous injection (IV) or intracarotid injection (ICD) using CD-1 male mice. Twenty-four hours before the experiment, mice were shaved on the dorsal and ventral side. The dorsal and ventral sides were imaged using the parameters: excitation-740 nm and emission-790 nm with IVIS Lumina III at various time point (pre-injection, 10 minutes, 30 minutes, 1 h, 2 h, 3 h, 4 h, 6 h, 24 h post-injection). Mice were saline-perfused and various tissues (brain, heart, lung, liver, kidney, spleen, and lymph nodes) were collected for ex-vivo imaging with IVIS Lumina III to detect the tissue distribution (biodistribution) by quantifying the fluorescent signals from each organ. A naïve mouse was used as a negative control. A diagram of these assays can be seen below (**Figure 7**).

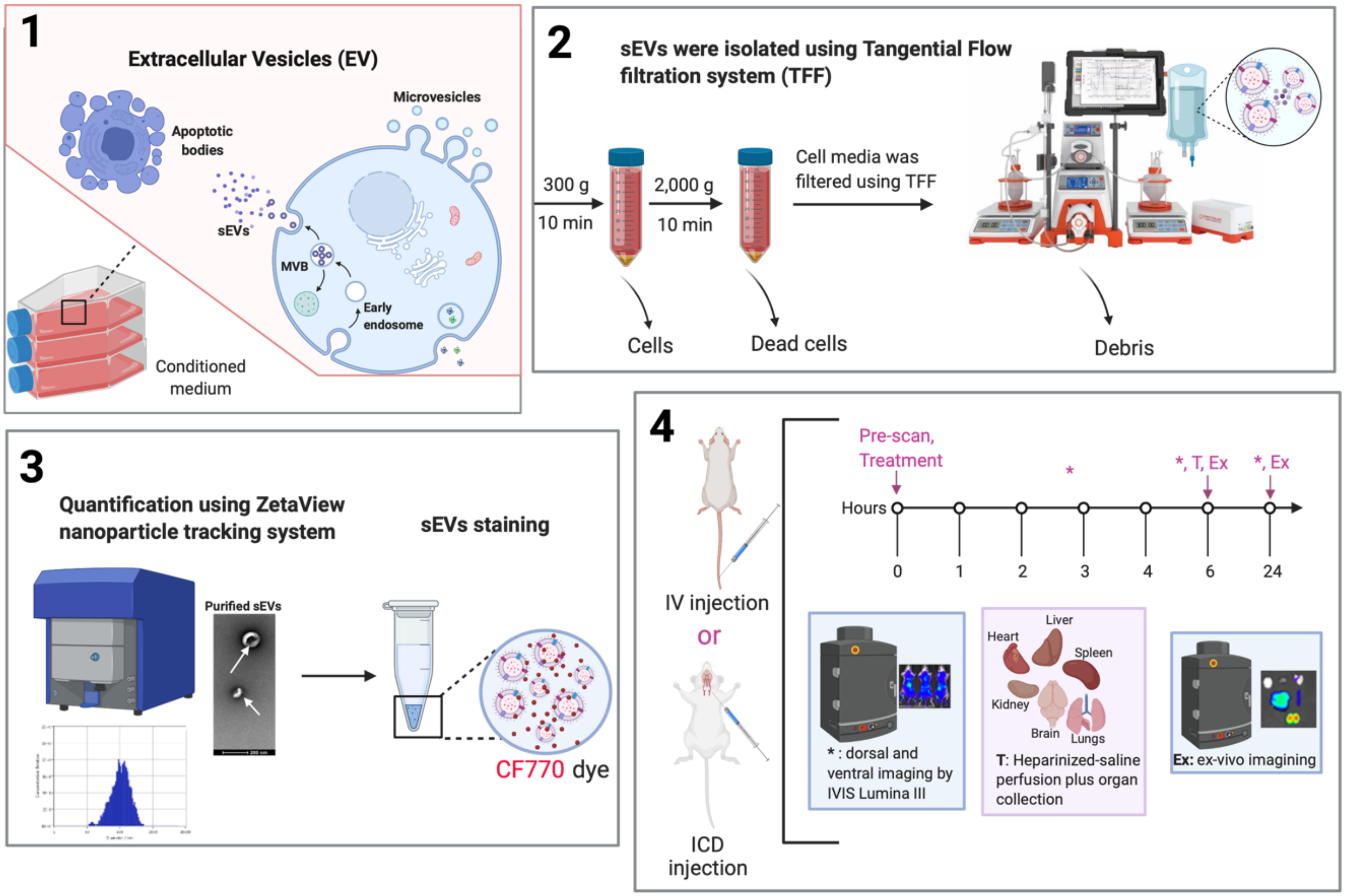

Figure 7. Methodology for *in vivo* biodistribution of CF770-labeled small EVs from Immortalized human brain microvascular endothelial cells after a single bolus administration (IV and ICD) in mice. IV, intravenous injection. IC, intracarotid injection. sEVs, small extracellular vesicles. Illustration created using BioRender.

1.21 Statistical Analysis

All statistical tests were performed using GraphPad Prism version 9 software (www.graphpad.com). The following tests were performed, unless stated differently in the caption of each figure. One-way ANOVA (analysis of variance) test was performed followed by Tukey's multiple comparison test when the means of the test columns was compared individually to the mean of the control column. Two-way ANOVA with Tukey's multiple comparison test was used to determine which specific groups differed from each other. Normal distribution was assumed for all tests. Statistical significance was showed as: *=$p<0.05$, **=$p<0.01$, ***=$p<0.001$, ****=$p<0.0001$.

RESULTS

1.22 Integrating siRNA against α-synuclein into the pre-miR-451 backbone

Evidence provided by Reshke, et al. showed that integration of siRNA sequences into the pre-miR-451 hairpin structure leads to their enrichment in small EVs (**Figure 8A**). In order to use this system to target α-synuclein (**Figure 8B**), siRNAs targeting α-synuclein were first tested to identify those with the maximum potential to knockdown α-synuclein. Thus, siRNAs targeting α-synuclein were obtained from Thermo Fisher Scientific and a patent from Alnylam Pharmaceuticals (**Table 2 and Table 3**). α-synuclein knockdown was quantified by transfecting the siRNAs into human embryonic kidney (HEK293T) cells using RNAiMAX and measuring reduction in α-synuclein mRNA (RT-qPCR) and protein levels (western blot) (**Figure *10***). The siRNA sequences with the most potent knockdown were sequence #1 (sq1, 96.74%), sequence #3 (sq3, 97.98%) and sequence #5 (sq5, 88.78%). Therefore, these sequences were integrated into the pre-miR-451 structure. The specific oligonucleotide sequences (shown in **Table *4***) were cloned into the modified pUC19 construct encoding the 5' and 3' regions of the pre-miR-451 backbone with BbsI sites flanking an EcoRV site in the middle to allow insertion of new siRNA sequences (**Figure *11*A**). BamHI and NheI sites flank the whole pre-miR-451 sequence. The plasmids were subjected to 1% gel electrophoresis to confirm that the pre-miR-451 backbone was disrupted, and the α-synuclein-targeting oligonucleotide was inserted. As shown in the gel, digestion with BbsI and BamHI restriction sites illustrated no digestion and full digestion, respectively. This indicates proper integration of the sequence of the α-synuclein-targeting oligonucleotide into the modified pUC19 construct (**Figure *11*B**). As a control, an oligonucleotide targeting GFP was integrated into the pre-miR-451 backbone (same as shown in Reshke, et al.). These constructs containing oligonucleotide against α-synuclein or GFP in pUC19 vector were verified by DNA sequencing.

Stable human immortalized cerebral endothelial (hCMEC/D3) and HEK239T cell lines were produced via transduction with lentiviral vectors to allow stable expression of the re-programmed pre-miR-451 backbone containing siRNA targeting α-synuclein or GFP (**Figure *11*C**). The hCMEC/D3 cells were selected to produce small EVs due to their stability, ease of growth and their ability to maintain a normal BBB phenotype[318]. These cells have been shown to express a BBB phenotype including endothelial markers (CD34, CD31, CD40, CD105, VE-cadherin), junction-associated proteins (PECAM-1, JAM-1), tight junction proteins (claudin-3,-5, occluding), as well as scaffolding proteins (beta catenin, zonula occludens-protein-1 and 2), among others[324]. On the other hand, HEK293T cells were selected as positive control for transduction since they are easy, reliable and divide rapidly. Further in this project, HEK293T cells were used to produce small EVs as negative control since they do not express any BBB phenotypes or human brain endothelial properties compared to hCMEC/D3 cells. After transduction, both stable cells containing siRNA against α-synuclein in pre-miR-451 backbone were validated by observing the GFP fluorescent signals using ZOE Fluorescent Cell Imager (**Figure *11*C**) since CMV promoter in pre-miR-451 vector drives GFP expression in cells (cells fluoresce green). Ultimately, the sq3 oligonucleotide sequence, siRNA that achieved the maximum silencing of α-synuclein (97.98%), was further selected to assess the siRNA delivery by small EVs in cell culture.

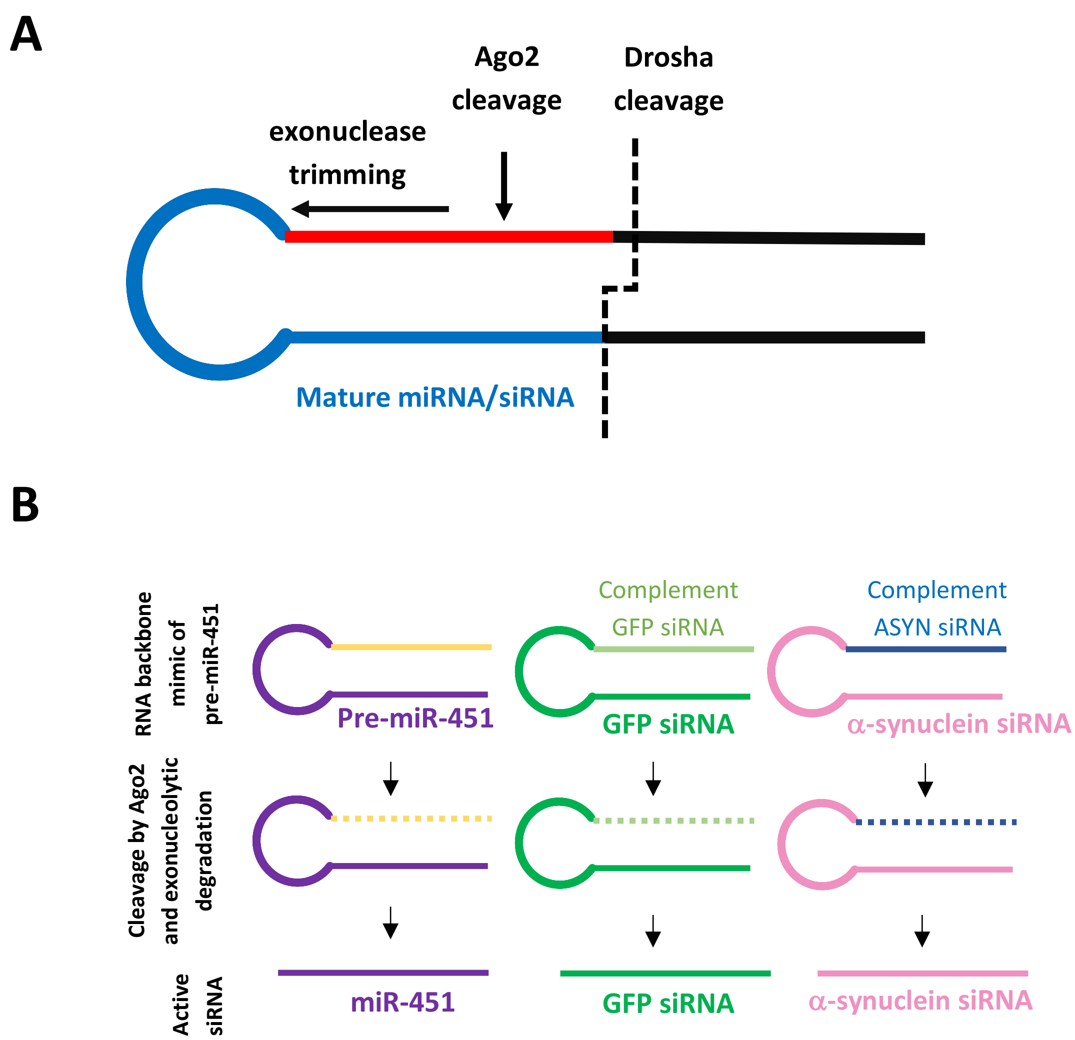

Figure 8. Reprogramming the pre-miR-451 backbone with siRNAs. (A) Schematic of the predicated pre-miR-451 secondary structure, showing its cleavage by Drosha, Ago2 and subsequent trimming by exonucleases. **(B)** Schematic illustrating the reprogramming of the pre-miR-451 hairpin loop structure with siRNA targeting GFP or α-synuclein siRNA sequences. If the pre-miR-451 hairpin structure is maintained, any siRNA sequence can be inserted and processed by Dicer-independent pathway into a mature siRNA.

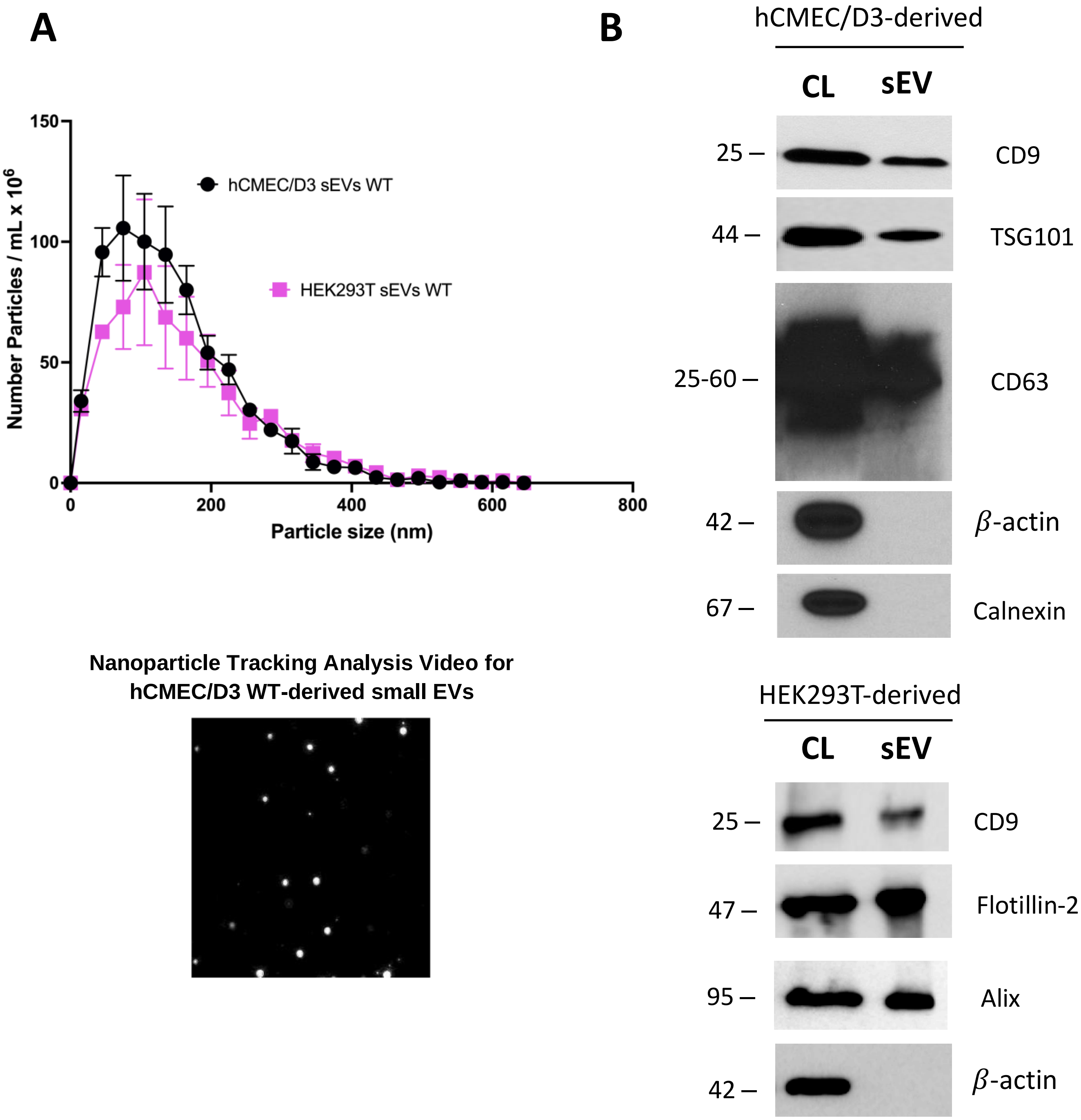

Figure 9. Characterization of small EVs. Wild-type small EVs were collected from the media of human immortalized cerebral endothelial hCMEC/D3 cells and human embryonic kidney HEK293T cells by differential ultracentrifugation. **(A)** Size distribution and concentration of purified EV particles (pelleted at 100,000 x g) diluted 10^6 in PBS were measured by nanoparticle tracking analysis (NTA) on the Zetaview® (n=3). Distribution of small EVs were observed at the screen shot from NTA video. **(B)** Western blots of equal amounts of proteins from small EVs or hCMEC/D3 cells were probed with antibodies recognizing small EV-specific biomarkers (CD9, TSG101, CD63, Flotillin-2, Alix) or a protein normally excluded from small EVs (calnexin, β-actin) to confirm the enrichment of small EV (CL – cell lysate, sEV – small extracellular vesicles). The error bars represent as mean ± SEM of three independent experiments.

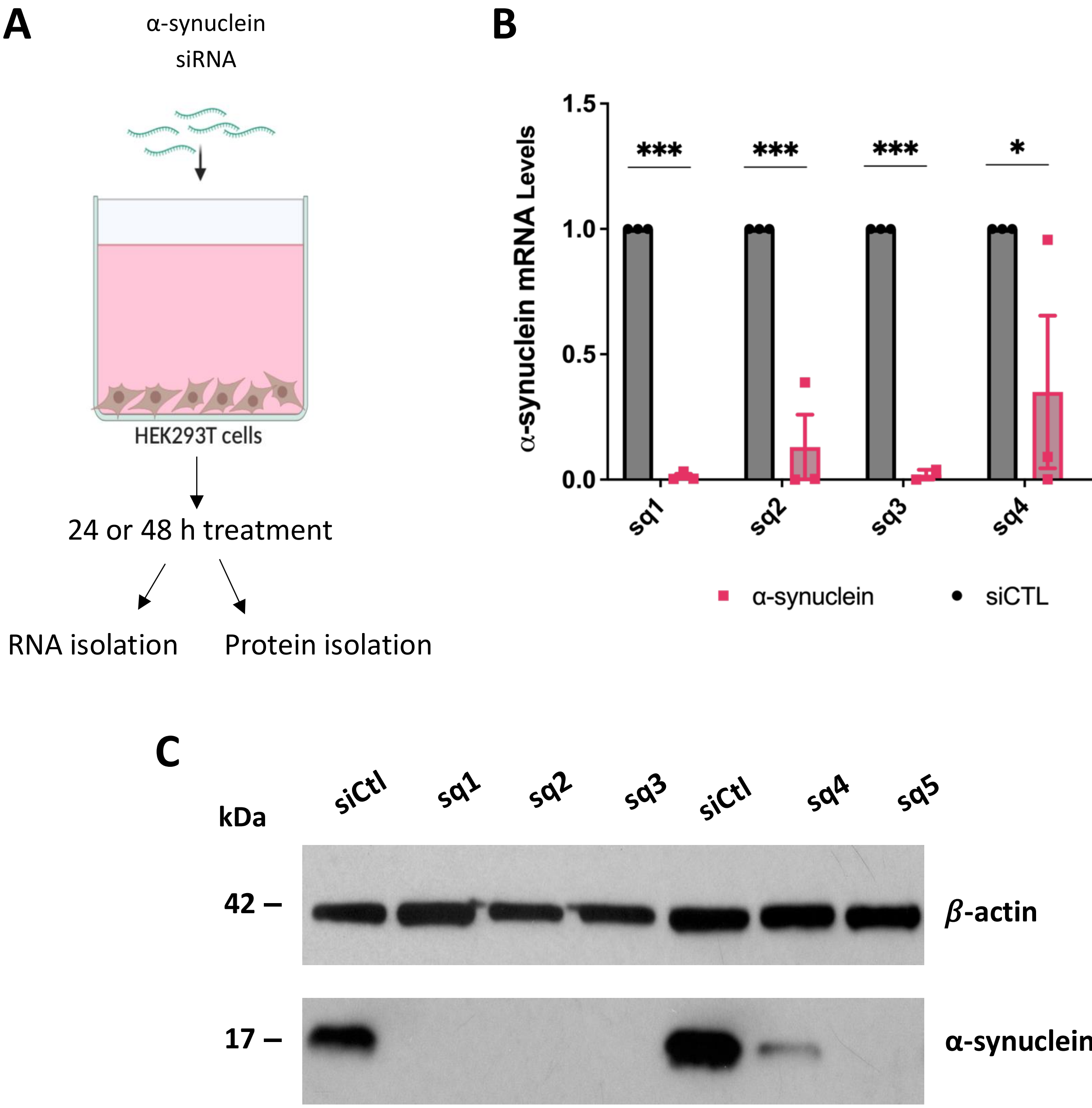

Figure 10. α-synuclein Knockdown measured by RT-qPCR and Western Blot in HEK293T cells. (A) Schematic of the α-synuclein siRNA transfection into human embryonic kidney HEK293T cells (Illustration created using BioRender). The potency of α-synuclein siRNA was verified by transfecting the siRNAs into HEK293T cells using Lipofectamine RNAiMAX and measuring the reduction α-synuclein in HEK293T cells by **(B)** RT-qPCR (mRNA levels) (n=3) and **(C)** Western blot (protein levels). α-synuclein siRNA sequences were obtained from Thermofisher and a patent from Alnylam Pharmaceuticals (Table 2 and Table 3). *β*-actin and hGAPDH were used as controls. For statistics, a two-way ANOVA with Holmes-Sidak test was used. Data are presented as mean ± SEM. *=p<0.05, **=p<0.01, ***=p<0.001, ****=p<0.0001.

1.23 Small EVs packaged with α-synuclein siRNA integrated in the pre-miR-451 backbone efficiently deliver siRNA to human neuron-like cells

Next, we sought to test whether small EVs packaged with α-synuclein siRNA reprogrammed into the pre-miR-451 backbone could efficiently deliver these siRNA. The validation of siRNA delivery by small EVs was performed by quantifying endogenous α-synuclein knockdown in neuron-like cells in cell culture. Even though it has been demonstrated in previous studies that small EVs are capable of delivering their cargo into the cytoplasm of target cells, there are also other studies showing that not all cells produce small EVs capable of delivering siRNA to target cells[199]. Therefore, our first step was to directly incubate small EVs with neuron-like cells to demonstrate that these small EVs are capable of producing a functional change. These experiments used the sq3 siRNA sequence, siRNA that achieved the maximum silencing of α-synuclein (97.98%) when transfected with RNAiMax into HEK293T cells (**Figure *10***).

Small EVs from two stable cell lines, hCMEC/D3 and HEK293T, stably expressing either siRNA targeting GFP or α-synuclein integrated in the pre-miR-451 backbone were isolated using TFF system (more details in methods section, **Figure 5**). In 2018, ISEV proposed comprehensive MISEV guidelines regarding the isolation and characterization of EVs. Therefore, we followed these guidelines and showed isolated small EVs derived from hCMEC/D3 and HEK293T were ~120 nm in size (**Figure 9A and B**) and expressed specific small EV markers such as CD9, CD63, Alix, Flotillin-2, and TSG101, analyzed by western blotting (**Figure 9C**). Thus, the absence of markers such as the endoplasmic reticulum protein calnexin, was an indication that the isolated small EV population was indeed small EVs and not contaminating vesicles from other compartments of the cell. Even though these markers indicate a pure small EV population, it is important to consider that up to this date there is no ideal method to isolate a pure population of small EVs and isolated small EVs preparation are often “contaminated” by co-isolated proteins (i.e., albumin, alpha-1-antitrypsin), smaller or larger vesicles, and lipoprotein particles of similar density as small EVs. As well, the size and concentration of these small EVs were measured using the ZetaView® which is a Nanoparticle Tracking Analysis (NTA) instrument (**Figure 9A and B**). The size and concentration of particles in the NTA instrument are calculated by capturing the amount of laser light scattering and Brownian movement of particles in the solution on a single-particle level[325], more details in the parameters in **section 1.12**.

After isolation, small EVs from two stable cell lines, hCMEC/D3 and HEK293T, stably expressing either siRNA targeting GFP or α-synuclein integrated in the pre-miR-451 backbone were directly incubated with neuron-like cells in cell culture. The human neuroblastoma cell line SH-SY5Y was treated for 7 days with 10 µM retinoic acid (RA) in order to be differentiated into mature neuron-like cells[326]. Retinoic acid is a common inducing agent used to induce SH-SY5Y in order to reassemble mature neurons which results in an increase in several relevant mature neuronal markers such as formation of neurites and expression of neuro-specific proteins, including β-III tubulin (**Figure 14B**). Differentiated SH-SY5Y cells were incubated with isolated small EVs for 72 h at a ratio of $5x10^4$ small EVs per cell. HEK293T and hCMEC/D3 derived small EVs containing α-synuclein siRNA integrated in the pre-miR-451 backbone showed a knockdown of α-synuclein mRNA in differentiated SH-SY5Y of 60-70% (**Figure *12*B**) compared to wild-type small EVs and small EVs packaged with a negative control GFP siRNA integrated in the pre-miR-451 backbone. This data suggests that α-synuclein siRNA packaged in small EVs has reached the neuronal cytoplasm and engaged its target resulting in RNA silencing of endogenous α-synuclein expression. At the protein level, HEK293T small EVs containing α-synuclein siRNA integrated in the pre-miR-451 backbone reduced α-synuclein levels by 43% (**Figure *12*C**).

In regard to hCMEC/D3, small EVs containing α-synuclein siRNA integrated in the pre-miR-451 backbone showed a trend in α-synuclein reduction, however it was not statistically significant. This could be due to the outliers which can be overcome by increasing the experimental biological replicates. In contrast to mRNA expression, protein levels were lower which indicate that, in order to have a greater impact, they require longer gene down-regulation[121]. All these results suggest that small EVs deliver their siRNA cargo into the cytosol of neuron-like cells in an efficient enough manner to produce a change in function.

Previous studies have indicated that in order to silence a target mRNA in cells, between 300-2,000 copies of siRNA molecules in the cytoplasm of each cell are required[184–186]. Specifically, 300 copies of siRNA molecules per cell were needed to reduce 50% of target mRNA in which the siRNA was microinjected directly into the cytoplasm of the target cell[185]. Therefore, we sought to quantify the amount of α-synuclein siRNA molecules per small EVs required to silence α-synuclein mRNA levels. Our data indicate that an average number of α-synuclein siRNA molecules per small EV was determined to be an average of around 0.0248 (**Figure *13*A**). In reference to previous results, $5x10^4$ small EVs per cell were added suggesting 1,240 α-synuclein siRNA per cell were needed in order to obtain 60-70% α-synuclein mRNA reduction. In comparation to other studies, lipid nanoparticles (LNPs, the current clinical delivery vehicles) only deliver between 0.05% and 1% of their siRNA cargo into the cytoplasm of target cells. This suggest that if our small EVs at a dose of 1,240 α-synuclein siRNA per cell cause target reduction, then our small EVs would appear to deliver a great proportion of their siRNA cargo into the cytoplasm compared to LNPs. This result was consistent with Reshke, et al. data where they showed 1,000 GFP siRNA molecules per cell were needed to observe a target reduction.

Additionally, a dose response experiment was performed in order to test the minimum and maximum number of small EVs needed per neuron-like cell to reduce α-synuclein mRNA levels in cell culture (**Figure *6*B**). The α-synuclein levels were reduced with 2.5×10^4 small EVs per cell, but a lower concentration of small EVs did not reduce α-synuclein levels significantly. Similarly, treating cells with higher concentrations of small EVs, three times the amount of small EVs per cell (1.50×10^5) did not cause a plateau in α-synuclein levels. This demonstrates that a reduced dose of small EVs was relatively efficient in obtaining ~85% α-synuclein reduction at the mRNA levels. However, it is important to consider the appropriate degree of reduction necessary to safely, and effectively reduce α-synuclein expression levels with no resulting implication to its normal functional activity. In addition, previous studies have suggested that α-synuclein protein is present in small EVs[327,328]. One could interpret that our stable cell lines expressing α-synuclein siRNA can presumably have lower α-synuclein levels due to the expression of α-synuclein siRNA in the cytoplasm of these cells. Therefore, lower amounts of α-synuclein protein gets packaged into small EVs, ultimately leading to the reduction of α-synuclein mRNA seen in the differentiated SH-SY5Y cells. This interpretation was overcome in **Figure *13*A** where we detected α-synuclein siRNA molecules and we did not see any effect in their controls. In summary, this data suggests that small EVs packaged with α-synuclein siRNA integrated in the pre-miR-451 backbone can sufficiently deliver and reduce α-synuclein in neuron-like cells at the mRNA level.

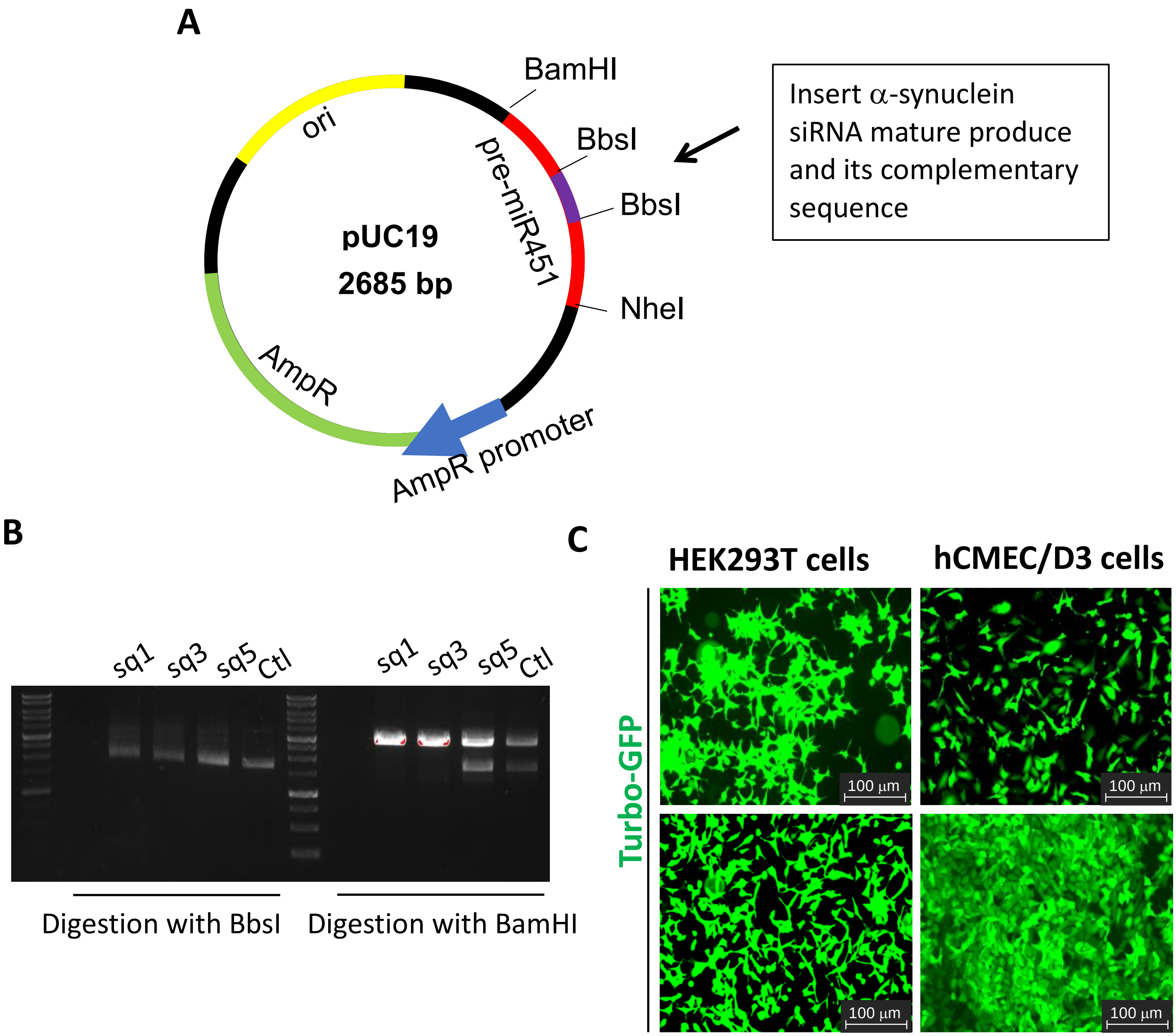

Figure 11. Reprogramming the pre-miR-451 hairpin structure with α-synuclein siRNA. (A) An illustration of the pUC19 vector containing synthetic pre-miR-451 with BbsI sites (Type II s). The published siRNA sequences were adapted to reprogram pre-miR-451 to target α-synuclein (Table 2 and 3). **(B)** These were cloned between the BamHI and NdeI sites of pUC19 construct specifically within the BbsI sites (Type II s). 1% Electrophoresis gel showing the digestion of pUC19 constructs containing α-synuclein oligonucleotide sequences with BbsI and BamHI restriction sites, specifically. **(C)** Constructs encoding reprogrammed pre-miR-451 in pUC19 were moved into a vector allowing production of lentiviral particles. Lentiviral particles were produced using standard methods from transfected HEK293T cells and were concentrated by ultracentrifugation. Dilutions of these lentiviral particle stocks were added to cell growth media and after 3 days, cells were spilt into media containing puromycin to select for transduced cells. Transduction was confirmed by observing the GFP fluorescent signals by ZOE Fluorescent Cell Imager. Top panel: Transduced cells 2 days after puromycin selection. Bottom panel: Transduced cells 4 days after puromycin selection.

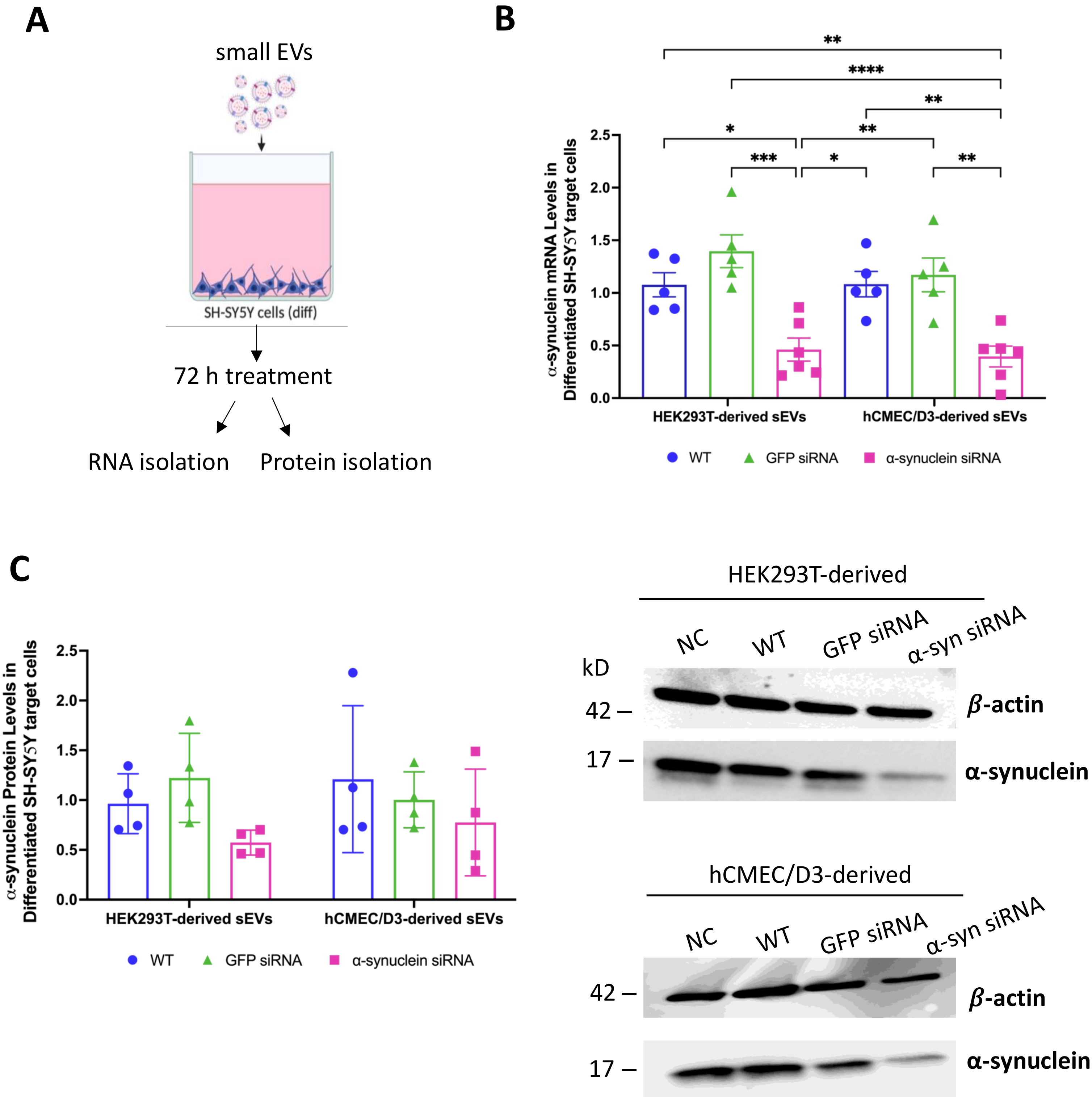
A
small EVs
SH-SY5Y cells (diff)
72 h treatment
RNA isolation
Protein isolation
B
α-synuclein mRNA Levels in Differentiated SH-SY5Y target cells
HEK293T-derived sEVs
hCMEC/D3-derived sEVs
WT
GFP siRNA
α-synuclein siRNA
C
α-synuclein Protein Levels in Differentiated SH-SY5Y target cells
HEK293T-derived sEVs
hCMEC/D3-derived sEVs
WT
GFP siRNA
α-synuclein siRNA
HEK293T-derived
NC
WT
GFP siRNA
α-syn siRNA
kD
42 –
17 –
β-actin
α-synuclein
hCMEC/D3-derived
NC
WT
GFP siRNA
α-syn siRNA
42 –
17 –
β-actin
α-synuclein

Figure 12. Small EVs packaged with α-synuclein siRNA integrated in the pre-miR-451 backbone efficiently deliver siRNA to human neuron-like cell line. (A) Schematic of the direct small EVs treatment of differentiated neuron-like cells (Illustration created using BioRender). Small EVs from various cell lines (HEK293T and hCMEC/D3) stably expressing either GFP siRNA or α-synuclein siRNA integrated in the pre-miR-451 backbone were isolated using the Tangential Flow Filtration (TFF) system. Differentiated SH-SY5Y cells treated 7 days with 10 μM retinoic acid (RA) were directly incubated with isolated small EVs for 72 h. 50, 000 small EVs per cell. Negative control (NC) and wild-type (WT) small EVs were used as controls. The knockdown of α-synuclein levels was measured by **(B)** RT-qPCR (mRNA levels) (n=5) and **(C)** western blot (protein levels) (n=4). Wild-type small EVs were normalized to the no treated sample and small EVs containing GFP siRNA and α-synuclein siRNA were normalized to the wild-type sample. sEVs – small extracellular vesicles. For statistics, a one-way ANOVA with Tukey's multiple comparison test was used. Data are presented as mean ± SEM. *=$p<0.05$, **=$p<0.01$, ***=$p<0.001$, ****=$p<0.0001$.

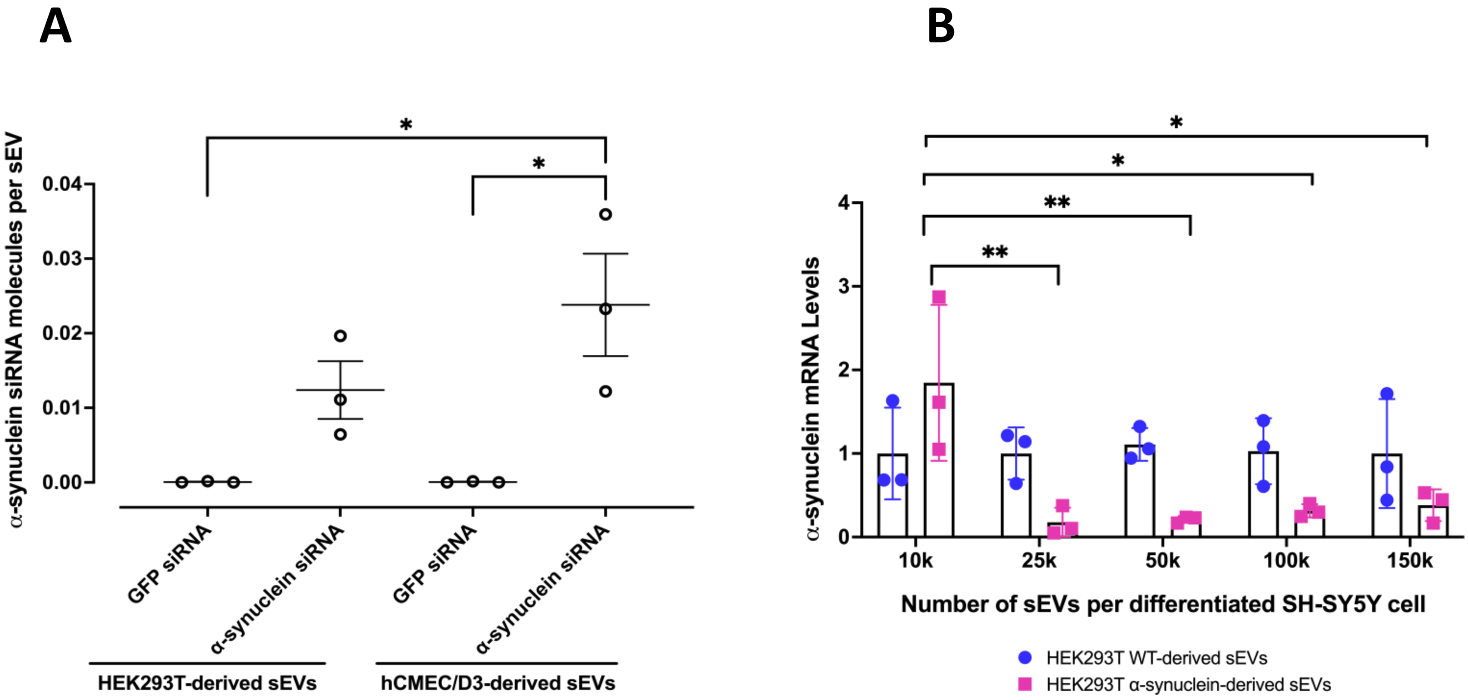

Figure 13. Packing efficiency of small EVs α-synuclein siRNA reprogrammed into pre-miR-451 hairpin structure. Small EVs from various cell lines (HEK293T and hCMEC/D3) stably expressing either GFP siRNA or α-synuclein siRNA integrated in the pre-miR-451 hairpin structure were isolated using the Tangential Flow Filtration (TFF) system. **(A)** Copy number of α-synuclein siRNA molecules in small EVs after stable expression from the pre-miR-451 backbone in the indicated cell types (n=3). For statistics, a one-way ANOVA with Tukey's multiple comparison test was used. **(B)** Different amount of small EVs were directly incubated for 72 h with differentiated SH-SY5Y cells treated 7 days with 10 μM RA, and mRNA levels were quantified by RT-qPCR (n=3). Small EVs containing GFP siRNA and α-synuclein siRNA were normalized to the wild-type sample. sEVs – small extracellular vesicles. For statistics, a one-way ANOVA with Tukey's multiple comparison test was used. Data are presented as mean ± SEM. *=$p<0.05$, **=$p<0.01$, ***=$p<0.001$, ****=$p<0.0001$.

1.24 Small EVs packaged with α-synuclein siRNA integrated in the pre-miR-451 backbone cross an *in vitro* human BBB model and reduce α-synuclein mRNA levels in neuron-like cells

Selecting the appropriate *in vitro* BBB model is critical when assessing the potential for small therapeutic transport. The aim was to assess the ability of small EVs packaged with α-synuclein siRNA integrated in the pre-miR-451 hairpin structure to cross the BBB and efficiently knockdown α-synuclein in neuron-like cells. In this project, the *in vitro* human BBB model using endothelial cells derived from iPSCs, as described by Ribecco-Lutkiewicz et al.[62], was implemented.

This model is a reproducible, scalable and transgene-free human BBB model composed of induced brain endothelial cells (iBECs), generated from human amniotic fluid-derived induced pluripotent stem cells (AF-iPSCs). Importantly, this model has a functional RMT pathway that transports natural ligands across the BBB formed by iBECs. The iBECs are used to assemble an *in vitro* BBB model in a transwell, a static system, where iBECs are seeded in the upper chamber (luminal side) and neuron-like derived from SH-SY5Y were seeded in the lower chamber (abluminal side) (**Figure 14A**). As well, this *in vitro* human iPSC BBB model exhibits the critical components of the BBB, including high barrier integrity measured by TEER (around 550 Ωcm^2) and polarized expression of efflux transporters[62]. The TEER measurement indicates the barrier impermeability or "tightness" of the tight junctions between iBEC cells. In comparison, TEER measurements of the common two commercially available primary human brain microvascular endothelial cells (hBCMECs) and human immortalised endothelial cells (hCMEC/D3) ranged from 30-100 Ωcm^2 [62,329]. These human immortalised hCMEC/D3 cells, when grown in coculture with astrocytes, yield higher TEER values of approximately 140 Ωcm^2 [330,331], indicating a specific tightening response to astrocytic interactions. TEER measurements have been observed to increase in stem cell-based models (iPSC-derived BECs) and neuronal progenitor cells, specifically when exposed to chemical treatments such as retinoic acid or astrocyte conditioned media, resulting in values of 3000–4000 $\Omega.cm^2$ [332]. However, these chemical treatments often require specialized and costly methods to culture cells.

Prior to treating this model with small EVs, the TEER Ωcm^2 of confluent iBECs monolayer cultures on gelatin coated transwell inserts were measured. The human *in vitro* BBB model showed average iBEC values of 500 Ωcm^2 (ranging between 200-600 Ωcm^2) 48 h after seeding onto the inserts (**Figure 14E**). To visualize the small EVs, α-synuclein siRNA packaged small EVs were isolated from hCMEC/D3 and HEK293T cells using Tangential Flow Filtration (TFF) and labeled with CellTracker red dye (CMPTX, Ex/Em 577/602 nm). CellTracker red dye freely passes through the cell membrane and, once inside the cell, its chloromethyl group reacts with the intracellular thiol groups in a reaction mediated by glutathione S-transferase which leads to its retention inside the cell[333]. The most widely used method to fluorescently label isolated small EVs is by using dyes such as PKH, DiD and DiR, for their visualization and cellular uptake in recipient cells[334,335]. These dyes are lipophilic and often label small EVs non-specifically as well as labeling other components which are present in the isolated small EVs population; thereby generating false positive signals[336–338]. Moreover, it has been reported that lipophilic dyes can form self-aggregates and micelles resembling small EVs which might also generate false signals[339]. Therefore, labeling small EVs with a fluorescent chloromethyl derivative and membrane-permeant dye that is non-fluorescent until it is activated by intracellular binding can overcome some of the lipophilic dye challenges. As well, another major benefit of using this dye is that it does not disrupt the membrane and integrity of small EVs.

After labeling the hCMEC/D3 and HEK293T small EVs, they were added to the upper chamber of the BBB at 50,000 small EVs per differentiated SH-SY5Y neuron-like cell (**Figure 14A**). At 60 min, 2.5 h, 4.5 h, and 24 h, media from the upper and lower chambers was collected and the fluorescent values of the CellTracker red dye (CMPTX, Ex/Em 577/602 nm) were measured using a microplate reader (**Figure 14C**). A previous study has reported delivery rates in the abluminal side of a variety of antibody-based macromolecules including human IgG (0.16%), human Fc (0.17%), human transferrin (0.19%), and 10-kDa dextan (1.48%) across iBECs using BEC-like cells derived from human induced pluripotent stem cells[340]. The results from our experiments showed that ~2.4% of small EVs derived from hCMEC/D3 cells and ~1.3% of small EVs derived from HEK293T cells were found on the abluminal side of the BBB after 1 h. Even though there are fewer studies regarding small EV delivery to the BBB, one study has reported that tumor-derived small EVs (Br-EVs) can cross the endothelial barrier at a rate of 0.16% (after 3 h) in their BBB chip model[160], meaning that our small EVs cross iBECs better than Br-EVs. This suggests that small EVs from both cell lines could cross the iBECs at a higher amount than monoclonal antibodies/Br-EVs and could also indicate that small EVs have unique transcytosis properties which influence their uptake into the BBB. Furthermore, this data demonstrates that there was a difference in percentage uptake between small EVs derived from hCMEC/D3 versus HEK293T, suggesting that the different cell source of small EVs can contribute to their efficiency in crossing the iBECs.

In addition, ~4% of small EVs from human immortalised (hCMEC/D3) cells were detected in the abluminal side of the transwell system after 24 h; substantially more than small EVs from HEK293T (2%). Another interpretation of this data could be that even though the TEER values were around 500 Ωcm^2 (ranging between 300-600 Ωcm^2) prior to small EVs treatment, after 24 h these TEER values were observed to decrease (**Figure 14F**), suggesting a potential increase in barrier permeability of the tight junctions between iBEC cells. Despite that this could indicate that the observed percentage uptake at 24 h was due to leakage of small EVs through the tight junctions of the iBECs, only six inserts had a low TEER value (< 20 Ωcm^2), and the majority of other inserts (< 110 Ωcm^2) had a higher TEER values compared to the common two commercially available primary human brain endothelial cells (30-100 Ωcm^2). Approximately 4.75% of Cell tracker red dye was detected in the lower chamber, indicating that there were 7.125×10^9 small EVs derived from hCMED/D3 fluorescing red after 24 h. Therefore, if 5×10^4 small EVs per differentiated SH-SY5Y neuron-like cell were added, this suggests that around 8,906.25 small EVs crossed the BBB per iBEC cell after 24 h. This data showed on average 2.474 small EVs cross one iBEC cell per second. This data does not correlate with previous studies where they have shown the maximal transport activity ($V_{max,}$ molecules per second) for BBB nutrients transports were 600 glucose molecules per second, 2,300 monocarboxylic acid molecules per second, and 3,000 neutral amino acid molecules per second[341].

After 24 h, the transwell inserts were imaged using ZOE Cell Imager in order to observe the small EVs labeled with Cell tracker red dye in iBECs in the upper chamber transwell insert (**Figure 14D**). The percent of red dye in the iBECs was 1.96%, indicating that there were 603 iBECs fluorescing red out of 30,844 total iBECs detected after 24 h. This could indicate that small EVs labeled with Cell Tracker red are co-localizing with iBECs after 24 h, however there were not available to fully transcytose across the iBECs into the lower chamber. It is important to note that the red fluorescent signal detected also could indicate that small EVs did not cross the BBB model since they are co-cultured with iBECs after 24 h however, it could also indicate the Cell tracker red dye diffused inside the iBECs. It could be also a possibility that these small EVs might be degraded by lysosomes in the cytoplasm of iBECs, resulting in the Cell tracker red dye being released free into the cytoplasm of iBECs[342,343]. To answer these, other experiments need to be performed such as determining the percentage of leakage of dye, using another dye to compare results, and/or measuring the permeability of radiolabeled small molecules (^{14}C-Sucrose, ^{3}H-Cyclosporine) in parallel with small EV permeability. Moreover, the observed association between the physical characteristics of our small EVs (specifically hCMEC/D3 derived small EVs) and their ability to breach the BBB model (4% uptake) indicates an important factor that should be taken into consideration for further studies. Despite this percentage of uptake being promising, the caveat regarding the collection of upper/lower chamber media is that it was only performed twice (n=2, **Figure 14C**) due to the COVID-19 shutdown and challenges obtaining these inserts from the NRC-HHT facility.

Furthermore, iBEC cells from the transwell inserts (upper chamber) were collected after 72 h and RT-qPCR was performed (**Figure 15A**). iBECs showed ~74% reduction in the levels of α-synuclein mRNA treated with HEK293T-derived small EVs packaged with α-synuclein siRNA compared to ~62% when small EVs from the human endothelial cells were used. As well, SH-SY5Y neuron-like cells, seeded on the far side of the BBB from the lower chamber were collected after 72 h and RT-qPCR was performed (**Figure 15B**). Human immortalized hCMEC/D3 derived small EVs packaged with α-synuclein siRNA showed an approximately 40% α-synuclein knockdown at the mRNA level. In contrast, HEK293T-derived small EVs did not show any reduction in α-synuclein mRNA levels in neuron-like cells. This data indicates that HEK293T-derived small EVs can reduce α-synuclein mRNA level better than hCMEC/D3-derived small EVs in iBECs, however previous data have shown that hCMEC/D3 derived small EVs can cross the iBECs in a larger percentage (**Figure 14C**).

One interpretation here could be the possibility that these small EVs derived from hCMEC/D3 express some specific endothelial receptors that enhance their crossing of the iPSC BBB model better than the HEK293T derived small EVs. However, the fate of small EVs inside the cytoplasm of iBECs following internalization, is unknown. It is possible there are different mechanisms for the two population of small EVs – (i) HEK293T cell-derived small EVs which fuse and deliver its cargo to iBECs; (ii) hCMEC/D3 cell-derived small EVs can undergo receptor-mediated transcytosis and be recycled across the intact BBB to deliver its cargo to differentiated SH-SY5Y cells on the lower chamber. This could be a viable interpretation since the reduction in α-synuclein mRNA levels in iBECs is higher than in differentiated SH-SY5Y cells for HEK293T derived small EVs. Therefore, these populations of small EVs can be internalized by iBECs at lower rates (2%), can release their siRNA cargo into the cytoplasm, and can produce a functional change. However, it was not able to fully transcytose since there was negligible reduction in α-synuclein mRNA levels in differentiated SH-SY5Y cells. While the other population of small EVs derived from hCMEC/D3 cells, were able to successfully cross the intact iBEC cell barrier (4%) after 24 h. These small EVs were internalized by differentiated SH-SY5Y cells and efficiently deliver their siRNA cargo into the cytoplasm to lower α-synuclein mRNA levels. This point raises quite a few questions i) is the fusion machinery on iBEC cells saturated at some point? ii) if so, when do they start to cross the BBB? iii) are there specific BBB receptor/ligand interaction that enhances uptake? iv) if so, how can they help the small EVs to be delivered across the intact BBB? Studies have reported that modification in the surface proteins of small EVs increased their uptake into the BBB. One example of the modification was by engineering small EVs to express a small peptide in their surface, neuron-specific RVG, which increased delivery of RVG-small EVs to the brain[120,121]. Our data adds to the growing body of evidence that a specific type of small EVs could cross the intact BBB and transfer its cargo to its target cell on the far side of the BBB.

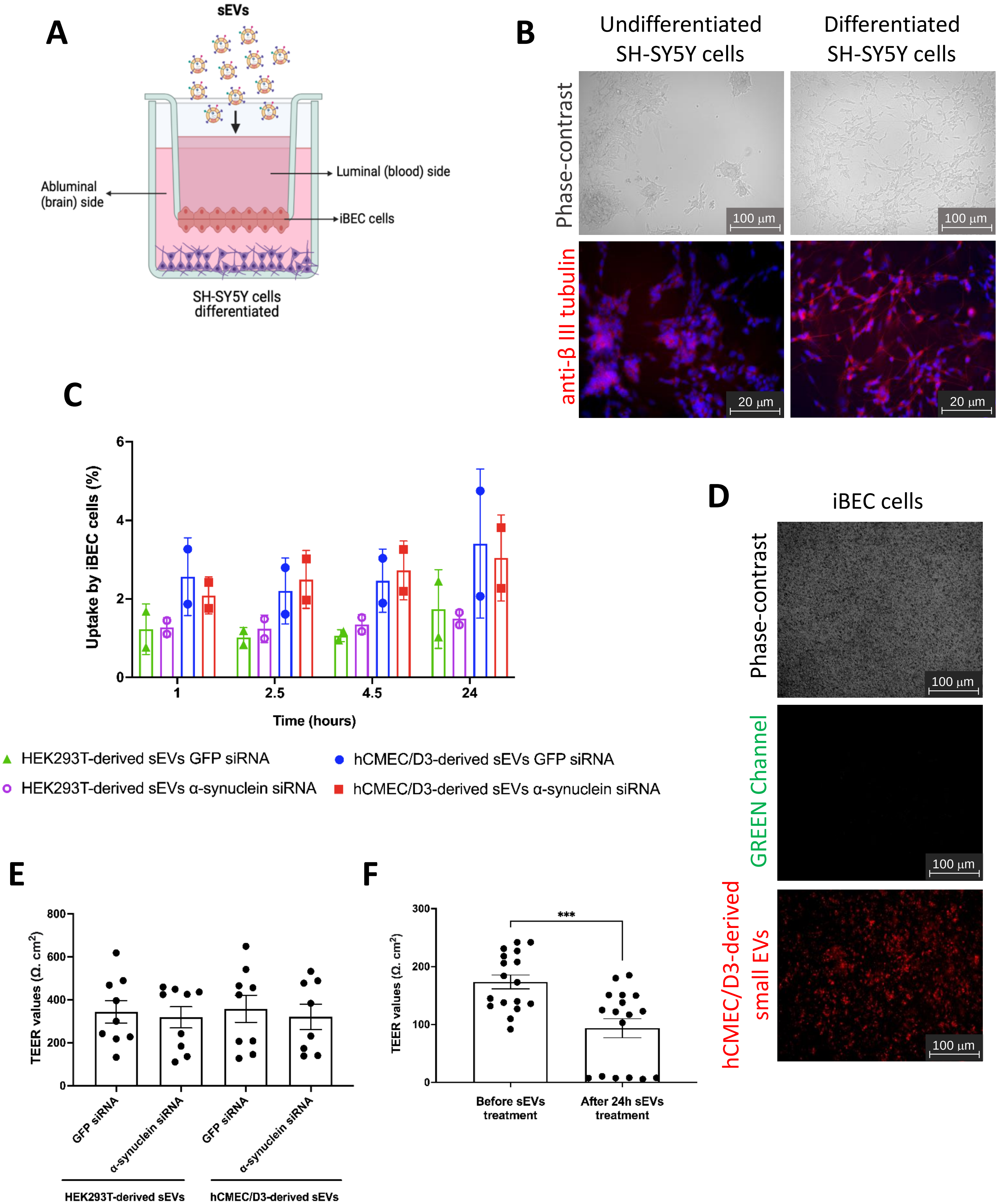
A
sEVs
Abluminal (brain) side
Luminal (blood) side
iBEC cells
SH-SY5Y cells differentiated
B
Undifferentiated SH-SY5Y cells
Differentiated SH-SY5Y cells
Phase-contrast
anti-β III tubulin
100 µm
20 µm
C
Uptake by iBEC cells (%)
Time (hours)
1
2.5
4.5
24
HEK293T-derived sEVs GFP siRNA
HEK293T-derived sEVs α-synuclein siRNA
hCMEC/D3-derived sEVs GFP siRNA
hCMEC/D3-derived sEVs α-synuclein siRNA
D
iBEC cells
Phase-contrast
GREEN Channel
hCMEC/D3-derived small EVs
100 µm
E
TEER values (Ω. cm²)
GFP siRNA
α-synuclein siRNA
HEK293T-derived sEVs
hCMEC/D3-derived sEVs
F
TEER values (Ω. cm²)
***
Before sEVs treatment
After 24h sEVs treatment

Figure 14. α-synuclein knockdown efficiency and uptake in the *in vitro* human BBB model using α-synuclein siRNA packaged small EVs. (A) Overview of the NRC *in vitro* human BBB model which consists of endothelial cells (iBECs) generated from proprietary amniotic fluid-derived induced pluripotent stem cells (iPSCs) (Illustration created using BioRender). It is assembled where iBECs are seeded in the upper chamber (luminal side) and human neuron-like cells (SH-SY5Y) in the lower chamber (abluminal side) of a 24-well transwell system. **(B)** Phase-contrast image by ZOE Cell Imager and immunofluorescence image stained with anti-β III tubulin antibody, illustrating undifferentiated and differentiated SH-SY5Y cells treated 7 days with 10 µM retinoic acid (RA). **(C)** α-synuclein siRNA packaged small EVs were isolated from hCMEC/D3 cells and HEK293T cells using Tangential Flow Filtration (TFF) system, labeled with CellTracker^{TM} Red CMPTX dye and added to the upper chamber. At 60 minutes, 2:30 h, 4:30 h, and 24 h, media from the upper and lower chambers was collected and the fluorescent values were measured by Clariostar microplate reader. The percentage uptake was calculated by using a std curve and plotting the lower chamber values (n=2). **(D)** Phase-contrast image and fluorescence channels by ZOE Cell Imager, illustrating small EVs labeled with Cell tracker red co-cultured with iBEC cells in the upper chamber transwell insert. **(E)** Transendothelial electrical resistance (TEER, Ωcm^2) of confluent iBECs monolayer transwell inserts were measured prior to treating the small EVs using CellZscope apparatus (Nanoanalytics). **(F)** Comparation of TEER values before small EV treatment vs. treatment of small EVs after 24 h. sEVs – small extracellular vesicles. For statistics, an unpaired t-test was used. Data are presented as mean ± SEM. *=$p<0.05$, **=$p<0.01$, ***=$p<0.001$, ****=$p<0.0001$. Scale bar, 100µm.

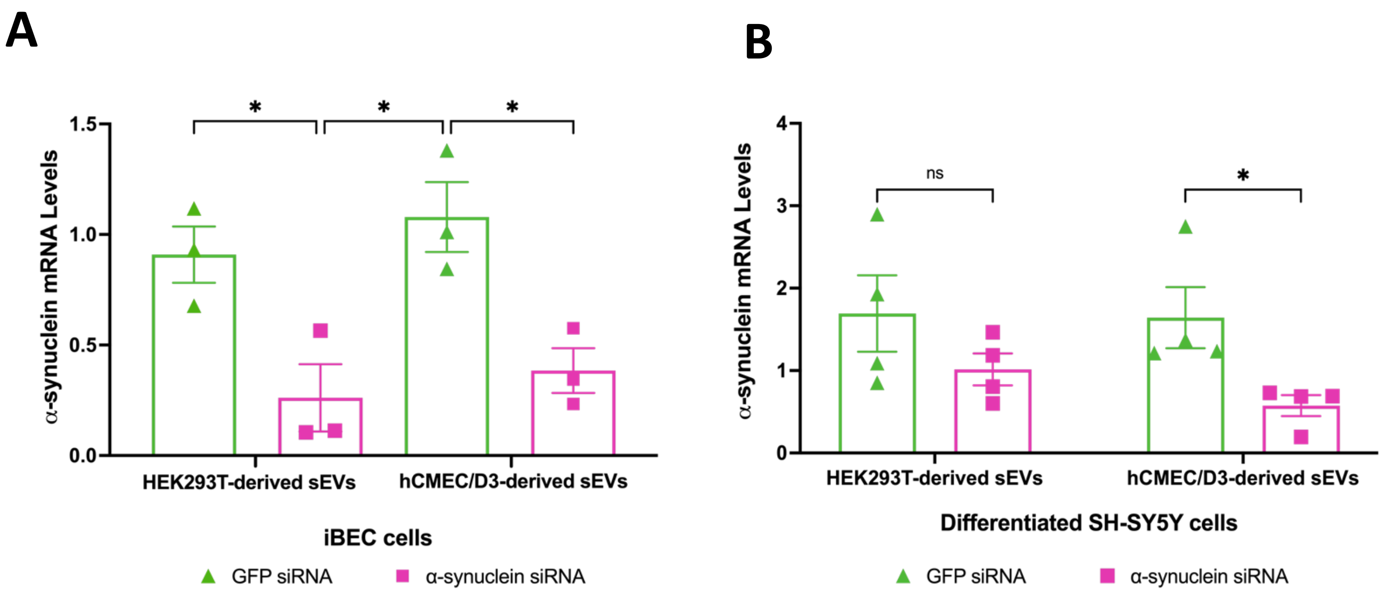

Figure 15. Small EVs packaged with α-synuclein siRNA integrated in the pre-miR-451 backbone efficiently deliver siRNA to neuron-like cells in the *in vitro* human iPSC BBB model. α-synuclein siRNA packaged small EVs were isolated from hCMEC/D3 cells and HEK293T cells using Tangential Flow Filtration (TFF) system, labeled with CellTracker^{TM} Red CMPTX dye and added to the upper chamber. **(A)** iBEC cells (n=3) and **(B)** differentiated SH-SY5Y cells treated 7 days with 10 µM retinoic acid (RA) (n=4) were collected after 72 h and α-synuclein mRNA levels were measured by RT-qPCR. Small EVs containing GFP siRNA and α-synuclein siRNA were normalized to the non-treated sample. sEVs – small extracellular vesicles. For statistics, a one-way ANOVA with Tukey's multiple comparison test was used. Data are presented as mean ± SEM. *=p<0.05, **=p<0.01, ***=p<0.001, ****=p<0.0001.

1.25 *In vivo* biodistribution of small EVs in mice

For *in vivo* analysis of small EV distribution, intravenous (IV) injection of small EVs has been the preferred (~78%) administration route reported in small EV biodistribution publications[344]. The main aim here was to compare two different routes of administration, a single bolus intravenous (IV) or intra-carotid (ICD) injection, using small EVs produced by immortalized human brain endothelial hCMEC/D3 cells. Ultimately, this was done in order to assess whether the route of administration can influence the biodistribution patterns in mice. Several studies have reported that small EVs frequently accumulate in the liver, spleen, and kidney tissues after IV injection. Therefore, the rationale to test the ICD route of administration was to enhance the amount of small EVs crossing the BBB and ultimately reaching the brain due to the fact that the internal carotid artery supplies blood to the brain, which appears at the point in the neck (intracarotid) where the common carotid arteries divide[345,346]. Thus, ICD injection bypasses the liver and kidney tissues and first goes to the brain which can potentially increase the amount of small EVs reaching the BBB. As mentioned previously, it has been reports that there are difference in the biodistribution of small EVs according to their producer cells. Therefore, human brain endothelial derived small EVs were used since they express BBB phenotypes and through homotypic interactions can potentially enhance their transmigration across the BBB.

HCMEC/D3-derived small EVs were labeled with CF770-SE dye and injected via IV or ICD. This near-infrared fluorescent cyanine-based succinimidyl ester dye (CF770-SE, Ex/Em 770/797), also known as N-hydroxysuccinimide (NHS) esters, is amine-reactive, where its succinimidyl ester group reacts with an amine group on proteins to form a stable amide linkage on the surface of the small EV. Additionally, this CF770-SE dye produces light in the near-infrared

(IR) wavelength which makes it highly sensitive and provides strong tissue penetration for *in vivo* fluorescence imaging.

After a single bolus IV injection, a whole-body scan of mice (dorsal and ventral) at various time points using IVIS Lumina III was performed to localize CF770-label. After 6 h, mice were saline-perfused and various tissues (brain, heart, lung, liver, kidney, spleen and lymph nodes) were collected for ex-vivo imaging in order to detect the biodistribution by quantifying the fluorescent signals from each organ. A more detailed experiment plan is shown in **Figure *7***. As shown in **Figure *16*** and **Figure *17***, there was no statistically significant difference between the two routes of administration following the analysis of the whole-body scans. In both routes of administration, small EVs were predominantly localized in the liver and kidneys, indicating a rapid uptake and excretion into the urine (**Figure *16*A** and **Figure *17*A**). This data correlates with previous biodistributions studies where the most frequent accumulation of small EVs after IV injection were also reported to be in the liver, spleen and kidney[347]. Consequently, the rationale was to reduce the amount of small EVs that distribute to the liver and kidney, and increase the delivery to the brain[346]. Therefore, the ICD route of administration of small EVs was attempted. Unexpectedly, the biodistribution of small EVs appeared to be unchanged by the ICD route of administration despite it has direct access to the carotid artery (a major blood vessel in the neck) which supplies blood to the brain, neck, and face. Additionally, this data shows that small EVs get cleared relatively rapidly and enter the brain in small quantities. This data suggests that the difference in the first pass of circulation using ICD route (direct access to the carotid artery) did not matter since these small EVs did not get cleared any more rapidly or did not enter the brain more quickly. Relatively, they followed a very similar distribution as the IV route. Another interpretation could be that even though small EVs get cleared rapidly from the system, small EVs still get into brain in small quantities specifically in the first minutes after ICD or IV injection. This could indicate that the uptake rate in which the small EVs cross the BBB potentially becomes saturated and ultimately slows down compared to their rapid clearance out of the system.

After 6 h, organs were saline-heparin perfused and scanned ex-vivo (**Figure *16*B** and **Figure *17*B**). The total radiant efficiency of each organ was quantified, indicating the same results as before that the liver ($9 \times 10^{10}/2 \times 10^{11}$) and kidney ($8 \times 10^{10}/1 \times 10^{11}$) were the main organs of IV and ICD distribution, respectively. However, looking into other organs beside these two, the amount of small EVs detected in the brain was around 2×10^9 in IV route and 8×10^8 ICD route of administration (**Figure *16*C and Figure *17*C**)which indicates that there were some quantities of small EVs detected in the brain. However, these detected small EVs in the brain do not necessarily indicate that small EVs have indeed crossed the BBB. There is a possibility that small EVs have accumulated in the blood vessels and the radiant efficiency calculated represents the small EVs surrounding the brain without crossing the BBB. In order to confirm the delivery of these small EVs across the BBB, additional assays can be performed including confocal microscope to see small EV distribution inside the brain and the target gene reduction in a transgenic mouse model to confirm small EV delivery across the BBB.

In addition, five lymph nodes (mandibular, axial/brachial, inguinal, mesenteric, and popliteal) organs were also quantified in both routes of administration. The objective of the ex-vivo scan of the lymph nodes was to observe the small EV distribution in the lymphatic system since lymph circulates through the body in a similar way to blood. The mesenteric lymph node was the one with the highest radiant efficiency ($\sim 4 \times 10^8$) detected in both routes of administration. This was not unexpected since this lymph node is located near the mesentery membrane which attaches the intestine to the abdominal wall and holds it in place. This data suggests that small EVs can be detected in the lymphatic system and correlates with previous results where they are predominantly localized in the small intestines, liver and kidneys[347]. Overall, these results demonstrate that despite the difference in routes of administrations, small EVs accumulated largely in the liver, spleen, small intestines and kidneys; and only a small amount of small EVs were detected in the brain.

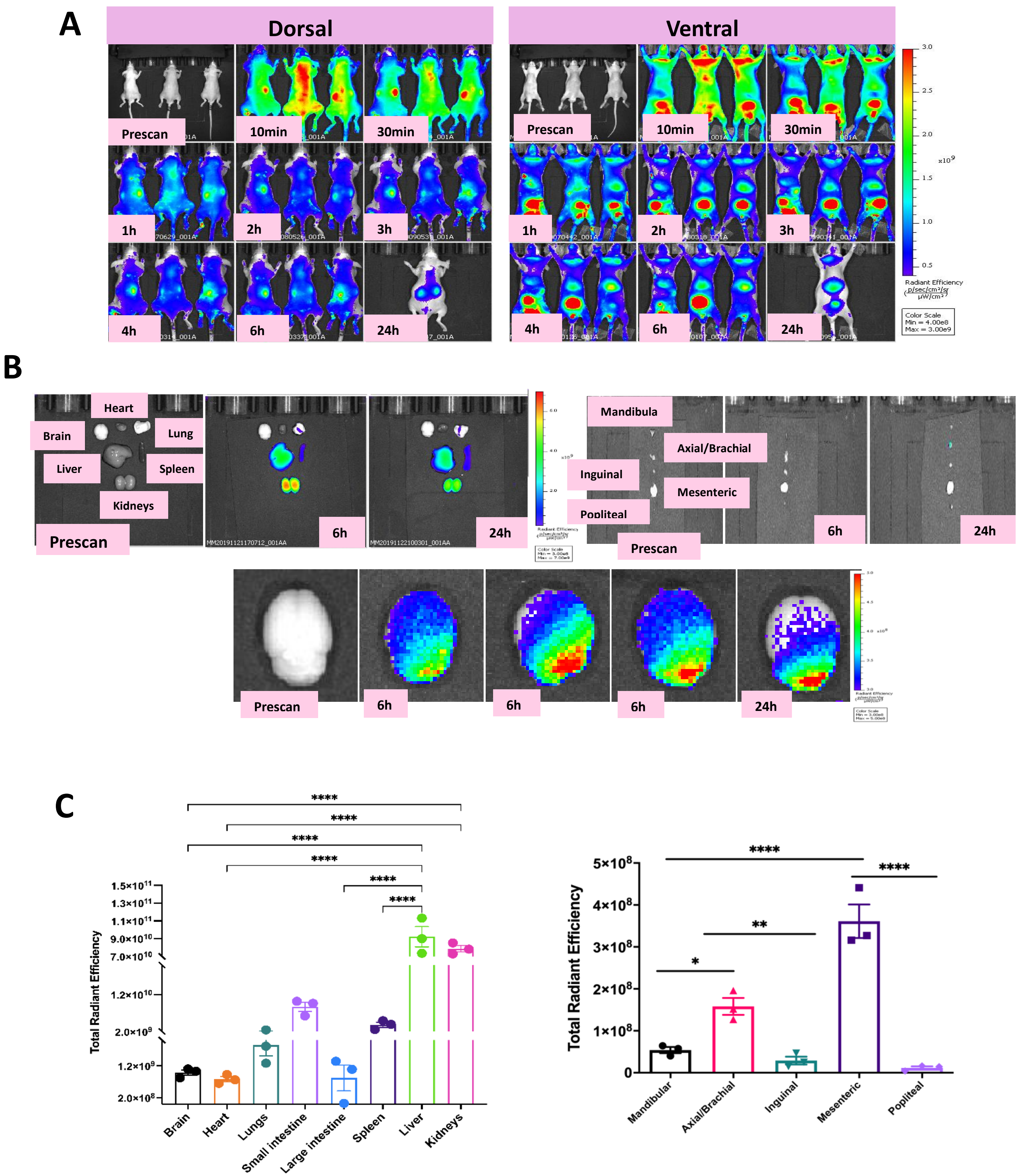
A
Dorsal
Ventral
Prescan
10min
30min
1h
2h
3h
4h
6h
24h
Radiant Efficiency
Color Scale
Min = 4.00e8
Max = 3.00e9
B
Brain
Heart
Lung
Liver
Spleen
Kidneys
Prescan
6h
24h
Mandibula
Axial/Brachial
Inguinal
Mesenteric
Popliteal
C
Total Radiant Efficiency
Brain
Heart
Lungs
Small intestine
Large intestine
Spleen
Liver
Kidneys
Mandibular
Axial/Brachial
Inguinal
Mesenteric
Popliteal

Figure 16. Biodistribution of CFF70-labeled small EVs from human immortalized cerebral endothelial after a single bolus IV injection in CD-1 mice. Human immortalized cerebral endothelial hCMEC/D3-derived small EVs were labeled with CF770 dye and free dye was removed using Zeba Spin desalting columns (7 kDa, Thermo Scientific) before administration. **(A)** Imaging (dorsal and ventral) parameters using excitation-740 nm and emission-790 nm in IVIS Lumina III at various point times (pre-scan, 10 min, 30 min, 1 h, 2 h, 3 h, 4 h, 6 h, 24 h). **(B)** Ex-vivo imaging of organs (brain, heart, liver, lung, spleen, kidney), and lymph nodes in IVIS Lumina III at various point times. **(C)** Quantification of ex vivo imaging, total radiant efficiency of organs at average of 3 mice for 6 h. All mice were males at 6-8 weeks, n=4, and naïve mice (n = 1) was used for pre-scan of ex-vivo organs (saline-perfused). For statistics, a two-way ANOVA with Tukey's multiple comparison test was used. Data are presented as mean ± SEM. $*=p<0.05$, $**=p<0.01$, $***=p<0.001$, $****=p<0.0001$.

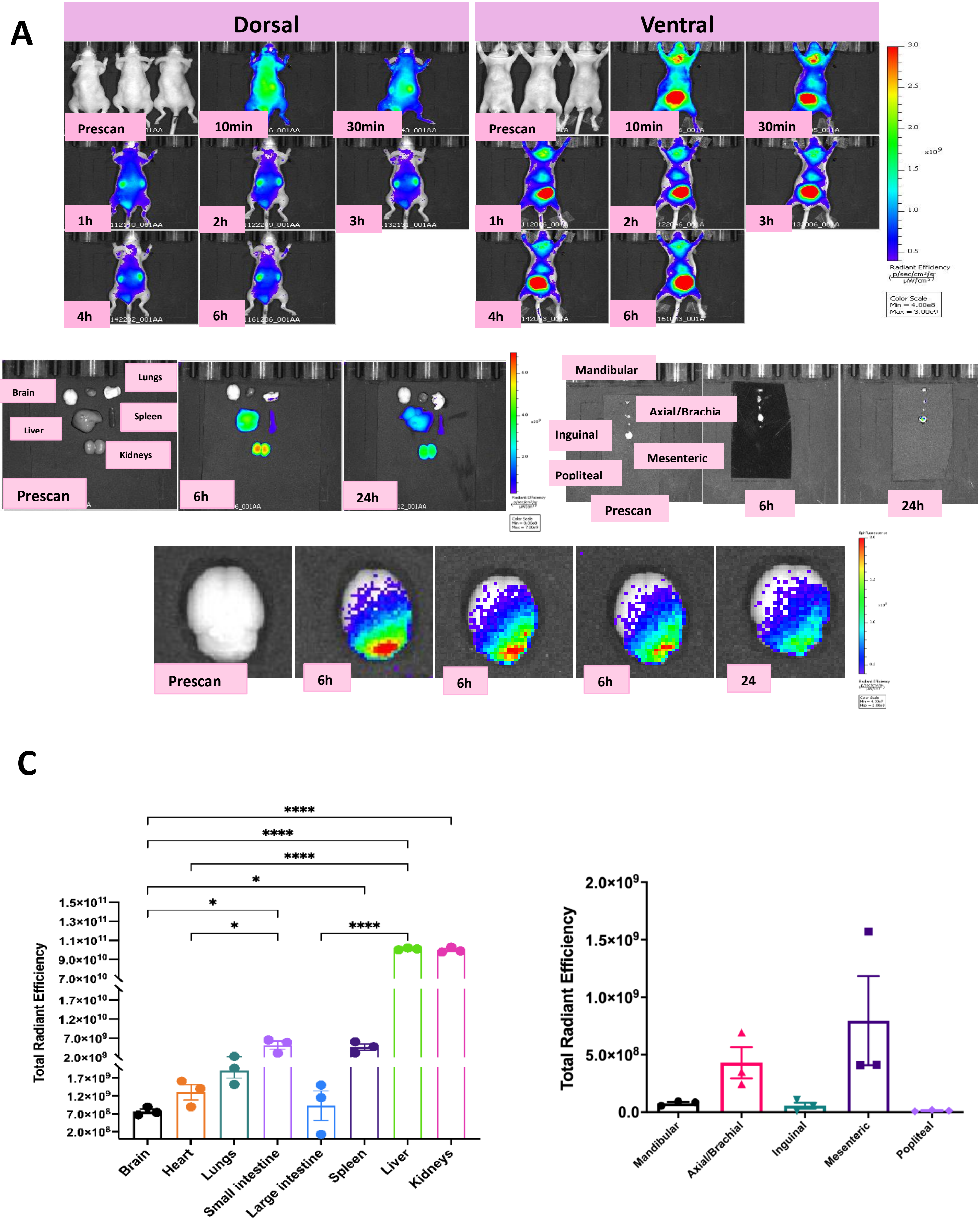

A
Dorsal
Ventral
Prescan
10min
30min
1h
2h
3h
4h
6h
Radiant Efficiency
Color Scale
Min = 4.00e8
Max = 3.00e9
B
Brain
Lungs
Spleen
Liver
Kidneys
Prescan
6h
24h
Mandibular
Axial/Brachia
Inguinal
Mesenteric
Popliteal
24
C
Total Radiant Efficiency
Brain
Heart
Lungs
Small intestine
Large intestine
Spleen
Liver
Kidneys
Mandibular
Axial/Brachial
Inguinal
Mesenteric
Popliteal

Figure 17. Biodistribution of CFF70-labeled small EVs from human immortalized cerebral endothelial after a single bolus ICD injection in CD-1 mice. Human immortalized cerebral endothelial hCMEC/D3-derived small EVs were labeled with CF770 dye and free dye was removed using Zeba Spin desalting columns (7 kDa, Thermo Scientific) before administration. **(A)** Imaging (dorsal and ventral) parameters using excitation-740 nm and emission-790 nm in IVIS Lumina III at various point times (pre-scan, 10 min, 30 min, 1 h, 2 h, 3 h, 4 h, 6 h, 24 h). **(B)** Ex-vivo imaging of organs (brain, heart, liver, lung, spleen, kidney), and lymph nodes in IVIS Lumina III at various point times. **(C)** Quantification of ex vivo imaging, total radiant efficiency of organs at average of 3 mice for 6 h. All mice were males at 6-8 weeks, n=4, and naïve mice (n = 1) was used for pre-scan of ex-vivo organs (saline-perfused). For statistics, a two-way ANOVA with Tukey's multiple comparison test was used. Data are presented as mean ± SEM. *=$p<0.05$, **=$p<0.01$, ***=$p<0.001$, ****=$p<0.0001$.

DISCUSSION

The present study confirms and extends a previous study by Reshke et al. on the use of small EVs containing specific siRNA integrated in the pre-miR-451 backbone to selectively induce the downregulation of a gene. Firstly, we were able to successfully integrate siRNA against α-synuclein into the re-programmed pre-miR-451 backbone and produce stable cell lines, namely human brain endothelial cells (hCMEC/D3) and human embryonic kidney cells (HEK293T), expressing this construct. Using this strategy, we were able to isolate small EVs from both stable cell lines and reduce the expression of endogenous α-synuclein in differentiated neuron-like cells by direct treatment of small EVs in culture or crossing *in vitro* iPSC BBB transwell model. This data suggests that small EVs packaged with α-synuclein siRNA integrated in the pre-miR-451 backbone can sufficiently deliver and reduce α-synuclein in neuron-like cells at the mRNA level. We have also demonstrated that small EVs isolated from two different cell types, hCMEC/D3 and HEK293T, showed BBB crossing in the *in vitro* iPSC BBB transwell model, however there were significant differences in percentage uptake across the iBECs. As well, we reported a reduction of endogenous α-synuclein mRNA expression in iBECs for HEK293T-derived small EVs, but they did not deliver its cargo to neuron-like cells in the far side of the lower chamber of the *in vitro* iPSC BBB model; while hCMEC/D3-derived small EVs were able to silence α-synuclein gene expression in neuron-like cells. We also sought to determine the *in vivo* biodistribution of CF770-labeled hCMEC/D3-derived small EVs using two different routes of administration, IV and ICD, for future exploration of its delivery to the CNS. Our data adds to the growing evidence that a specific type of small EVs could cross the intact BBB and transfer its cargo to its target cell on the other side of the BBB.

Small EVs are promising nanocarriers for delivering therapeutics to the brain due to their biocompatibility, low immunogenicity, special tissue target ligands, stability, and long circulation half-life in normal conditions[148]. Previous studies confirmed the transfer of endogenous siRNA, mRNA or miRNA from isolated small EVs to target cells in a biologically active form resulting in a change in cellular function[150,206]. This led to the suggestion that small EVs are internalized by target cells and escape from the endo-lysosomal degradation ultimately delivering their cargoes into the cytoplasm of target cells. Therefore, there has been an increased interest for the development of small EVs as delivery vehicles for exogenous nucleic acid-based cargoes, specifically siRNA. Despite the tremendous excitement for the development of small EV-based therapeutics, their clinical development is hampered by the lack of reliable methods for packing therapeutics into them. Current methods involve packing small EVs with therapeutics after their isolation from parental cells. The most common packing strategies include a) passive incubation with isolated small EVs or b) active packing with transfection and electroporation. Studies using electroporation reported <0.1% siRNA packing, attributed to siRNA precipitation[121]. Similarly, packing cholesterol-conjugated siRNA resulted in siRNA incorporation predominantly on the surface of small EVs resulting in inefficient delivery[201]. Therefore, increased intracellular delivery of siRNA can only be achieved by incorporating it inside intact small EVs. Many studies that have observed an effect with small EVs packaged with siRNA could be due to the high physiological doses of small EVs or excessive amounts of siRNA packed onto small EVs[120,142,200]. Therefore, whether small EVs are actually efficient at delivering their RNA cargo into target cells has not been fully tested beside reports from our lab[199]. The main roadblock in advancing small EVs-based therapy into the clinical settings is the lack of efficient, robust, and scalable methods for packing siRNA molecules into small EVs.

We were able to overcome this challenge by packing small EVs during their biogenesis which required hijacking of the endogenous packing machinery of the parental cells in order to produce small EVs that contain specific siRNA molecule. We first tested the efficiency of small EVs in delivering its siRNA cargo into target cells in culture. The data presented in this thesis used two independent methods to demonstrate that small EVs packaged with siRNA targeting α-synuclein in the pre-miR-451 backbone efficiently reduced both endogenous α-synuclein mRNA and protein expression levels in neuron-like SH-SY5Y cells (**Figure *12*B, C and Figure 15**). Then, using absolute quantification of siRNA and small EVs, we calculated the amount of α-synuclein siRNA molecules per small EVs required to silence α-synuclein mRNA levels. Our results demonstrated that small EVs containing 1,240 copies of α-synuclein siRNA molecules per cell were sufficient to silence ~60-70% endogenous α-synuclein mRNA expression in target cells. This correlates with previous studies that have established that between 300 – 2,000 copies of a specific siRNA are required to observe a specific gene knockdown in cultured cells[184–186]. Then, if our small EVs at a dose of 1,240 siRNAs per cell can silence a target (**Figure *13*A**), these small EVs would appear to deliver a large proportion of their siRNA cargo into the cytoplasm, compared with ~0.05 - 1% of siRNA reported for LNPs[184,186,196]. This provides evidence that small EVs are highly efficient delivery nanocarriers and have the ability to achieve biological functions in target tissues.

In addition, the average number of α-synuclein siRNA molecules per small EV was determined to be around 0.0248. This number of siRNA molecules per small EV is lower compared to other studies. An absolute copy number average of one miRNA per EV to one miRNA per 100 EVs as well as one specific miRNA copy per 10^6 small EVs has been reported[207,208,348]. Reshke et al. also reported from the pre-miR-451 hairpin, siRNA targeting GFP or SOD1 were enriched up to one copy per small EV on average[199]. It is possible that the observed lower copy number in our data was influenced by RNA-binding proteins (RBPs). RBPs have been observed to be associated in the transit of most RNAs from the nucleus to specific cellular localizations, as well as modulating RNA packaging into EVs[202,349]. Thus, there are more than 500 RBPs in mammalian cells[350] and about 25% of RBPs content has been reported to be presented in EVs[203]. Therefore, it could be an assumption that the pre-miR-451 containing α-synuclein siRNA has a sequence which is bound by a RBP which retains it in the cytoplasm and limits its packaging into small EVs. This further suggests the possibility that RBPs regulate these siRNAs by retaining them in the cytoplasm of cells, ultimately leading to their low number observed in small EVs. However, evidence is lacking regarding the distribution of these RBPs in small EVs population and their specific role in loading RNAs into these vesicles[351–353]. To our understanding, there are also not many studies illustrating the absolute number of siRNA molecules inside small EVs[207,208], and our data provides a contribution to this field. Of note, several studies have described subpopulation of small EVs with different surface markers and size[144,354,355]. Therefore, another possibility could be that one subpopulation of small EVs is more efficient in delivery their RNA content into the cytoplasm while other subpopulation of small EVs get degraded by lysosomes inside the cell. As a result, it is important to consider the absolute copy number of specific siRNA per small EVs to better determine the proper therapeutic siRNA dose required to silence a specific target gene and to understand the endosomal pathway of siRNAs in the cytoplasm of target cells.

The BBB is composed of a protective layer of cells that shields the brain from toxins and infectious agents, but it also restricts the entry of almost all therapeutic, including protein and nucleic acid-based medicines and ~98% of small molecule drugs. Crossing the BBB and delivering therapeutics to the CNS at therapeutic levels is a major challenge in the treatment of neurodegenerative disorders, including PD. Current attempts to silence α-synuclein require 11 h infusions into the spinal cord (antisense oligonucleotide, Ionis Pharmaceuticals)[356] or direct injection of adeno-associated virus into the brain (Voyageur Therapeutics)[357]. Finding a delivery approach that is non-invasive and allows for maximum effectiveness is important for successful treatments in brain. To date, the main approach to deliver therapeutics across the BBB is to utilize endogenous transport mechanisms. Small EVs have been shown to express a selected number of parent cell-derived surface proteins[358,359], some of which are tissue specific relating to the cell source. In this study, we prepared and utilized small EVs derived from hCMEC/D3 and HEK293T cells. The hypothesis was that small EVs derived from brain cells would more likely display brain-specific surface molecules for a more effective delivery across the *in vitro* BBB model.

Even though the amount of small EVs produced by brain cells has been reported to be slightly variable[358,360], the size and concentration of small EVs derived from hCMEC/D3 were consistent throughout this study, shown using Nanoparticle Tracking analysis (NTA) on the Zetaview® (**Figure 9**). Our data demonstrated that hCMEC/D3-derived small EVs had greatly enhanced internalization by iBECs, around 4% of small EVs derived hCMEC/D3 cells were detected in the abluminal side of the transwell system after 24 h; substantially more than small EVs from HEK293T (2%). A major limitation of our data is that these calculations are based on the detection of fluorescent signal from Cell tracker dye alone at different point times. However, we observed that iBECs showed a ~74% reduction in α-synuclein mRNA levels using HEK293T-derived small EVs containing α-synuclein siRNA, while these small EVs did not reduce α-synuclein mRNA levels in the neuron-like cells seeded in the lower chamber. In contrast, hCMEC/D3-derived small EVs containing α-synuclein siRNA integrated in the pre-miR-451 backbone showed approximately 40% α-synuclein knockdown at the mRNA level in neuron-like cells at the far side of the BBB (lower chamber). Therefore, small EVs (hCMED/D3) were available to transcytose across the iBECs in order to reach the abluminal side and deliver its content to neuron-like cells in the lower chamber, while the HEK293T-derived small EVs did not. This suggests that small EVs from both cell lines were internalized by iBECs but their transcytosis mechanism across the barrier formed by iBECs could possibly be different. Further experiments need to be performed to solidify these findings such as inhibiting or labeling specific markers of early/late endosomes to better understand intracellular trafficking of small EVs in iBECs. As well as, tracking and locating a specific siRNA sequence packaged into small EVs inside the iBECs using fluorescence in situ hybridization (FISH). Additionally, this *in vitro* transwell model does not include astrocytes and pericytes (NVU cells); therefore, it has a limited application, lacking both the BBB's physical structure and brain microenvironment. Therefore, the reliability of these results can be measured using the combination of other models including microfluidic BBB models and/or brain-on-a-chip models. Notably, small EVs even from the same cell type can be heterogeneous and have differences in size and surface membranes proteins[361]. Therefore, multiple mechanisms may be involved in small EVs uptake at the BBB.

As mentioned in previously, there are different transport routes across the BBB (**Figure 2**). Our data alone is not sufficient to specifically determine a route for the transport of small EVs through the *in vitro* BBB model. Therefore, with the incorporation of previously published studies into our results, we will discuss the possible transport routes of HEK293T- and hCMEC/D3-derived small EVs across the iBECs.

Firstly, the percentage uptake of HEK293T-derived small EVs was lower compared to hCMED/D3-derived small EVs, as well as HEK293T-derived small EVs did not show reduction of endogenous α-synuclein in the neuron-like cells seeded in the lower chamber. This could indicate the possibility that HEK293T-derived small EVs did not passively diffuse through TJs and cross the iBECs via paracellular diffusion route. Interestingly, it has been showed that under inflamed conditions (addition of activated TNF-α, a proinflammatory cytokine) mimicking stroke-like pathology, the small EVs can cross the *in vitro* BBB by paracellular diffusion route[162]. Using the same model, they showed that in the absence of TNF-α, small EVs were not found in the abluminal side of the model, indicating the effects of CNS diseases in the transport route or efficiency of small EV transport through the BBB[162]. Further, it has been reported that TNF-α significantly downregulates BBB specific surface markers including VE-cadherin, ZO-1, and claudin-5 and translocates them from on the luminal side to the cytoplasmic side of BECs[362]. It has yet not been reported that small EVs can cross BBB through the paracellular transport route under normal conditions[162].

Another possible transport mechanisms that could be involved is receptor-mediated transcytosis (RMT). Small EVs play an important role in cell-to-cell communication. Therefore, the surface of small EVs has been demonstrated to be enriched in cell-targeting adhesion molecules (e.g., tetraspanins and integrins), antigen-presenting molecules (e.g., major histocompatibility complex class I and II), and membrane trafficking proteins[363]. Beside these common surface markers, small EVs can also carry cell type specific surface proteins found on the plasma membrane of the cell source. Noteworthy, the differential transcytosis observed in **Figure 14 and Figure 15** could possibly be due to the presence of specific receptors on small EVs derived from hCMEC/D3 mediating homotypic interactions via binding to ligands on iBECs compared to HEK293T-derived small EVs. This could suggest a possible RMT pathway. This assumption can be supported by previous observation that brain endothelial small EVs contained several receptors which has been reported to carry BBB specific surface markers including transferrin receptor (TfR), the low-density lipoprotein (LDL) receptor related proteins (LRP), cell cycle control protein

50A (TMEM30A/CDC50A), and Fc-Binding Proteins (e.g., FcγBP)[103,364–366]. As well, this assumption correlates with previous studies where the difference in the distribution of small EVs was dependent on their cellular origin[347].

Even though, the transcytosis mechanisms deployed by small EVs to traffic through the BBB is still not clear, there have been a couple of studies suggesting the potential of small EVs to use the RMT pathway. For instance, a study showed macrophage-derived small EVs internalized by hCMED/D3 cells *in vitro* in a saturable manner using various pathways including clathrin-/caveolae-mediated transcytosis, implying a possible RMT pathway[367]. These macrophage-derived small EVs inherited integrin lymphocyte function-associated antigen 1 (LFA-1) from their parental cells, a protein that interacts with endothelial carbohydrate-binding C-type lectin receptors (ICAM-1) and regulates their internalization across the BBB[367]. More importantly, the LFA-1 and ICAM-1 also mediated cellular uptake of these macrophage-derived small EVs in hCMEC/D3 cells [367]. This indicates a potential mechanism of endocytosis mediated by the interaction of LFA-1 and ligand ICAM-1, which have been shown to be expressed on macrophages-derived small EVs and hCMEC/D3 cells, respectively[162]. Additionally, an *in vitro* study showed that the inhibition of clathrin-dependent endocytosis by pre-treatment of brain endothelial cells with chlorpromazine and a Cdc42/Rac1 GTPase inhibitors, significantly decreased the uptake of breast cancer-derived small EVs[160]. In addition, these authors further confirmed these findings by showing that the small EVs partially colocalized with transferrin, a marker of clathrin-dependent endocytosis. Kuroda et al. investigated the mechanism of binding and internalization of PKH67-labeled small EVs derived from brain-metastatic cancer cell line (SK- Mel-28) in hCMEC/D3 cells. CD46 was determined to be a major receptor for SK-Mel-28 derived small EVs *in vitro* uptake[368], indicating a RMT pathway.

All these studies and our data suggest that the mechanism of uptake of small EVs by the brain is a selective process which potentially is dependent on the different properties of small EVs, specifically on the interaction between surface receptors in small EVs and ligands in BECs. However, the specific mechanism(s) of such transport are not well understood and the evidence regarding the interaction of small EVs with the BBB has limitations. Some limitations of these studies mentioned above include: (i) lack of *in vivo* evidence, (ii) lack of proper labeling methods to track small EVs trafficking (e.g., PKH, a lipophilic dye, can form self-aggregates and micelles leading to generation of a false signal of small EVs), (iii) quantification of the exact number of small EVs crossing the BBB and (iv) usage of cancer cell-derived small EVs. For example, it has been shown that cancer cell-derived small EVs can express tropism to their parental cells, limiting their interaction to non-cancer cells[369]. Then, if we consider the fact that receptor-mediated transcytosis (RMT) could be the only and significant approach for the delivery of small EVs through the BBB, therefore the direct interaction and affinity of small EVs to the luminal surface of BECs should be explored. There is a need to understand this field better and further studies will be needed to determine the significance of these findings.

As mentioned above, small EVs have the natural ability to cross the BBB. Several studies have reported that a large amount of systemically injected small EVs rapidly accumulate in the liver, spleen, lung, and kidney tissues[347]. This is due to quick renal clearance out of the system, extensive capillary networks and specialized immune cells with phagocytic receptors[370]. Therefore, we compared two different routes of administration, IV or ICD injection, using small EVs produced by hCMEC/D3-derived small EVs. We observed that despite the difference in routes of administrations, the biodistribution of small EVs for both routes, was largely to the liver, spleen, small intestines, and kidneys; and only a small amount of small EVs were detected in the brain. Although we observed a 4% uptake of hCMEC/D3-derived small EVs with a 40% endogenous α-synuclein reduction in neuron-like cells using an *in vitro* transwell system, a large fraction of small EVs were retained in the peripheral circulation following systemic injection into mice and ultimately cleared out of the system.

Recent studies have demonstrated that small EVs can be decorated with targeting ligands that specifically direct small EVs to the CNS and facilitate their crossing across the BBB. The pioneering study by Alvarez-Erviti et al. used engineered small EVs for brain-targeted delivery of BACE1 siRNA (electroporated into small EVs) to the CNS[120]. To do so, they enhanced the targeting properties of small EVs by transfecting the parental cells with a plasmid encoding Lamp2b, an EVs membrane protein, fused with RVG peptide. The parental cells produced engineered small EVs with the targeting peptide on their surface, resulting in an increased brain small EVs accumulation after IV administration. Hung et al. used an improved version of targeted small EVs by introducing a glycosylation motif (GNSTM) on their surface[371]. Engineered Lamp2b-GNSTM-RVG-small EVs isolated from parental cells showed an enhanced accumulation in brain tissue after IV injection compared to unmodified small EVs. Therefore, Lamp2b has been utilized to modify small EV surface by genetically modifying parental cells to treat different CNS disorders. Specifically, systemic administration of engineered RVG small EVs packed with miR-124 by electroporation showed an increase in cortical neural progenitors, resulting in protection against ischemic injury - in a mouse stroke model[372]. Accordingly, a phase 1/2 clinical trial testing mesenchymal stromal cell (MSC)-derived EVs packed with miR-124 is underway for the treatment of acute ischemic stroke (NCT03384433).

Beside using parental cell genetic modification, post-isolation approaches for small EV surface modification for CNS therapy have been implemented. As mentioned previously, targeting natural BBB receptor on the luminal surface of BECs is an alternative approach to increase transcytosis of small EVs across the BBB. Ye et al. conjugated a KLA-LDL on small EVs surface by using a simple coincubation with the peptide of interest[373]. LDL binds to LDL membrane-bound receptors present on the luminal site of the BECs promoting RMT while KLA is a pro-apoptotic peptide which promotes anti-glioma formulation. In this study, they showed that IV injected KLA-LDL conjugated small EVs encapsulated with methotrexate was observed to achieve an increase of these target small EVs in the glioma site ultimately showing an increased in the survival period of mice bearing a glioma. In another study, Tian et al., conjugated cyclo(Arg-Gly-Asp-D-Tyr-Lys) peptide c(RGDyK) on MSC-derived small EVs surface using orthogonal copper-free azide alkyde cyclo-addition (click chemistry)[374]. This peptide c(RGDyK) has a high affinity to integrin a_vb_3 which is overexpressed in BECs after ischemia. After IV administration of c(RGDyK) small EVs packed with curcumin, they showed a suppression in the inflammatory response and cellular apoptosis in the ischemic region. Even though the capacity of c(RGDyK)-conjugated small EVs to bind endothelial integrins (a_vb_3) at the luminal surface increased, these data was dependent on the overexpression of a_vb_3 during pathological conditions. This leads to the possibility that c(RGDyK)-conjugated small EVs get internalized either by interacting with endothelial integrins (a_vb_3) using RMT and/or non-specific paracellular transport after the BBB disruption. However, performing pharmacokinetic analyses would be essential to address the elimination of modified small EVs following injection into the blood circulation. Whether the cellular intensity of integrins/receptors in different tissue endothelial cells contributes to the removal of modified small EVs, even before BBB crossing, is another issue that requires further consideration. Therefore, decorating small EVs by either genetically modifying their parental cells or conjugating small EVs post-isolation with targeting ligands can be useful to develop therapeutic small EVs for the targeting of diseased CNS sites.

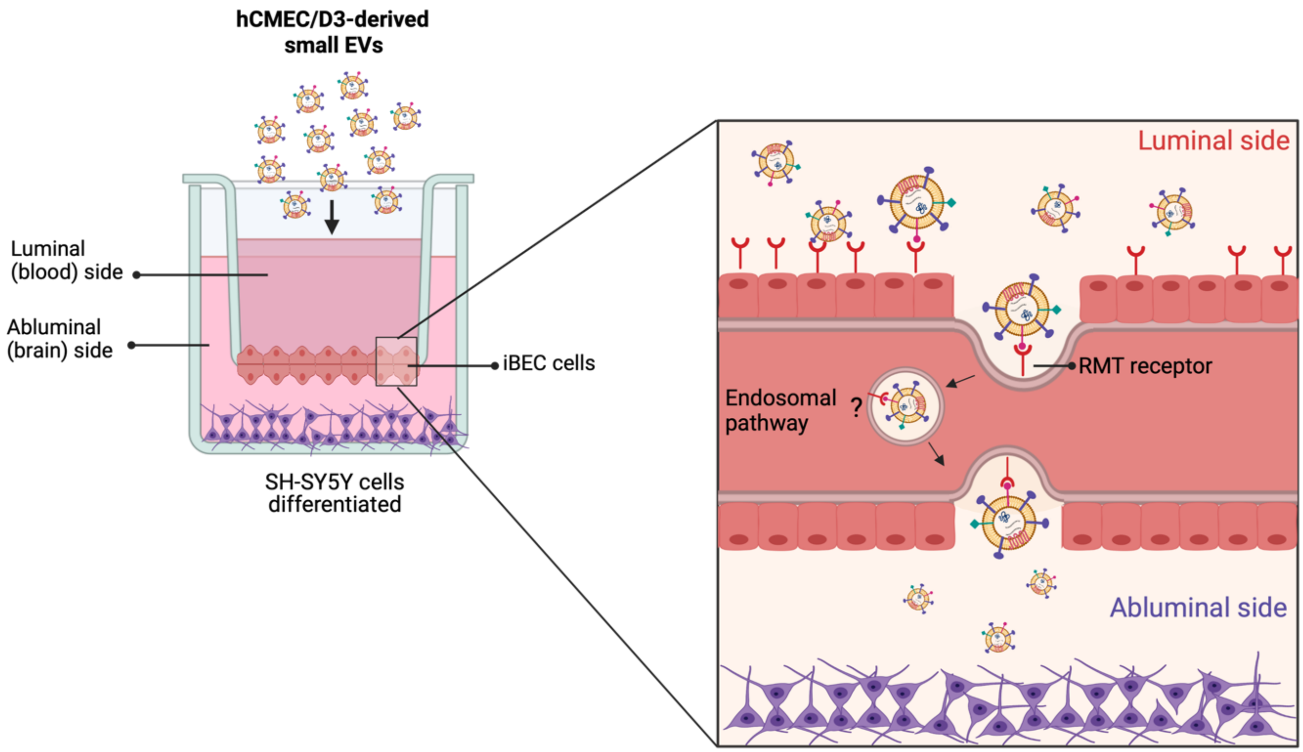

Figure 18. Proposed transport mechanism of hCMEC/D3-derived small EVs across the *in vitro* iPSCs BBB Transwell model. Overview of the *in vitro* human BBB model which consists of endothelial cells (iBECs) generated from proprietary amniotic fluid-derived induced pluripotent stem cells (iPSCs). It is assembled where iBECs are seeded in the upper chamber (luminal side) and human differentiated neuron-like cells (SH-SY5Y) in the lower chamber (abluminal side) of a 24-well transwell system. Isolated small EVs derived from human immortalized cerebral endothelial (hCMEC/D3) were placed in the upper chamber of the transwell system and after 24 h incubation, they showed an approximate 4% uptake across the iBECs. This suggests a potential homotypic interaction between specific receptors on the surface of small EVs derived from hCMEC/D3 and ligands on iBECs compared to HEK293T-derived small EVs (2% uptake), suggesting a RMT pathway. After internalization the specific endosomal pathway of small EVs is not well understood, however these small EVs derived from hCMEC/D3 were available to reduce endogenous α-synuclein mRNA level in the neuron-like cells seeded at the lower chamber.

Even though we demonstrated that small EVs can cross the *in vitro* BBB transwell model, there are limitations to this study, and in general in the field of small EVs and BBB. The main current limitations include scale-up of small EVs production, yielding a high purified small EVs population, proper standardization for isolation and characterization protocols, poor/low packing efficiency, tracking small EVs *in vivo*, pharmacokinetics and poor understanding of transcytosis mechanisms[33,375,376]. Therefore, there are necessary steps that must be taken into consideration before studying small EVs-based drug delivery to the CNS. Firstly, it is important to demonstrate how to reduce the non-specific biodistribution of small EVs to other tissues and how to specifically direct them to the diseased area in the brain. Secondly, the lack of *in vivo* evidence for small EVs trafficking mechanisms across the BBB is a big gap in the field since there have been studies reported that NVU cells (pericytes, astrocytes, microglia, and olidodendrocytes) can uptake the small EVs after their crossing the BECs[377]. This limits the amount of small EVs that can actually reach the specific target brain region. The mechanisms by which small EVs are internalized by these NVU cells have not been yet identified. Therefore, beside the specific interaction of small EVs with different NVU cells, it should also be important to determine the mechanism(s) with the addition of different cell types to mimic the NVU under pathological conditions in order to develop a better therapeutic approach. Lastly, another challenge that needs to be addressed more thoroughly is the ability of small EVs to migrate to remote areas in the brain after crossing the BBB, more specifically deep brain regions for neurodegenerative disorders like the SNpc for PD.

Overall, our findings suggest that small EVs-derived from hCMEC/D3 indeed cross the iBECs more efficiently and highlights the possibility of various transcytosis mechanisms involved according to the parental cell from where the small EVs are derived. As well, we showed the potential of small EVs to deliver and reduce mRNA levels of endogenous α-synuclein using the pre-miR-451 backbone strategy to package small EVs with siRNA against α-synuclein. It is important to note that this *in vitro* process does not fully recapitulate developmental BBB transcytosis. Dedicated studies involving fluid flow, shear forces, and tissue microenvironment are required to further develop this system for more advanced diseases modelling and therapeutic application. In accordance with previous studies and our data, small EVs could be considered as nanocarrier vehicles for drug delivery to the brain parenchyma. Therefore, understanding the various possible mechanisms of small EVs passing through BBB and related challenges could help the field to investigate the small EVs – BECs interaction(s) on the surface of BBB and further facilitate small EVs crossing ultimately resulting in an increased efficiency of the drug delivery to the abluminal side of the BBB. Although this assertion requires further confirmation, the possibility remains that tissue-specificity of delivery could be improved by using autologous tissue small EVs. Therefore, hCMEC/D3-derived small EVs could potentially be exploited as brain-selective nanocarriers for therapeutic delivery across the BBB.

CONCLUSION & FUTURE DIRECTION

The main aim of this project was to test the ability of small EVs packaged with α-synuclein siRNA integrated into the pre-miR-451 backbone to efficiently be delivered to neuron-like cells and knockdown α-synuclein *in vitro* by direct treatment or using human *in vitro* BBB model. The data obtained has shown a reduction of endogenous α-synuclein at the mRNA and protein level specifically in human SH-SY5Y neuron-like cells. This demonstrates a potential opportunity to silence toxic genes in neurodegenerative disorders. Although, there was also evidence that small EVs derived from human brain endothelial cells cross the *in vitro* BBB, it is important to highlight that this approach cannot truly recapitulate the complex anatomical and functional relationships of the NVU or *in vivo* pharmacokinetic distribution. Therefore, a next step could potentially be to evaluate the crossing of these small EVs *in vivo* in transgenic mouse models of PD. As well, to increase small EV penetration into the brain parenchyma, the small EV surface could potentially be engineered with BBB-crossing specific receptors[53] (FC5 or IGF1R) to further increase the uptake and transcytosis and the amount of small EVs that reaches a target brain region. Overall, this method has the potential to overcome the limitation of inefficient packing of small EVs with siRNA, which hinders small EVs research and could help to bring small EV-based therapeutics one step closer to clinical use for treating neurodegenerative disorders. These results indicate that human brain endothelial cells may serve as a promising cell source for small EVs-based CNS treatments.

REFERENCE

1. René, C. A. & Parks, R. J. Delivery of Therapeutic Agents to the Central Nervous System and the Promise of Extracellular Vesicles. *Pharm. 2021, Vol. 13, Page 492* **13**, 492 (2021).
2. Ray Dorsey, E. *et al.* Global, regional, and national burden of Parkinson's disease, 1990–2016: a systematic analysis for the Global Burden of Disease Study 2016. *Lancet Neurol.* **17**, 939–953 (2018).
3. Gratpain, V. *et al.* Extracellular vesicles for the treatment of central nervous system diseases. *Adv. Drug Deliv. Rev.* **174**, 535–552 (2021).
4. Kesselheim, A. S., Hwang, T. J. & Franklin, J. M. Two decades of new drug development for central nervous system disorders. *Nat. Rev. Drug Discov. 2015 1412* **14**, 815–816 (2015).
5. Butlen-Ducuing, F. *et al.* Regulatory watch: Challenges in drug development for central nervous system disorders: A European Medicines Agency perspective. *Nat. Rev. Drug Discov.* **15**, 813–814 (2016).
6. B Pincus, B. J., Kramer, B. & Hopkins Hospital, J. COMPARATIVE STTJDY OF THE CONCENTRATION OF VARIOUS ANIONS AND CATIONS IN CEREBRO-SPINAL FLUID AND SERUM. more, and the Harriet Lane Home, the.
7. LS, K. & GM, S. STUDIES ON THE RELATIONSHIP OF THE CHEMICAL CONSTITUENTS OF BLOOD AND CEREBROSPINAL FLUID. *J. Exp. Med.* **42**, 565–592 (1925).
8. Das Sauerstoff-Bedürfniss des Organismus; eine farbenanalytische Studie. (Book, 1885) [WorldCat.org]. https://www.worldcat.org/title/sauerstoff-bedurfniss-des-organismus-eine-farbenanalytische-studie/oclc/9718332.
9. Risau, W. & Wolburg, H. *Development of the blood-brain barrier*. (1990).
10. Daneman, R. & Prat, A. The Blood-Brain Barrier. *Cold Spring Harb. Lab. Press* (2015) doi:10.1101/cshperspect.a020412.
11. BV, Z. The blood-brain barrier in health and chronic neurodegenerative disorders. *Neuron* **57**, 178–201 (2008).
12. Zeissig, S. *et al.* Changes in expression and distribution of claudin 2, 5 and 8 lead to discontinuous tight junctions and barrier dysfunction in active Crohn's disease. *Gut* **56**, 61–72 (2007).
13. Laksitorini, M. D., Yathindranath, V., Xiong, W., Hombach-Klonisch, S. & Miller, D. W. Modulation of Wnt/β-catenin signaling promotes blood-brain barrier phenotype in cultured brain endothelial cells. *Sci. Rep.* **9**, (2019).
14. NR, S., SA, L. & KM, D. Barrier mechanisms in the developing brain. *Front. Pharmacol.* **3**, 1–18 (2012).
15. WA, B. & NH, G. Small molecules as central nervous system therapeutics: old challenges, new directions, and a philosophic divide. *Future Med. Chem.* **11**, 489–493 (2019).
16. Banks, W. A. Characteristics of compounds that cross the blood-brain barrier. *BMC Neurol. 2009 91* **9**, 1–5 (2009).
17. D, S. & NM, M. Pericyte physiology. *FASEB J.* **7**, 1031–1038 (1993).
18. Brown, L. S. *et al.* Pericytes and Neurovascular Function in the Healthy and Diseased Brain. *Front. Cell. Neurosci.* **13**, 282 (2019).
19. Uemura, M. T., Maki, T., Ihara, M., Lee, V. M. Y. & Trojanowski, J. Q. Brain

Microvascular Pericytes in Vascular Cognitive Impairment and Dementia. *Frontiers in Aging Neuroscience* vol. 12 (2020).
20. Larson, D. M., Wrobleski, M. J., Sagar, G. D., Westphale, E. M. & Beyer, E. C. Differential regulation of connexin43 and connexin37 in endothelial cells by cell density, growth, and TGF-beta1. *https://doi.org/10.1152/ajpcell.1997.272.2.C405* **272**, (1997).
21. Hirschi, K. K., Burt, J. M., Hirschi, K. D. & Dai, C. Gap Junction Communication Mediates Transforming Growth Factor-β Activation and Endothelial-Induced Mural Cell Differentiation. *Circ. Res.* **93**, 429–437 (2003).
22. Choudhary, M. *et al.* Tumor-induced loss of mural Connexin 43 gap junction activity promotes endothelial proliferation. *BMC Cancer 2015 151* **15**, 1–13 (2015).
23. AP, S. *et al.* Pericyte loss influences Alzheimer-like neurodegeneration in mice. *Nat. Commun.* **4**, (2013).
24. Abbott, N. J., Patabendige, A. A. K., Dolman, D. E. M., Yusof, S. R. & Begley, D. J. Structure and function of the blood–brain barrier. *Neurobiol. Dis.* **37**, 13–25 (2010).
25. Ding, S. *et al.* Overcoming blood–brain barrier transport: Advances in nanoparticle-based drug delivery strategies. *Materials Today* vol. 37 112–125 (2020).
26. Mahringer, A., Ott, M. & Fricker, G. The blood–brain barrier: An introduction to its structure and function. *Top. Med. Chem.* **10**, (2014).
27. GR, G., C, H. & BA, M. Bidirectional control of arteriole diameter by astrocytes. *Exp. Physiol.* **96**, 393–399 (2011).
28. Ezan, P. *et al.* Deletion of Astroglial Connexins Weakens the Blood–Brain Barrier: *http://dx.doi.org/10.1038/jcbfm.2012.45* **32**, 1457–1467 (2012).
29. Lutz, S. E., Raine, C. S. & Brosnan, C. F. Loss of astrocyte connexins 43 and 30 does not significantly alter susceptibility or severity of acute experimental autoimmune encephalomyelitis in mice. *J. Neuroimmunol.* **245**, 8–14 (2012).
30. C, I. The Neurovascular Unit Coming of Age: A Journey through Neurovascular Coupling in Health and Disease. *Neuron* **96**, 17–42 (2017).
31. Lochhead, J. J., Yang, J., Ronaldson, P. T. & Davis, T. P. Structure, Function, and Regulation of the Blood-Brain Barrier Tight Junction in Central Nervous System Disorders. *Frontiers in Physiology* vol. 11 (2020).
32. Cecchelli, R. *et al.* Modelling of the blood - Brain barrier in drug discovery and development. *Nat. Rev. Drug Discov.* **6**, 650–661 (2007).
33. Matsumoto, J., Stewart, T., Banks, W. A. & Zhang, J. The Transport Mechanism of Extracellular Vesicles at the Blood-Brain Barrier. *Curr. Pharm. Des.* **23**, 6206–6214 (2018).
34. FP, D. *et al.* Comparative permeabilities of the paracellular and transcellular pathways of corneal endothelial layers. *J. Membr. Biol.* **242**, 41–51 (2011).
35. Levin, V. A. Relationship of octanol/water partition coefficient and molecular weight to rat brain capillary permeability. *J. Med. Chem.* **23**, 682–684 (2002).
36. S, O., H, Y., Y, K., T, A. & T, T. mRNA expression levels of tight junction protein genes in mouse brain capillary endothelial cells highly purified by magnetic cell sorting. *J. Neurochem.* **104**, 147–154 (2008).
37. Barar, J., Rafi, M. A., Pourseif, M. M. & Omidi, Y. Blood-brain barrier transport machineries and targeted therapy of brain diseases. *BioImpacts* **6**, 225–248 (2016).
38. Ohtsuki, S. & Terasaki, T. Contribution of Carrier-Mediated Transport Systems to the Blood–Brain Barrier as a Supporting and Protecting Interface for the Brain; Importance

for CNS Drug Discovery and Development. *Pharm. Res. 2007 249* **24**, 1745–1758 (2007).
39. Pulgar, V. M. Transcytosis to Cross the Blood Brain Barrier, New Advancements and Challenges. *Front. Neurosci.* **0**, 1019 (2019).
40. TUMA, P. L. & HUBBARD, A. L. Transcytosis: Crossing Cellular Barriers. *https://doi.org/10.1152/physrev.00001.2003* **83**, 871–932 (2003).
41. S, H. & WA, B. Role of the immune system in HIV-associated neuroinflammation and neurocognitive implications. *Brain. Behav. Immun.* **45**, 1–12 (2015).
42. JC, V. & RD, B. Transcytosis of protein through the mammalian cerebral epithelium and endothelium. II. Adsorptive transcytosis of WGA-HRP and the blood-brain and brain-blood barriers. *J. Neurocytol.* **22**, 67–80 (1993).
43. René, C. A. & Parks, R. J. Delivery of therapeutic agents to the central nervous system and the promise of extracellular vesicles. *Pharmaceutics* **13**, (2021).
44. JM, L. & EV, S. Targeting receptor-mediated transport for delivery of biologics across the blood-brain barrier. *Annu. Rev. Pharmacol. Toxicol.* **55**, 613–631 (2015).
45. J, P. & CI, W. Exploiting transferrin receptor for delivering drugs across the blood-brain barrier. *Drug Discov. Today. Technol.* **20**, 49–52 (2016).
46. Mayor, S. & Pagano, R. E. Pathways of clathrin-independent endocytosis. *Nat. Rev. Mol. Cell Biol. 2007 88* **8**, 603–612 (2007).
47. Zhao, Z. *et al.* Central role for PICALM in amyloid-β blood-brain barrier transcytosis and clearance. *Nat. Neurosci.* **18**, 978–987 (2015).
48. K, B. *et al.* Tissue-type plasminogen activator crosses the intact blood-brain barrier by low-density lipoprotein receptor-related protein-mediated transcytosis. *Circulation* **111**, 2241–2249 (2005).
49. WM, P., J, E. & J, Y. Human blood-brain barrier transferrin receptor. *Metabolism.* **36**, 892–895 (1987).
50. HT, M. & E, B. Molecular mechanism and physiological functions of clathrin-mediated endocytosis. *Nat. Rev. Mol. Cell Biol.* **12**, 517–533 (2011).
51. RG, P. & K, S. The multiple faces of caveolae. *Nat. Rev. Mol. Cell Biol.* **8**, 185–194 (2007).
52. P, C. *et al.* Apical-to-basolateral transport of amyloid-β peptides through blood-brain barrier cells is mediated by the receptor for advanced glycation end-products and is restricted by P-glycoprotein. *J. Alzheimers. Dis.* **22**, 849–859 (2010).
53. Stanimirovic, D. B., Sandhu, J. K. & Costain, W. J. Emerging Technologies for Delivery of Biotherapeutics and Gene Therapy Across the Blood–Brain Barrier. *BioDrugs* **32**, 547–559 (2018).
54. Andjelkovic, A. V., Stamatovic, S. M., Phillips, C. M., Martinez-Revollar, G. & Keep, R. F. Modeling blood-brain barrier pathology in cerebrovascular disease in vitro: current and future paradigms. *Fluids and barriers of the CNS* vol. 17 44 (2020).
55. Song, H. W. *et al.* transcriptomic comparison of human and mouse brain microvessels. **10**, 12358 (2020).
56. A, B., TR, G. & R, G. Comparative transcriptomics in human and mouse. *Nat. Rev. Genet.* **18**, 425–440 (2017).
57. Wang, M. M. *et al.* Expression of periaxin (PRX) specifically in the human cerebrovascular system: PDZ domain-mediated strengthening of endothelial barrier function. *Sci. Reports 2018 81* **8**, 1–15 (2018).
58. O'Brown, N. M., Pfau, S. J. & Gu, C. Bridging barriers: a comparative look at the blood–

brain barrier across organisms. *Genes Dev.* **32**, 466 (2018).
59. Roux, G. Le *et al.* Proof-of-Concept Study of Drug Brain Permeability Between in Vivo Human Brain and an in Vitro iPSCs-Human Blood-Brain Barrier Model. *Sci. Reports 2019 91* **9**, 1–11 (2019).
60. Andjelkovic, A. V., Stamatovic, S. M., Phillips, C. M., Martinez-Revollar, G. & Keep, R. F. Modeling blood-brain barrier pathology in cerebrovascular disease in vitro: current and future paradigms. *Fluids and barriers of the CNS* vol. 17 44 (2020).
61. Danica B Stanimirovic†, Mahmud Bani-Yaghoub, M. P. & A. S. H. Blood–brain barrier models: in vitro to in vivo translation in preclinical development of CNS- targeting biotherapeutics. (2014).
62. Ribecco-Lutkiewicz, M. *et al.* A novel human induced pluripotent stem cell blood-brain barrier model: Applicability to study antibody-triggered receptor-mediated transcytosis OPEN. **8**, 1873 (2018).
63. Butt, A. M., Jones, H. C. & Abbott, N. J. Electrical resistance across the blood-brain barrier in anaesthetized rats: a developmental study. *J. Physiol.* **429**, 47 (1990).
64. Tarbell, J. M. Shear stress and the endothelial transport barrier. *Cardiovasc. Res.* **87**, 320 (2010).
65. JG, D., ZS, X., AJ, W., N, Y. & PC, S. Effect of shear stress on iPSC-derived human brain microvascular endothelial cells (dhBMECs). *Fluids Barriers CNS* **14**, (2017).
66. Lippmann, E. S., Al-Ahmad, A., Azarin, S. M., Palecek, S. P. & Shusta, E. V. A retinoic acid-enhanced, multicellular human blood-brain barrier model derived from stem cell sources. *Sci. Rep.* **4**, 1–10 (2014).
67. Bernas, M. J. *et al.* Establishment of primary cultures of human brain microvascular endothelial cells to provide an in vitro cellular model of the blood-brain barrier. *Nat. Protoc.* **5**, 1265–1272 (2010).
68. Weksler, B. B. *et al.* Blood-brain barrier-specific properties of a human adult brain endothelial cell line. *FASEB J.* **19**, 1872–1874 (2005).
69. HC, H. *et al.* In vitro models of the blood-brain barrier: An overview of commonly used brain endothelial cell culture models and guidelines for their use. *J. Cereb. Blood Flow Metab.* **36**, 862–890 (2016).
70. SM, S., N, S., RF, K. & AV, A. PDCD10 (CCM3) regulates brain endothelial barrier integrity in cerebral cavernous malformation type 3: role of CCM3-ERK1/2-cortactin cross-talk. *Acta Neuropathol.* **130**, 731–750 (2015).
71. Ponio, J. B.-D. *et al.* Instruction of Circulating Endothelial Progenitors In Vitro towards Specialized Blood-Brain Barrier and Arterial Phenotypes. *PLoS One* **9**, e84179 (2014).
72. Cecchelli, R. *et al.* A Stable and Reproducible Human Blood-Brain Barrier Model Derived from Hematopoietic Stem Cells. *PLoS One* **9**, e99733 (2014).
73. Katt, M. E., Xu, Z. S., Gerecht, S. & Searson, P. C. Human Brain Microvascular Endothelial Cells Derived from the BC1 iPS Cell Line Exhibit a Blood-Brain Barrier Phenotype. *PLoS One* **11**, e0152105 (2016).
74. Lippmann, E. S. *et al.* Derivation of blood-brain barrier endothelial cells from human pluripotent stem cells. *Nat. Biotechnol. 2012 308* **30**, 783–791 (2012).
75. Bagchi, S. *et al.* In-vitro blood-brain barrier models for drug screening and permeation studies: An overview. *Drug Design, Development and Therapy* vol. 13 3591–3605 (2019).
76. Helms, H. C. *et al.* In vitro models of the blood–brain barrier: An overview of commonly used brain endothelial cell culture models and guidelines for their use. *J. Cereb. Blood*

Flow Metab. **36**, 862 (2016).
77. Mantle, J. L., Min, L. & Lee, K. H. Minimum Transendothelial Electrical Resistance Thresholds for the Study of Small and Large Molecule Drug Transport in a Human in Vitro Blood–Brain Barrier Model. *Mol. Pharm.* **13**, 4191–4198 (2016).
78. K, H., A, K., T, O. & Y, D. Memantine transport by a proton-coupled organic cation antiporter in hCMEC/D3 cells, an in vitro human blood-brain barrier model. *Drug Metab. Pharmacokinet.* **30**, 182–187 (2015).
79. V, S., YV, K., S, L. & KS, K. Human astrocytes/astrocyte-conditioned medium and shear stress enhance the barrier properties of human brain microvascular endothelial cells. *Brain Res.* **1147**, 39–50 (2007).
80. AG, K. *et al.* Volume flow and wall shear stress quantification in the human conjunctival capillaries and post-capillary venules in vivo. *Biorheology* **44**, 375–386 (2007).
81. L, C. *et al.* Development of a humanized in vitro blood-brain barrier model to screen for brain penetration of antiepileptic drugs. *Epilepsia* **48**, 505–516 (2007).
82. G, A., D, M., A, P., RD, K. & EL, G. A 3D neurovascular microfluidic model consisting of neurons, astrocytes and cerebral endothelial cells as a blood-brain barrier. *Lab Chip* **17**, 448–459 (2017).
83. S, J. *et al.* A Three-Dimensional Arrayed Microfluidic Blood-Brain Barrier Model With Integrated Electrical Sensor Array. *IEEE Trans. Biomed. Eng.* **65**, 431–439 (2018).
84. Booth, R. & Kim, H. A MULTI-LAYERED MICROFLUIDIC DEVICE FOR IN VITRO BLOOD-BRAIN BARRIER PERMEABILITY STUDIES.
85. Oddo, A. *et al.* Advances in Microfluidic Blood–Brain Barrier (BBB) Models. *Trends Biotechnol.* **37**, 1295–1314 (2019).
86. Griep, L. M. *et al.* BBB ON CHIP: microfluidic platform to mechanically and biochemically modulate blood-brain barrier function. *Biomed. Microdevices 2012 151* **15**, 145–150 (2012).
87. GN, G. *et al.* Tissue-engineered blood-brain barrier models via directed differentiation of human induced pluripotent stem cells. *Sci. Rep.* **9**, (2019).
88. EH, N. *et al.* A Simplified, Fully Defined Differentiation Scheme for Producing Blood-Brain Barrier Endothelial Cells from Human iPSCs. *Stem cell reports* **12**, 1380–1388 (2019).
89. M, T. *et al.* The blood-brain barrier: structure, function and therapeutic approaches to cross it. *Mol. Membr. Biol.* **31**, 152–167 (2014).
90. Stanimirovic, D. B., Sandhu, J. K. & Costain, W. J. Emerging Technologies for Delivery of Biotherapeutics and Gene Therapy Across the Blood–Brain Barrier. *BioDrugs* **32**, 547–559 (2018).
91. Hughes, M. P. *et al.* AAV9 intracerebroventricular gene therapy improves lifespan, locomotor function and pathology in a mouse model of Niemann–Pick type C1 disease. *Hum. Mol. Genet.* **27**, 3079 (2018).
92. Wurster, C. D. & Ludolph, A. C. Nusinersen for spinal muscular atrophy. *Ther. Adv. Neurol. Disord.* **11**, (2018).
93. Stevens, D., Claborn, M. K., Gildon, B. L., Kessler, T. L. & Walker, C. Onasemnogene Abeparvovec-xioi: Gene Therapy for Spinal Muscular Atrophy: *https://doi.org/10.1177/1060028020914274* **54**, 1001–1009 (2020).
94. J, L. & BE, Z. Endoscopic-Assisted Ommaya Reservoir Placement: Technical Note. *Cureus* **9**, (2017).

95. de Yebenes, J. G., Fahn, S., Jackson-Lewis, V. & Mena, M. A. The effect of intracerebroventricular infusion of (+)-4-propyl-9-hydroxynapthoxacine (PHNO) through a totally implanted drug delivery system in rats with dopamine deficiency. *Mov. Disord.* **2**, 291–299 (1987).
96. Sheikov, N., McDannold, N., Sharma, S. & Hynynen, K. Effect of focused ultrasound applied with an ultrasound contrast agent on the tight junctional integrity of the brain microvascular endothelium. *Ultrasound Med. Biol.* **34**, 1093 (2008).
97. Brewster, M. E., Raghavan, K., Pop, E. & Bodor, N. Enhanced delivery of ganciclovir to the brain through the use of redox targeting. *Antimicrob. Agents Chemother.* **38**, 817 (1994).
98. J, R., K, L., M, G. & J, S. Prodrug approaches for CNS delivery. *AAPS J.* **10**, 92–102 (2008).
99. Saint-Pol, J., Gosselet, F., Duban-Deweer, S., Pottiez, G. & Karamanos, Y. Targeting and Crossing the Blood-Brain Barrier with Extracellular Vesicles. *Cells* **9**, 851 (2020).
100. WM, P. Delivery of Biologics Across the Blood-Brain Barrier with Molecular Trojan Horse Technology. *BioDrugs* **31**, 503–519 (2017).
101. Bendix Johnsen, K. *et al.* Targeting transferrin receptors at the blood-brain barrier improves the uptake of immunoliposomes and subsequent cargo transport into the brain parenchyma. doi:10.1038/s41598-017-11220-1.
102. T, M. & EH, M. Transferrin and transferrin receptor function in brain barrier systems. *Cell. Mol. Neurobiol.* **20**, 77–95 (2000).
103. B, D. *et al.* A new function for the LDL receptor: transcytosis of LDL across the blood-brain barrier. *J. Cell Biol.* **138**, 877–889 (1997).
104. PL, G., TJ, M. & WM, P. Human blood-brain barrier leptin receptor. Binding and endocytosis in isolated human brain microvessels. *J. Clin. Invest.* **99**, 14–18 (1997).
105. Xia, C.-F., Boado, R. J. & Pardridge, W. M. Antibody-Mediated Targeting of siRNA Via the Human Insulin Receptor Using Avidin-Biotin Technology. *Mol. Pharm.* **6**, 747 (2009).
106. A, M., J, T., S, N. & D, S. Selection of phage-displayed llama single-domain antibodies that transmigrate across human blood-brain barrier endothelium. *FASEB J.* **16**, 240–242 (2002).
107. MW, B. Transport of iron in the blood-brain-cerebrospinal fluid system. *J. Neurochem.* **69**, 443–454 (1997).
108. J, H. & WM, P. Examination of blood-brain barrier transferrin receptor by confocal fluorescent microscopy of unfixed isolated rat brain capillaries. *J. Neurochem.* **70**, 883–886 (1998).
109. Zhang, Y. *et al.* An RNA-Sequencing Transcriptome and Splicing Database of Glia, Neurons, and Vascular Cells of the Cerebral Cortex. *J. Neurosci.* **34**, 11929–11947 (2014).
110. He, L. *et al.* Single-cell RNA sequencing of mouse brain and lung vascular and vessel-associated cell types. *Sci. Data 2018 51* **5**, 1–11 (2018).
111. R, R., A, S., GC, S., JJ, L. & RE, F. Studies of the mechanism of iron transport across the blood-brain barrier. *Ann. Neurol.* **32 Suppl**, S43–S50 (1992).
112. Bickel, U., Yoshikawa, T., Landaw, E. M., Faull, K. F. & Pardridge, W. M. Pharmacologic effects in vivo in brain by vector-mediated peptide drug delivery. *Proc. Natl. Acad. Sci. U. S. A.* **90**, 2618 (1993).
113. Deguchi, Y., Kurihara, A. & Pardridge, W. M. Retention of biologic activity of human

epidermal growth factor following conjugation to a blood-brain barrier drug delivery vector via an extended poly(ethylene glycol) linker. *Bioconjug. Chem.* **10**, 32–37 (1999).
114. Lee, H. J., Zhang, Y., Zhu, C., Duff, K. & Pardridge, W. M. Imaging Brain Amyloid of Alzheimer Disease in Vivo in Transgenic Mice with an Aβ Peptide Radiopharmaceutical: *http://dx.doi.org/10.1097/00004647-200202000-00010* **22**, 223–231 (2016).
115. Y, Z. & WM, P. Delivery of beta-galactosidase to mouse brain via the blood-brain barrier transferrin receptor. *J. Pharmacol. Exp. Ther.* **313**, 1075–1081 (2005).
116. Agents shuttle across blood-brain barrier to treat Hunter syndrome. *Nat. Biotechnol.* **39**, 253 (2021).
117. Kariolis, M. S. *et al.* Brain delivery of therapeutic proteins using an Fc fragment blood-brain barrier transport vehicle in mice and monkeys. *Sci. Transl. Med.* **12**, 1359 (2020).
118. Qian, Z. M., Li, H., Sun, H. & Ho, K. Targeted Drug Delivery via the Transferrin Receptor-Mediated Endocytosis Pathway. *Pharmacol. Rev.* **54**, 561–587 (2002).
119. Bien-Ly, N. *et al.* Transferrin receptor (TfR) trafficking determines brain uptake of TfR antibody affinity variants. *J. Exp. Med.* **211**, 233–244 (2014).
120. Alvarez-Erviti, L. *et al.* Delivery of siRNA to the mouse brain by systemic injection of targeted exosomes. *Nat. Biotechnol.* **29**, 306–309 (2011).
121. Cooper, J. M. *et al.* Systemic exosomal siRNA delivery reduced alpha-synuclein aggregates in brains of transgenic mice. *Mov. Disord.* **29**, 1476–1485 (2014).
122. Kumar, P. *et al.* Transvascular delivery of small interfering RNA to the central nervous system. *Nat. 2007 4487149* **448**, 39–43 (2007).
123. Tuffereau, C. *et al.* The Rabies Virus Glycoprotein Receptor p75NTR Is Not Essential for Rabies Virus Infection. *J. Virol.* **81**, 13622 (2007).
124. TL, L. Rabies virus binding to an acetylcholine receptor alpha-subunit peptide. *J. Mol. Recognit.* **3**, 82–88 (1990).
125. Qinghua Wang, Shang Cheng, Fen Qin, Ailing Fu & Chen Fu. Application progress of RVG peptides to facilitate the delivery of therapeutic agents into the central nervous system. *RSC Adv.* **11**, 8505–8515 (2021).
126. F, D. *et al.* PLGA-based nanoparticles: an overview of biomedical applications. *J. Control. Release* **161**, 505–522 (2012).
127. Yuan, Z.-Y., Hu, Y.-L. & Gao, J.-Q. Brain Localization and Neurotoxicity Evaluation of Polysorbate 80-Modified Chitosan Nanoparticles in Rats. *PLoS One* **10**, e0134722 (2015).
128. Voigt, N. *et al.* Toxicity of polymeric nanoparticles in vivo and in vitro. *J. Nanopart. Res.* **16**, (2014).
129. Sharma, D., Ali, A. A. E. & Trivedi, L. R. An Updated Review On:Liposomes as Drug Delivery System. *Pharmatutor* **6**, 50 (2018).
130. T, H. *et al.* Preparation, biodistribution and neurotoxicity of liposomal cisplatin following convection enhanced delivery in normal and F98 glioma bearing rats. *PLoS One* **7**, (2012).
131. Montesinos, R. N. Liposomal Drug Delivery to the Central Nervous System. *Liposomes* (2017) doi:10.5772/INTECHOPEN.70055.
132. E, W., C, D. P., C, L. & TB, C.-P. Development and Evaluation of Lipid Nanoparticles for Drug Delivery: Study of Toxicity In, Vitro and In Vivo. *J. Nanosci. Nanotechnol.* **16**, 1321–1330 (2016).
133. Puapermpoonsiri, U., Lipipun, V. & Vardhanabhuti, N. Synergistic Effect of Phospholipid-Based Liposomes and Propylthiouracil on U-937 Cell Growth. *http://dx.doi.org/10.1080/00032710500364316* **15**, 215–227 (2008).

134. Akinc, A. *et al.* The Onpattro story and the clinical translation of nanomedicines containing nucleic acid-based drugs. *Nature Nanotechnology* vol. 14 1084–1087 (2019).
135. Schoenmaker, L. *et al.* mRNA-lipid nanoparticle COVID-19 vaccines: Structure and stability. *Int. J. Pharm.* **601**, 120586 (2021).
136. SLN, M., XO, B. & AM, W. Extracellular Vesicles: Unique Intercellular Delivery Vehicles. *Trends Cell Biol.* **27**, 172–188 (2017).
137. M, Z. *et al.* Exosome-based nanocarriers as bio-inspired and versatile vehicles for drug delivery: recent advances and challenges. *J. Mater. Chem. B* **7**, 2421–2433 (2019).
138. Osorio-Querejeta, I. *et al.* MiR-219a-5p Enriched Extracellular Vesicles Induce OPC Differentiation and EAE Improvement More Efficiently Than Liposomes and Polymeric Nanoparticles. *Pharm. 2020, Vol. 12, Page 186* **12**, 186 (2020).
139. Foster, B. P. *et al.* Extracellular vesicles in blood, milk and body fluids of the female and male urogenital tract and with special regard to reproduction. *http://dx.doi.org/10.1080/10408363.2016.1190682* **53**, 379–395 (2016).
140. Van Dommelen, S. M. *et al.* Microvesicles and exosomes: Opportunities for cell-derived membrane vesicles in drug delivery. *Journal of Controlled Release* vol. 161 635–644 (2012).
141. Rufino-Ramos, D. *et al.* Extracellular vesicles: Novel promising delivery systems for therapy of brain diseases. *J. Control. Release* **262**, 247–258 (2017).
142. El-Andaloussi, S. *et al.* Exosome-mediated delivery of siRNA in vitro and in vivo. *Nat. Protoc.* **7**, 2112–2126 (2012).
143. Théry, C., Amigorena, S., Raposo, G. & Clayton, A. Isolation and Characterization of Exosomes from Cell Culture Supernatants and Biological Fluids. *Curr. Protoc. Cell Biol.* **30**, 3.22.1-3.22.29 (2006).
144. Zhang, H. *et al.* Identification of distinct nanoparticles and subsets of extracellular vesicles by asymmetric flow field-flow fractionation. *Nat. Cell Biol. 2018 203* **20**, 332–343 (2018).
145. Ma, L. *et al.* Discovery of the migrasome, an organelle mediating release of cytoplasmic contents during cell migration. *Cell Res. 2015 251* **25**, 24–38 (2014).
146. J, A. *et al.* Retrovirus-like Gag Protein Arc1 Binds RNA and Traffics across Synaptic Boutons. *Cell* **172**, 262-274.e11 (2018).
147. ED, P. *et al.* The Neuronal Gene Arc Encodes a Repurposed Retrotransposon Gag Protein that Mediates Intercellular RNA Transfer. *Cell* **172**, 275-288.e18 (2018).
148. Théry, C., Zitvogel, L. & Amigorena, S. Exosomes: Composition, biogenesis and function. *Nat. Rev. Immunol.* **2**, 569–579 (2002).
149. Van Der Meel, R. *et al.* Extracellular vesicles as drug delivery systems: Lessons from the liposome field. *Journal of Controlled Release* vol. 195 72–85 (2014).
150. Skog, J. *et al.* Glioblastoma microvesicles transport RNA and proteins that promote tumour growth and provide diagnostic biomarkers. *Nat. Cell Biol.* **10**, 1470–1476 (2008).
151. HM, van D., N, M., KW, W. & DM, P. Extracellular Vesicles Exploit Viral Entry Routes for Cargo Delivery. *Microbiol. Mol. Biol. Rev.* **80**, 369–386 (2016).
152. T, T. *et al.* Exosome uptake through clathrin-mediated endocytosis and macropinocytosis and mediating miR-21 delivery. *J. Biol. Chem.* **289**, 22258–22267 (2014).
153. KJ, S. *et al.* Exosome uptake depends on ERK1/2-heat shock protein 27 signaling and lipid Raft-mediated endocytosis negatively regulated by caveolin-1. *J. Biol. Chem.* **288**, 17713–17724 (2013).

154. D, F. *et al.* Cellular internalization of exosomes occurs through phagocytosis. *Traffic* **11**, 675–687 (2010).
155. H, C. V., JJ, G.-F., RM, S. & P, V. Cellular uptake of extracellular vesicles is mediated by clathrin-independent endocytosis and macropinocytosis. *J. Control. Release* **266**, 100–108 (2017).
156. Théry, C. *et al.* Minimal information for studies of extracellular vesicles 2018 (MISEV2018): a position statement of the International Society for Extracellular Vesicles and update of the MISEV2014 guidelines. *https://doi.org/10.1080/20013078.2018.1535750* **7**, (2018).
157. Tauro, B. J. *et al.* Comparison of ultracentrifugation, density gradient separation, and immunoaffinity capture methods for isolating human colon cancer cell line LIM1863-derived exosomes. *Methods* **56**, 293–304 (2012).
158. Konoshenko, M. Y., Lekchnov, E. A., Vlassov, A. V & Laktionov, P. P. Isolation of Extracellular Vesicles: General Methodologies and Latest Trends. (2018) doi:10.1155/2018/8545347.
159. Busatto, S. *et al.* Tangential Flow Filtration for Highly Efficient Concentration of Extracellular Vesicles from Large Volumes of Fluid. *Cells* **7**, 273 (2018).
160. Morad, G. *et al.* Tumor-Derived Extracellular Vesicles Breach the Intact Blood−Brain Barrier via Transcytosis. (2019) doi:10.1021/acsnano.9b04397.
161. RJ, K. *et al.* Human vascular endothelial cells transport foreign exosomes from cow's milk by endocytosis. *Am. J. Physiol. Cell Physiol.* **310**, C800–C807 (2016).
162. Chen, C. C. *et al.* Elucidation of Exosome Migration Across the Blood–Brain Barrier Model In Vitro. *Cell. Mol. Bioeng.* **9**, 509–529 (2016).
163. Banks, W. A. *et al.* Transport of Extracellular Vesicles across the Blood-Brain Barrier: Brain Pharmacokinetics and Effects of Inflammation. *Int. J. Mol. Sci. Artic.* doi:10.3390/ijms21124407.
164. Haraszti, R. A. *et al.* High-resolution proteomic and lipidomic analysis of exosomes and microvesicles from different cell sources. *J. Extracell. Vesicles* **5**, (2016).
165. S, C. *et al.* Surface Glycoproteins of Exosomes Shed by Myeloid-Derived Suppressor Cells Contribute to Function. *J. Proteome Res.* **16**, 238–246 (2017).
166. Antimisiaris, S. G., Mourtas, S. & Marazioti, A. Exosomes and Exosome-Inspired Vesicles for Targeted Drug Delivery. *Pharmaceutics* **10**, (2018).
167. Sun, D. *et al.* A Novel Nanoparticle Drug Delivery System: The Anti-inflammatory Activity of Curcumin Is Enhanced When Encapsulated in Exosomes. *Mol. Ther.* **18**, 1606 (2010).
168. MJ, H. *et al.* Exosomes as drug delivery vehicles for Parkinson's disease therapy. *J. Control. Release* **207**, 18–30 (2015).
169. Armstrong, J. P. K., Holme, M. N. & Stevens, M. M. Re-Engineering Extracellular Vesicles as Smart Nanoscale Therapeutics. *ACS Nano* **11**, 69–83 (2017).
170. Nash, L. A. *et al.* Survival Motor Neuron Protein is Released from Cells in Exosomes: A Potential Biomarker for Spinal Muscular Atrophy. *Sci. Reports 2017 71* **7**, 1–15 (2017).
171. Yang, T. *et al.* Exosome Delivered Anticancer Drugs Across the Blood-Brain Barrier for Brain Cancer Therapy in Danio Rerio. *Pharm Res* (2015) doi:10.1007/s11095-014-1593-y.
172. Mendonç, M. C. P., Kont, A., Aburto, M. R., Cryan, J. F. & O'driscoll, C. M. Advances in the Design of (Nano)Formulations for Delivery of Antisense Oligonucleotides and Small

Interfering RNA: Focus on the Central Nervous System. *Cite This Mol. Pharm.* **18**, 1491–1506 (2021).

173. CA, S. & D, C. FDA-Approved Oligonucleotide Therapies in 2017. *Mol. Ther.* **25**, 1069–1075 (2017).
174. Rinaldi, C. & Wood, M. J. A. Antisense oligonucleotides: the next frontier for treatment of neurological disorders. *Nat. Rev. Neurol. 2017 141* **14**, 9–21 (2017).
175. B, C. & GJ, H. Small RNA sorting: matchmaking for Argonautes. *Nat. Rev. Genet.* **12**, 19–31 (2011).
176. Bartlett, D. W. & Davis, M. E. Insights into the kinetics of siRNA-mediated gene silencing from live-cell and live-animal bioluminescent imaging. *Nucleic Acids Res.* **34**, 322–333 (2006).
177. Ameres, S. L., Martinez, J. & Schroeder, R. Molecular Basis for Target RNA Recognition and Cleavage by Human RISC. *Cell* **130**, 101–112 (2007).
178. Watts, J. K. & Corey, D. R. Gene silencing by siRNAs and antisense oligonucleotides in the laboratory and the clinic. *J. Pathol.* **226**, 365 (2012).
179. Subramanian, R. R. *et al.* Enhancing antisense efficacy with multimers and multi-targeting oligonucleotides (MTOs) using cleavable linkers. *Nucleic Acids Res.* **43**, 9123 (2015).
180. Xu, C.-F. & Wang, J. Delivery systems for siRNA drug development in cancer therapy. (2014) doi:10.1016/j.ajps.2014.08.011.
181. DV, M. *et al.* Potent and persistent in vivo anti-HBV activity of chemically modified siRNAs. *Nat. Biotechnol.* **23**, 1002–1007 (2005).
182. Dar, S. A., Thakur, A., Qureshi, A. & Kumar, M. siRNAmod: A database of experimentally validated chemically modified siRNAs. *Sci. Reports 2016 61* **6**, 1–8 (2016).
183. AD, J. *et al.* Sequence-dependent stimulation of the mammalian innate immune response by synthetic siRNA. *Nat. Biotechnol.* **23**, 457–462 (2005).
184. Pei, Y. *et al.* Quantitative evaluation of siRNA delivery in vivo. *RNA* **16**, 2553–2563 (2010).
185. Veldhoen, S., Laufer, S. D., Trampe, A. & Restle, T. Cellular delivery of small interfering RNA by a non-covalently attached cell-penetrating peptide: quantitative analysis of uptake and biological effect. *Nucleic Acids Res.* **34**, 6561 (2006).
186. Wittrup, A. *et al.* Visualizing lipid-formulated siRNA release from endosomes and target gene knockdown. *Nat. Biotechnol.* **33**, 870–876 (2015).
187. Chernikov, I. V., Vlassov, V. V. & Chernolovskaya, E. L. Current Development of siRNA Bioconjugates: From Research to the Clinic. *Front. Pharmacol.* **0**, 444 (2019).
188. GF, D. & MJ, D. Designing chemically modified oligonucleotides for targeted gene silencing. *Chem. Biol.* **19**, 937–954 (2012).
189. Baker, D. E. Eteplirsen. *Hosp. Pharm.* **52**, 302 (2017).
190. DJ, F. *et al.* Advanced siRNA Designs Further Improve In Vivo Performance of GalNAc-siRNA Conjugates. *Mol. Ther.* **26**, 708–717 (2018).
191. Janas, M. M. *et al.* Selection of GalNAc-conjugated siRNAs with limited off-target-driven rat hepatotoxicity. *Nat. Commun. 2018 91* **9**, 1–10 (2018).
192. PR, de P. B., SS, T.-A. & R, T.-A. Leading RNA Interference Therapeutics Part 2: Silencing Delta-Aminolevulinic Acid Synthase 1, with a Focus on Givosiran. *Mol. Diagn. Ther.* **24**, 61–68 (2020).
193. M, B. *et al.* Phase 3 Trial of RNAi Therapeutic Givosiran for Acute Intermittent

Porphyria. *N. Engl. J. Med.* **382**, 2289–2301 (2020).
194. O, K., D, S., O, S., B, C. & B, E. Trivalent, Gal/GalNAc-containing ligands designed for the asialoglycoprotein receptor. *Bioorg. Med. Chem.* **16**, 5216–5231 (2008).
195. Hu, B. *et al.* Therapeutic siRNA: state of the art. *Signal Transduct. Target. Ther. 2020 51* **5**, 1–25 (2020).
196. Gilleron, J. *et al.* Image-based analysis of lipid nanoparticle–mediated siRNA delivery, intracellular trafficking and endosomal escape. *Nat. Biotechnol. 2013 317* **31**, 638–646 (2013).
197. G, O., B, O., RL, C., AK, S. & G, L.-B. Preclinical and clinical development of siRNA-based therapeutics. *Adv. Drug Deliv. Rev.* **87**, 108–119 (2015).
198. K, G. Alnylam terminates revusiran program, stock plunges. *Nat. Biotechnol.* **34**, 1213–1214 (2016).
199. Reshke, R. *et al.* Reduction of the therapeutic dose of silencing RNA by packaging it in extracellular vesicles via a pre-microRNA backbone. *Nat. Biomed. Eng.* **4**, 52–68 (2020).
200. Kooijmans, S. A. A. *et al.* Electroporation-induced siRNA precipitation obscures the efficiency of siRNA loading into extracellular vesicles. *J. Control. Release* **172**, 229–238 (2013).
201. O'Loughlin, A. J. *et al.* Functional Delivery of Lipid-Conjugated siRNA by Extracellular Vesicles. *Mol. Ther.* **25**, 1580–1587 (2017).
202. O'Brien, K., Breyne, K., Ughetto, S., Laurent, L. C. & Breakefield, X. O. RNA delivery by extracellular vesicles in mammalian cells and its applications. *Nat. Rev. Mol. Cell Biol. 2020 2110* **21**, 585–606 (2020).
203. Sork, H. *et al.* Heterogeneity and interplay of the extracellular vesicle small RNA transcriptome and proteome. *Sci. Reports 2018 81* **8**, 1–12 (2018).
204. Baglio, S. R. *et al.* Human bone marrow- and adipose-mesenchymal stem cells secrete exosomes enriched in distinctive miRNA and tRNA species. *Stem Cell Res. Ther. 2015 61* **6**, 1–20 (2015).
205. Srinivasan, S., Yeri, A., Alexander, R. P., Das, S. & Correspondence, L. C. L. Small RNA Sequencing across Diverse Biofluids Identifies Optimal Methods for exRNA Isolation In Brief. *Cell* **177**, 446-462.e16 (2019).
206. Valadi, H. *et al.* Exosome-mediated transfer of mRNAs and microRNAs is a novel mechanism of genetic exchange between cells. *Nat. Cell Biol.* (2007) doi:10.1038/ncb1596.
207. Chevillet, J. R. *et al.* Quantitative and stoichiometric analysis of the microRNA content of exosomes. *Proc. Natl. Acad. Sci. U. S. A.* **111**, 14888 (2014).
208. L, S., L, T., N, V. & JD, S. Investigation of Content, Stoichiometry and Transfer of miRNA from Human Neural Stem Cell Line Derived Exosomes. *PLoS One* **11**, (2016).
209. Yang, S. *et al.* Conserved vertebrate mir-451 provides a platform for Dicer-independent, Ago2-mediated microRNA biogenesis. *Proc. Natl. Acad. Sci. U. S. A.* **107**, 15163–15168 (2010).
210. Gibbings, D. J., Ciaudo, C., Erhardt, M. & Voinnet, O. Multivesicular bodies associate with components of miRNA effector complexes and modulate miRNA activity. *Nat. Cell Biol.* **11**, 1143–1149 (2009).
211. Cifuentes, D. *et al.* A novel miRNA processing pathway independent of dicer requires argonaute2 catalytic activity. *Science (80-.).* **328**, 1694–1698 (2010).
212. Fields, C. R., Bengoa-Vergniory, N. & Wade-Martins, R. Targeting Alpha-Synuclein as a

Therapy for Parkinson's Disease. *Frontiers in Molecular Neuroscience* vol. 12 (2019).
213. Ozansoy, M. & Başak, A. N. The central theme of parkinson's disease: α-synuclein. *Mol. Neurobiol.* **42**, 460–465 (2012).
214. Kouli, A., Torsney, K. M. & Kuan, W.-L. Parkinson's Disease: Etiology, Neuropathology, and Pathogenesis. in *Parkinson's Disease: Pathogenesis and Clinical Aspects* 3–26 (Codon Publications, 2018). doi:10.15586/codonpublications.parkinsonsdisease.2018.ch1.
215. Xia, Q. *et al.* Proteomic identification of novel proteins associated with Lewy bodies. *Front. Biosci.* **13**, 3850 (2008).
216. AJ, L., M, S., LA, A. & C, D. The black stuff and Konstantin Nikolaevich Tretiakoff. *Mov. Disord.* **23**, 777–783 (2008).
217. Del Rey, N. L. G. *et al.* Advances in parkinson's disease: 200 years later. *Frontiers in Neuroanatomy* vol. 12 113 (2018).
218. T, P., N, J., A, F. & TD, S. The prevalence of Parkinson's disease: a systematic review and meta-analysis. *Mov. Disord.* **29**, 1583–1590 (2014).
219. DK, S., CM, T. & P, B. Parkinson Disease Epidemiology, Pathology, Genetics, and Pathophysiology. *Clin. Geriatr. Med.* **36**, 1–12 (2020).
220. A, A. & MA, S. The epidemiology of Parkinson's disease: risk factors and prevention. *Lancet. Neurol.* **15**, 1257–1272 (2016).
221. Maiti, P., Manna, J., Dunbar, G. L., Maiti, P. & Dunbar, G. L. Current understanding of the molecular mechanisms in Parkinson's disease: Targets for potential treatments. *Translational Neurodegeneration* vol. 6 (2017).
222. ME, C. *et al.* A case of probable Parkinson's disease after SARS-CoV-2 infection. *Lancet. Neurol.* **19**, 804–805 (2020).
223. P, B., A, N. & JD, B. Is COVID-19 a Perfect Storm for Parkinson's Disease? *Trends Neurosci.* **43**, 931–933 (2020).
224. M, M., KP, B. & JA, O. SARS-CoV-2 and the risk of Parkinson's disease: facts and fantasy. *Lancet. Neurol.* **20**, 94–95 (2021).
225. E, S. *et al.* Vagotomy and subsequent risk of Parkinson's disease. *Ann. Neurol.* **78**, 522–529 (2015).
226. BA, K. *et al.* The vermiform appendix impacts the risk of developing Parkinson's disease. *Sci. Transl. Med.* **10**, (2018).
227. Schapira, A. H. V., Chaudhuri, K. R. & Jenner, P. Non-motor features of Parkinson disease. *Nature Reviews Neuroscience* vol. 18 435–450 (2017).
228. Chaudhuri, K. R., Healy, D. G. & Schapira, A. H. V. Non-motor symptoms of Parkinson's disease: diagnosis and management. *Lancet Neurol.* **5**, 235–245 (2006).
229. P, M.-M., C, R.-B., MM, K. & KR, C. The impact of non-motor symptoms on health-related quality of life of patients with Parkinson's disease. *Mov. Disord.* **26**, 399–406 (2011).
230. TK, K. *et al.* The spectrum of nonmotor symptoms in early Parkinson disease. *Neurology* **80**, 276–281 (2013).
231. P, D., EC, H., Y, A. & AM, G. The substantia nigra of the human brain. II. Patterns of loss of dopamine-containing neurons in Parkinson's disease. *Brain* **122 (Pt 8)**, 1437–1448 (1999).
232. H, B. & K, D. T. Cortico-basal ganglia-cortical circuitry in Parkinson's disease reconsidered. *Exp. Neurol.* **212**, 226–229 (2008).
233. Kalia, L. V. & Lang, A. E. Parkinson's disease. *Lancet* **386**, 896–912 (2015).

234. Dickson, D. W. Parkinson's disease and parkinsonism: Neuropathology. *Cold Spring Harb. Perspect. Med.* **2**, (2012).
235. Polymeropoulos, M. H. *et al.* Mutation in the α-Synuclein Gene Identified in Families with Parkinson's Disease. *Science (80-.).* **276**, 2045–2047 (1997).
236. Peng, C., Gathagan, R. J. & Lee, V. M. Y. Distinct α-Synuclein strains and implications for heterogeneity among α-Synucleinopathies. *Neurobiol. Dis.* **109**, 209–218 (2018).
237. P, I. *et al.* Causal relation between alpha-synuclein gene duplication and familial Parkinson's disease. *Lancet (London, England)* **364**, 1169–1171 (2004).
238. Goedert, M., Spillantini, M. G., Del Tredici, K. & Braak, H. 100 years of Lewy pathology. *Nature Reviews Neurology* vol. 9 13–24 (2013).
239. R, B. & AHV, S. Parkinson disease. *Eur. J. Neurol.* **27**, 27–42 (2020).
240. MA, N. *et al.* Identification of novel risk loci, causal insights, and heritable risk for Parkinson's disease: a meta-analysis of genome-wide association studies. *Lancet. Neurol.* **18**, 1091–1102 (2019).
241. C, B., MA, N. & AB, S. The genetic architecture of Parkinson's disease. *Lancet. Neurol.* **19**, 170–178 (2020).
242. Bloem, B. R., Okun, M. S. & Klein, C. Seminar Parkinson's disease. *Lancet* **397**, 2284–2303 (2021).
243. AP, K. *et al.* α-Synucleinopathy associated with G51D SNCA mutation: a link between Parkinson's disease and multiple system atrophy? *Acta Neuropathol.* **125**, 753–769 (2013).
244. Proukakis, C. *et al.* A novel α-synuclein missense mutation in Parkinson disease. *Neurology* **80**, 1062 (2013).
245. JJ, Z. *et al.* The new mutation, E46K, of alpha-synuclein causes Parkinson and Lewy body dementia. *Ann. Neurol.* **55**, 164–173 (2004).
246. R, K. *et al.* Ala30Pro mutation in the gene encoding alpha-synuclein in Parkinson's disease. *Nat. Genet.* **18**, 106–108 (1998).
247. Maraganore, D. M. Rationale for Therapeutic Silencing of Alpha-Synuclein in Parkinson's Disease. *J. Mov. Disord.* **4**, 1–7 (2011).
248. Halliday, G. M., Holton, J. L., Revesz, T. & Dickson, D. W. Neuropathology underlying clinical variability in patients with synucleinopathies. doi:10.1007/s00401-011-0852-9.
249. Dettmer, U., Selkoe, D. & Bartels, T. New insights into cellular α-synuclein homeostasis in health and disease. *Curr. Opin. Neurobiol.* **36**, 15–22 (2016).
250. FN, E. Alpha-synuclein structure, functions, and interactions. *J. Res. Med. Sci.* **21**, (2016).
251. AJ, T. & E, R. N-Terminal acetylation is critical for forming α-helical oligomer of α-synuclein. *Protein Sci.* **21**, 601–605 (2012).
252. IG, Z. & GJ, P. Interaction of α-synuclein and a cell penetrating fusion peptide with higher eukaryotic cell membranes assessed by ^{19}F NMR. *Mol. Pharm.* **9**, 1024–1029 (2012).
253. Zigoneanu, I. G., Yang, Y. J., Krois, A. S., Haque, M. E. & Pielak, G. J. Interaction of α-synuclein with vesicles that mimic mitochondrial membranes. *Biochim. Biophys. Acta - Biomembr.* **1818**, 512–519 (2012).
254. Ulmer, T. S., Bax, A., Cole, N. B. & Nussbaum, R. L. Structure and Dynamics of Micelle-bound Human α-Synuclein. *J. Biol. Chem.* **280**, 9595–9603 (2005).
255. Trexler, A. J. & Rhoades, E. α-Synuclein binds large unilamellar vesicles as an extended helix. *Biochemistry* **48**, 2304 (2009).
256. Waxman, E. A., Mazzulli, J. R. & Giasson, B. I. Characterization of Hydrophobic Residue

Requirements for α-Synuclein Fibrillization. *Biochemistry* **48**, 9427 (2009).
257. OM, el-A. & GB, I. Aggregation and neurotoxicity of alpha-synuclein and related peptides. *Biochem. Soc. Trans.* **30**, 559–565 (2002).
258. LC, S., J, B., R, J., M, G. & RA, C. Fiber diffraction of synthetic alpha-synuclein filaments shows amyloid-like cross-beta conformation. *Proc. Natl. Acad. Sci. U. S. A.* **97**, 4897–4902 (2000).
259. MF, P., BJ, P., D, O., EE, W. & E, S. Aggregation of proteins with expanded glutamine and alanine repeats of the glutamine-rich and asparagine-rich domains of Sup35 and of the amyloid beta-peptide of amyloid plaques. *Proc. Natl. Acad. Sci. U. S. A.* **99**, 5596–5600 (2002).
260. KK, D., K, H., S, B., VL, B. & H, van der P. Part II: alpha-synuclein and its molecular pathophysiological role in neurodegenerative disease. *Neuropharmacology* **45**, 14–44 (2003).
261. Peelaerts, W. *et al.* α-Synuclein strains cause distinct synucleinopathies after local and systemic administration. *Nature* **522**, 340–344 (2015).
262. Outeiro, T. F. *et al.* Formation of toxic oligomeric α-synuclein species in living cells. *PLoS One* **3**, (2008).
263. Zambon, F. *et al.* Cellular α-synuclein pathology is associated with bioenergetic dysfunction in Parkinson's iPSC-derived dopamine neurons. *Hum. Mol. Genet.* **28**, 2001–2013 (2019).
264. A, R., KJ, A., J, K. & JA, C. The chaperone activity of α-synuclein: Utilizing deletion mutants to map its interaction with target proteins. *Proteins* **80**, 1316–1325 (2012).
265. Burré, J. *et al.* α-Synuclein Promotes SNARE-Complex Assembly in vivo and in vitro. *Science* **329**, 1663 (2010).
266. Samuel, F. *et al.* Effects of Serine 129 Phosphorylation on α-Synuclein Aggregation, Membrane Association, and Internalization. *J. Biol. Chem.* **291**, 4374–4385 (2016).
267. H, F. *et al.* alpha-Synuclein is phosphorylated in synucleinopathy lesions. *Nat. Cell Biol.* **4**, 160–164 (2002).
268. A, O. Implication of Alpha-Synuclein Phosphorylation at S129 in Synucleinopathies: What Have We Learned in the Last Decade? *J. Parkinsons. Dis.* **6**, 39–51 (2016).
269. E, D. *et al.* Alpha-Synuclein Oligomers Interact with Metal Ions to Induce Oxidative Stress and Neuronal Death in Parkinson's Disease. *Antioxid. Redox Signal.* **24**, 376–391 (2016).
270. Lu, Y., Prudent, M., Fauvet, B., Lashuel, H. A. & Girault, H. H. Phosphorylation of α-Synuclein at Y125 and S129 Alters Its Metal Binding Properties: Implications for Understanding the Role of α-Synuclein in the Pathogenesis of Parkinson's Disease and Related Disorders. *ACS Chem. Neurosci.* **2**, 667 (2011).
271. J, B. *et al.* Properties of native brain α-synuclein. *Nature* **498**, (2013).
272. Paul H. Weinreb, Weiguo Zhen, ‡, Anna W. Poon, Kelly A. Conway, ‡ and & Peter T. Lansbury, J. *,. NACP, A Protein Implicated in Alzheimer's Disease and Learning, Is Natively Unfolded†. *Biochemistry* **35**, 13709–13715 (1996).
273. W, W. *et al.* A soluble α-synuclein construct forms a dynamic tetramer. *Proc. Natl. Acad. Sci. U. S. A.* **108**, 17797–17802 (2011).
274. T, B., JG, C. & DJ, S. α-Synuclein occurs physiologically as a helically folded tetramer that resists aggregation. *Nature* **477**, 107–111 (2011).
275. Y, C. & JH, K. Lewy body pathology in fetal grafts. *Ann. N. Y. Acad. Sci.* **1184**, 55–67

(2010).
276. A, B. *et al.* Alpha-synuclein aggregation and cell death triggered by energy deprivation and dopamine overload are counteracted by D2/D3 receptor activation. *J. Neurochem.* **106**, 560–577 (2008).
277. L, C., M, W., J, S.-P. & M, G. S. Synaptic failure and α-synuclein. *Mov. Disord.* **31**, 169–177 (2016).
278. Kahle, P. J. *et al.* Subcellular Localization of Wild-Type and Parkinson's Disease-Associated Mutant α-Synuclein in Human and Transgenic Mouse Brain. *J. Neurosci.* **20**, 6365–6373 (2000).
279. J, B. The Synaptic Function of α-Synuclein. *J. Parkinsons. Dis.* **5**, 699–713 (2015).
280. BK, C. *et al.* Large α-synuclein oligomers inhibit neuronal SNARE-mediated vesicle docking. *Proc. Natl. Acad. Sci. U. S. A.* **110**, 4087–4092 (2013).
281. Zhang, S., Eitan, E., Wu, T. Y. & Mattson, M. P. Intercellular transfer of pathogenic α-synuclein by extracellular vesicles is induced by the lipid peroxidation product 4-hydroxynonenal. *Neurobiol. Aging* **61**, 52–65 (2018).
282. Diao, J. *et al.* Native α-synuclein induces clustering of synaptic-vesicle mimics via binding to phospholipids and synaptobrevin-2/VAMP2. *Elife* **2013**, (2013).
283. S, C., G, G., R, F.-C., OM, S. & TC, S. Alpha-synuclein cooperates with CSPalpha in preventing neurodegeneration. *Cell* **123**, 383–396 (2005).
284. Ghiglieri, V., Calabrese, V. & Calabresi, P. Alpha-synuclein: From early synaptic dysfunction to neurodegeneration. *Frontiers in Neurology* vol. 9 (2018).
285. H, J. *et al.* α-Synuclein negatively regulates protein kinase Cδ expression to suppress apoptosis in dopaminergic neurons by reducing p300 histone acetyltransferase activity. *J. Neurosci.* **31**, 2035–2051 (2011).
286. M, H. *et al.* alpha-Synuclein protects against oxidative stress via inactivation of the c-Jun N-terminal kinase stress-signaling pathway in neuronal cells. *J. Biol. Chem.* **277**, 11465–11472 (2002).
287. OS, G. *et al.* α-Synuclein expression in rat substantia nigra suppresses phospholipase D2 toxicity and nigral neurodegeneration. *Mol. Ther.* **18**, 1758–1768 (2010).
288. Park, M. J., Cheon, S.-M., Bae, H.-R., Kim, S.-H. & Kim, J. W. Elevated Levels of α-Synuclein Oligomer in the Cerebrospinal Fluid of Drug-Naïve Patients with Parkinson's Disease. *J. Clin. Neurol.* **7**, 215 (2011).
289. T, T. *et al.* Detection of elevated levels of α-synuclein oligomers in CSF from patients with Parkinson disease. *Neurology* **75**, 1766–1772 (2010).
290. Feany, M. B. & Bender, W. W. A Drosophila model of Parkinson's disease. *Nat. 2000 4046776* **404**, 394–398 (2000).
291. Lelan, F. *et al.* Effects of Human Alpha-Synuclein A53T-A30P Mutations on SVZ and Local Olfactory Bulb Cell Proliferation in a Transgenic Rat Model of Parkinson Disease. *Parkinsons. Dis.* **2011**, (2011).
292. Lin, X. *et al.* Conditional Expression of Parkinson's Disease-Related Mutant α-Synuclein in the Midbrain Dopaminergic Neurons Causes Progressive Neurodegeneration and Degradation of Transcription Factor Nuclear Receptor Related 1. *J. Neurosci.* **32**, 9248–9264 (2012).
293. T, K. *et al.* Familial Parkinson mutant alpha-synuclein causes dopamine neuron dysfunction in transgenic Caenorhabditis elegans. *J. Biol. Chem.* **281**, 334–340 (2006).
294. Cuvelier, E. *et al.* Overexpression of Wild-Type Human Alpha-Synuclein Causes

Metabolism Abnormalities in Thy1-aSYN Transgenic Mice. *Front. Mol. Neurosci.* **0**, 321 (2018).
295. L, B. *et al.* Structural and functional characterization of two alpha-synuclein strains. *Nat. Commun.* **4**, (2013).
296. Bousset, L. *et al.* Structural and functional characterization of two alpha-synuclein strains. *Nat. Commun. 2013 41* **4**, 1–13 (2013).
297. Jie Li, ‡,§, Vladimir N. Uversky, *,‡,§,‖ and & Anthony L. Fink*, §. Effect of Familial Parkinson's Disease Point Mutations A30P and A53T on the Structural Properties, Aggregation, and Fibrillation of Human α-Synuclein†. *Biochemistry* **40**, 11604–11613 (2001).
298. KA, C., JD, H. & PT, L. Accelerated in vitro fibril formation by a mutant alpha-synuclein linked to early-onset Parkinson disease. *Nat. Med.* **4**, 1318–1320 (1998).
299. Y, L. & H, Y. Environmental toxins and alpha-synuclein in Parkinson's disease. *Mol. Neurobiol.* **31**, 273–282 (2005).
300. Schieler, J. L. *et al.* Effect of oxidative stress on α-synuclein aggregation in Parkinson's disease. *Nanomedicine Nanotechnology, Biol. Med.* **2**, 317 (2006).
301. Ma, M.-R., Hu, Z.-W., Zhao, Y.-F., Chen, Y.-X. & Li, Y.-M. Phosphorylation induces distinct alpha-synuclein strain formation. *Sci. Reports 2016 61* **6**, 1–11 (2016).
302. VN, U., J, L. & AL, F. Metal-triggered structural transformations, aggregation, and fibrillation of human alpha-synuclein. A possible molecular NK between Parkinson's disease and heavy metal exposure. *J. Biol. Chem.* **276**, 44284–44296 (2001).
303. Braak, H. *et al.* Staging of brain pathology related to sporadic Parkinson's disease. *Neurobiol. Aging* **24**, 197–211 (2003).
304. Masuda-Suzukake, M. *et al.* Prion-like spreading of pathological α-synuclein in brain. *Brain* **136**, 1128–1138 (2013).
305. Volpicelli-Daley, L. A. *et al.* Exogenous α-Synuclein Fibrils Induce Lewy Body Pathology Leading to Synaptic Dysfunction and Neuron Death. *Neuron* **72**, 57–71 (2011).
306. KC, L. *et al.* Pathological α-synuclein transmission initiates Parkinson-like neurodegeneration in nontransgenic mice. *Science* **338**, 949–953 (2012).
307. Luk, K. C. *et al.* Pathological α-Synuclein Transmission Initiates Parkinson-like Neurodegeneration in Nontransgenic Mice. *Science (80-.).* **338**, 949–953 (2012).
308. Dehay, B. & Bezard, E. Intrastriatal injection of alpha-synuclein fibrils induces Parkinson-like pathology in macaques. *Brain* **142**, 3321–3322 (2019).
309. Peelaerts, W. *et al.* a-Synuclein strains cause distinct synucleinopathies after local and systemic administration. doi:10.1038/nature14547.
310. JH, K. *et al.* Transfer of host-derived α synuclein to grafted dopaminergic neurons in rat. *Neurobiol. Dis.* **43**, 552–557 (2011).
311. Hansen, C. *et al.* α-Synuclein propagates from mouse brain to grafted dopaminergic neurons and seeds aggregation in cultured human cells. *J. Clin. Invest.* **121**, 715–725 (2011).
312. J, M., J, G., J, W. & A, X. Prion-Like Mechanisms in Parkinson's Disease. *Front. Neurosci.* **13**, (2019).
313. McCormack, A. L. *et al.* α-synuclein suppression by targeted small interfering rna in the primate substantia nigra. *PLoS One* **5**, (2010).
314. MK, S. *et al.* Silencing of human alpha-synuclein in vitro and in rat brain using lentiviral-mediated RNAi. *Exp. Neurol.* **198**, 382–390 (2006).

315. Lewis, J. *et al.* In vivo silencing of alpha-synuclein using naked siRNA. *Mol. Neurodegener.* **3**, 19 (2008).
316. OS, G. *et al.* In vivo RNAi-mediated alpha-synuclein silencing induces nigrostriatal degeneration. *Mol. Ther.* **18**, 1450–1457 (2010).
317. TJ, C., DE, R., K, S.-C., JW, L. & FP, M. Is Alpha-Synuclein Loss-of-Function a Contributor to Parkinsonian Pathology? Evidence from Non-human Primates. *Front. Neurosci.* **10**, (2016).
318. Weksler, B. B. *et al.* Blood-brain barrier-specific properties of a human adult brain endothelial cell line. *FASEB J.* **19**, 1872–1874 (2005).
319. Momen-Heravi, F. Isolation of Extracellular Vesicles by Ultracentrifugation. *Methods Mol. Biol.* **1660**, 25–32 (2017).
320. Shang, M. *et al.* Extracellular Vesicles: A Brief Overview and Its Role in Precision Medicine. *Methods Mol. Biol.* **1660**, 1–14 (2017).
321. Royo, F. *et al.* Different EV enrichment methods suitable for clinical settings yield different subpopulations of urinary extracellular vesicles from human samples. *J. Extracell. Vesicles* **5**, (2016).
322. Musante, L., Saraswat, M., Ravidà, A., Byrne, B. & Holthofer, H. Recovery of urinary nanovesicles from ultracentrifugation supernatants. *Nephrol. Dial. Transplant.* **28**, 1425–1433 (2013).
323. Van Reis, R. *et al.* High Performance Tangential Flow Filtration. *Biotechnol Bioeng* **56**, 71–82 (1997).
324. Weksler, B., Romero, I. A. & Couraud, P. O. The hCMEC/D3 cell line as a model of the human blood brain barrier. *Fluids Barriers CNS* **10**, 1–10 (2013).
325. Holcar, M. *et al.* Enrichment of plasma extracellular vesicles for reliable quantification of their size and concentration for biomarker discovery. *Sci. Reports |* **10**, 21346 (123AD).
326. Agholme, L., Lindström, T., Kgedal, K., Marcusson, J. & Hallbeck, M. An in vitro model for neuroscience: Differentiation of SH-SY5Y cells into cells with morphological and biochemical characteristics of mature neurons. *J. Alzheimer's Dis.* **20**, 1069–1082 (2010).
327. Gustafsson, G. *et al.* Secretion and Uptake of α-Synuclein Via Extracellular Vesicles in Cultured Cells. *Cell. Mol. Neurobiol.* **38**, 1539 (2018).
328. Emmanouilidou, E. *et al.* Cell-Produced α-Synuclein Is Secreted in a Calcium-Dependent Manner by Exosomes and Impacts Neuronal Survival. *J. Neurosci.* **30**, 6838 (2010).
329. Srinivasan, B. *et al.* TEER measurement techniques for in vitro barrier model systems. *J. Lab. Autom.* **20**, 107 (2015).
330. Elbakary, B. & Badhan, R. K. S. A dynamic perfusion based blood-brain barrier model for cytotoxicity testing and drug permeation. *Sci. Reports 2020 101* **10**, 1–12 (2020).
331. BP, D. *et al.* Immortalized human cerebral microvascular endothelial cells maintain the properties of primary cells in an in vitro model of immune migration across the blood brain barrier. *J. Neurosci. Methods* **212**, 173–179 (2013).
332. Lippmann, E. S., Al-Ahmad, A., Azarin, S. M., Palecek, S. P. & Shusta, E. V. A retinoic acid-enhanced, multicellular human blood-brain barrier model derived from stem cell sources. *Sci. Reports 2014 41* **4**, 1–10 (2014).
333. Fisher Scientific, T. CellTracker fluorescent probes Product Information Sheet (Pub. No. MAN0001826 B.0).
334. Mondal, A., Ashiq, K. A., Phulpagar, P., Singh, D. K. & Shiras, A. Effective Visualization and Easy Tracking of Extracellular Vesicles in Glioma Cells. *Biol. Proced. Online* **21**, 1–

12 (2019).
335. Chuo, S. T. Y., Chien, J. C. Y. & Lai, C. P. K. Imaging extracellular vesicles: Current and emerging methods. *J. Biomed. Sci.* **25**, 1–10 (2018).
336. Takov, K., Yellon, D. M. & Davidson, S. M. Confounding factors in vesicle uptake studies using fluorescent lipophilic membrane dyes. *https://doi.org/10.1080/20013078.2017.1388731* **6**, (2017).
337. Pužar Dominkuš, P. *et al.* PKH26 labeling of extracellular vesicles: Characterization and cellular internalization of contaminating PKH26 nanoparticles. *Biochim. Biophys. Acta - Biomembr.* **1860**, 1350–1361 (2018).
338. Lai, C. P. *et al.* Visualization and tracking of tumour extracellular vesicle delivery and RNA translation using multiplexed reporters. *Nat. Commun. 2015 61* **6**, 1–12 (2015).
339. PK, W. *et al.* Tracking antigen-driven responses by flow cytometry: monitoring proliferation by dye dilution. *Cytometry. A* **73**, 1019–1034 (2008).
340. Ruano-Salguero, J. S. & Lee, K. H. Antibody transcytosis across brain endothelial-like cells occurs nonspecifically and independent of FcRn. *Sci. Rep.* **10**, 1–10 (2020).
341. Pardridge, W. M. Drug transport across the blood–brain barrier. *J. Cereb. Blood Flow Metab.* **32**, 1959 (2012).
342. Miranda, A. M. *et al.* Neuronal lysosomal dysfunction releases exosomes harboring APP C-terminal fragments and unique lipid signatures. *Nat. Commun. 2018 91* **9**, 1–16 (2018).
343. Eitan, E., Suire, C., Zhang, S. & Mattson, M. P. Impact of Lysosome Status on Extracellular Vesicle Content and Release. *Ageing Res. Rev.* **32**, 65 (2016).
344. Yi, Y. W. *et al.* Advances in analysis of biodistribution of exosomes by molecular imaging. *International Journal of Molecular Sciences* vol. 21 (2020).
345. Purves, D. *et al.* The Blood Supply of the Brain and Spinal Cord. (2001).
346. Joshi, S., Meyers, P. M. & Ornstein, E. Intracarotid delivery of drugs: The potential and the pitfalls. *Anesthesiology* vol. 109 543–564 (2008).
347. Wiklander, O. P. B. *et al.* Extracellular vesicle in vivo biodistribution is determined by cell source, route of administration and targeting. *J. Extracell. Vesicles* **4**, 1–13 (2015).
348. Li, M. *et al.* Analysis of the RNA content of the exosomes derived from blood serum and urine and its potential as biomarkers. *Philos. Trans. R. Soc. B Biol. Sci.* **369**, (2014).
349. Di Liegro, C. M., Schiera, G. & Di Liegro, I. Regulation of mRNA transport, localization and translation in the nervous system of mammals (Review). *Int. J. Mol. Med.* **33**, 747–762 (2014).
350. S, G., M, H., M, A. & T, T. Evolutionary conservation and expression of human RNA-binding proteins and their role in human genetic disease. *Adv. Exp. Med. Biol.* **825**, (2014).
351. Fabbiano, F. *et al.* RNA packaging into extracellular vesicles: An orchestra of RNA-binding proteins? *J. Extracell. Vesicles* **10**, (2020).
352. J, P.-B., A, B., M, L., F, D. & I, S. hnRNPA2B1 inhibits the exosomal export of miR-503 in endothelial cells. *Cell. Mol. Life Sci.* **77**, 4413–4428 (2020).
353. Teng, Y. *et al.* MVP-mediated exosomal sorting of miR-193a promotes colon cancer progression. *Nat. Commun. 2017 81* **8**, 1–16 (2017).
354. A, B., M, C., S, K., G, R. & C, T. Diverse subpopulations of vesicles secreted by different intracellular mechanisms are present in exosome preparations obtained by differential ultracentrifugation. *J. Extracell. vesicles* **1**, (2012).
355. Kowal, J. *et al.* Proteomic comparison defines novel markers to characterize

heterogeneous populations of extracellular vesicle subtypes. *Proc. Natl. Acad. Sci.* **113**, E968–E977 (2016).
356. Cole, T. A. *et al.* α-Synuclein antisense oligonucleotides as a disease-modifying therapy for Parkinson's disease. *JCI Insight* **6**, (2021).
357. Voyager's CNS gene therapy. *Nat. Biotechnol.* **37**, 204 (2019).
358. A, S. & M, S. Exosomes: vesicular carriers for intercellular communication in neurodegenerative disorders. *Cell Tissue Res.* **352**, 33–47 (2013).
359. M, R., C, S., S, S.-P. & M, P. Exosomes as intercellular signalosomes and pharmacological effectors. *Biochem. Pharmacol.* **81**, 1171–1182 (2011).
360. DD, T. & C, G.-T. Exosomes/microvesicles: mediators of cancer-associated immunosuppressive microenvironments. *Semin. Immunopathol.* **33**, 441–454 (2011).
361. J, M. Exosomes and Ectosomes in Intercellular Communication. *Curr. Biol.* **28**, R435–R444 (2018).
362. S, F., M, W., HH, M., D, R. & W, S. Simultaneous activation of several second messengers in hypoxia-induced hyperpermeability of brain derived endothelial cells. *J. Cell. Physiol.* **198**, 359–369 (2004).
363. Haqqani, A. S. *et al.* Method for isolation and molecular characterization of extracellular microvesicles released from brain endothelial cells. *Fluids Barriers CNS* **10**, 4 (2013).
364. Abulrob, A., Sprong, H., Henegouwen, P. V. B. E. & Stanimirovic, D. The blood–brain barrier transmigrating single domain antibody: mechanisms of transport and antigenic epitopes in human brain endothelial cells. *J. Neurochem.* **95**, 1201–1214 (2005).
365. AR, J. & EV, S. Blood-brain barrier transport of therapeutics via receptor-mediation. *Pharm. Res.* **24**, 1759–1771 (2007).
366. WM, P., JL, B. & PM, F. Selective transport of an anti-transferrin receptor antibody through the blood-brain barrier in vivo. *J. Pharmacol. Exp. Ther.* **259**, 66–70 (1991).
367. Yuan, D. *et al.* Macrophage exosomes as natural nanocarriers for protein delivery to inflamed brain. *Biomaterials* **142**, 1–12 (2017).
368. H, K. *et al.* Cluster of Differentiation 46 Is the Major Receptor in Human Blood-Brain Barrier Endothelial Cells for Uptake of Exosomes Derived from Brain-Metastatic Melanoma Cells (SK-Mel-28). *Mol. Pharm.* **16**, 292–304 (2019).
369. Qiao, L. *et al.* Tumor cell-derived exosomes home to their cells of origin and can be used as Trojan horses to deliver cancer drugs. *Theranostics* **10**, 3474–3487 (2020).
370. Fang, P. *et al.* Immune cell subset differentiation and tissue inflammation. *J. Hematol. Oncol.* **11**, (2018).
371. Hung, M. E. & Leonard, J. N. Stabilization of exosome-targeting peptides via engineered glycosylation. *J. Biol. Chem.* **290**, 8166–8172 (2015).
372. Yang, J., Zhang, X., Chen, X., Wang, L. & Yang, G. Exosome Mediated Delivery of miR-124 Promotes Neurogenesis after Ischemia. *Mol. Ther. - Nucleic Acids* **7**, 278–287 (2017).
373. G, J. *et al.* NRP-1 targeted and cargo-loaded exosomes facilitate simultaneous imaging and therapy of glioma in vitro and in vivo. *Biomaterials* **178**, 302–316 (2018).
374. T, T. *et al.* Surface functionalized exosomes as targeted drug delivery vehicles for cerebral ischemia therapy. *Biomaterials* **150**, 137–149 (2018).
375. Goulatis, L. I. & Shusta, E. V. Protein engineering approaches for regulating blood–brain barrier transcytosis. *Curr. Opin. Struct. Biol.* **45**, 109–115 (2017).
376. M, G., K, P., S, L.-P., K, S. & E, R. Manufacturing of Human Extracellular Vesicle-Based Therapeutics for Clinical Use. *Int. J. Mol. Sci.* **18**, (2017).

377. Hallal, S. *et al.* Extracellular Vesicles Released by Glioblastoma Cells Stimulate Normal Astrocytes to Acquire a Tumor-Supportive Phenotype Via p53 and MYC Signaling Pathways. *Mol. Neurobiol.* **56**, 4566 (2019).